ALMA MATER STUDIORUM - UNIVERSITÀ DI BOLOGNA
DOTTORATO DI RICERCA IN GEOFISICA
CICLO XXIX
SETTORE CONCORSUALE DI AFFERENZA 04/A4
SETTORE SCIENTIFICO DISCIPLINARE GEO/10

THE SEA LEVEL ACCELERATION AND ITS OBSERVATION FROM TIDE GAUGES

Presentata da:
Marco Olivieri

Relatore:
Prof. Giorgio Spada

Coordinatore Dottorato:
Prof. Nadia Pinardi

Anno Accademico 2016-17 — Ciclo XXIX

A Eleonora, ed in memoria di mio padre.

"Sale e scende la marea
che tutto copre e tutto crea"
(S.Sollima & S. Duncan Smith)

Abstract

TIDE gauges form a unique data set of sea–level observations that covers the last 200 years and more. Based on these data, models of the sea–level change have been created with the aim of assessing the global rate of sea–level rise and its acceleration. Such global models play a crucial role for the understanding of the ongoing climate change but these are also the roots for realistic scenarios of future sea level. Unfortunately, the sparse distribution of the tide gauge sites and the presence of long period oscillations pose some limitations that could compromise the reliability of the results.

In this dissertation I discuss the limits of using tide gauges data for the assessment of sea–level rise, with a focus on sea–level acceleration. The results confirm that long period oscillations, if not properly modeled, can bias the rate and the acceleration. Moreover, the limited number of observation points confined at coastlines can further disrupt the veracity of models. These findings are used to establish a new and more robust description of the century scale global mean sea level.

Preface

This project roots on the discussions with Prof. Giorgio Spada that followed the publication of the paper entitled “Intermittent sea-level acceleration” (Olivieri and Spada, 2013). While studying the century-long tide gauge time series, we learned that robust results strongly depend on the understanding of the local processes at the instrument location, on robust statistical approaches to the data, and on how the “coastal sea level” compares with the “global sea level”. These points are the main subjects of this dissertation, which include some original work and the results from a few papers published during these three years.

Despite the fact that my degree in Physics dates back to the early 90s, and that I am a researcher since 1999, I still felt motivations for a Ph.D. in Geophysics. The support by Prof. Giorgio Spada and by Prof. Maurizio Bonafede encouraged this effort.

As a general rule, I use the first singular person "I" when the text speaks about my own decisions. Conversely, I use "we" when referring to results obtained in collaboration with others to evidence the joint work and in most cases proper reference is given. Chapter 3 contains the results of a yet unpublished work by myself, Prof. Damiá Gomis, Gabriel Jordá and Prof. Giorgio Spada. Finally, I use "we", whenever the discourse is explanatory. Therein, "we" stands for "me and the reader".

Contents

List of Figures

List of Tables

CHAPTER 1

Introduction

1.1 The sea level

The height of the sea has been changing since oceans have existed. Nowadays, this change shows its dramatic interconnection with human activities (Pilkey and Cooper, 2004; Houghton et al., 2010), human life (McMichael et al., 2006) and wildlife (e.g. Regehr et al., 2016) with its rise at a rate of 1–2 mm yr^{-1} (e.g. Douglas, 1991; Church et al., 2004; Spada and Galassi, 2012) observed for the last century. Such a rise was worsened by the recent positive acceleration (Jevrejeva et al., 2008; Church et al., 2011; Olivieri and Spada, 2013; Spada et al., 2015). Conservative scenarios for the end of the century predict an average rise of ~ 0.8 m (Meehl et al., 2007) but this could widen up to 2.0 m according to semi-empirical models (Rahmstorf, 2007; Vermeer and Rahmstorf, 2009). The acceleration hypothesis, and its interconnection with climate change, explains the reason for a huge attention to sea–level change has been put globally by scientists, as well as by some of the politicians and

decision makers.

Why the sea level changes over time? The heating and cooling of the Earth surface, of the oceans and of the atmosphere modify the mass of the continental ice sheets inducing a change in the mass of the oceans, but the heating and cooling process also changes the volume of the seawater. At the same time, the meltwater load redistribution alters the Earth's gravity field. This change is responsible for a modification of the volume and shape of the ocean basins, and it also alters the ocean surface (Conrad, 2013). This simply explains how complex the interpretation and the modelization of the sea–level change can be, and how the different time scales characterizing the different processes are interconnected (e.g. Pirazzoli, 1986; Douglas, 1991; Cazenave and Nerem, 2004; Wöppelmann and Marcos, 2016). Without entering into the formalism of the problem, here I introduce the basic concepts related to it.

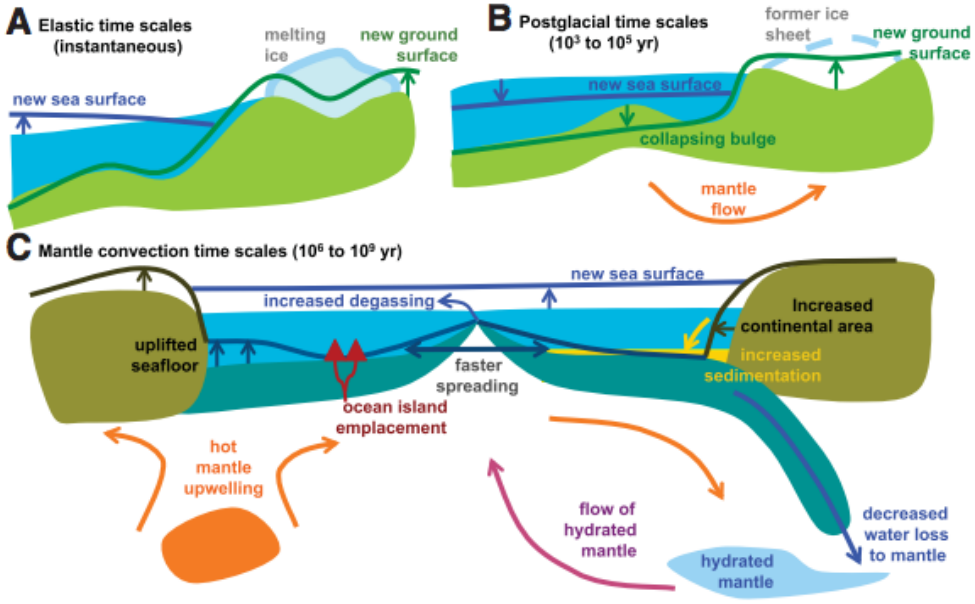

Figure 1.1: *Geodynamic processes, acting at different time scales, responsible for sea–level changes (reproduced under permission from Conrad, 2013).*

In Figure 1.1, reproduced from Conrad (2013), the processes related to the solid Earth dynamics are sketched and distinguished with respect to three different time scales: elastic, postglacial and mantle convec-

tion. The first shows the instantaneous "elastic" modification (Figure 1.1A) of sea level in consequence of the ice melting (Farrell, 1972; Farrell and Clark, 1976). The removal of the load induces two changes: the seafloor and bedrock react elastically by moving upwards while the seawater looses that portion of gravitational attraction produced by the melted ice mass. Different studies (Miller and Douglas, 2004; Leuliette and Miller, 2009) show that almost half of the observed sea–level rise at a century scale ($\sim$2 mm yr^{-1}) can be attributed to this mechanism and to the melting of the continental ice sheets.

At time scales between 10^3 and 10^4 years, Post Glacial Rebound (PGR) and Glacial Isostatic Adjustment (GIA) have an important role. In regions that where previously covered by large continental ice sheets (northern Europe and North America), the crust is presently subject to uplift in consequence of the still operating isostatic disequilibrium. In the periphery of these regions (Figure 1.1B), isostatic subsidence is causing the lateral forebulges to collapse (Farrell and Clark, 1976). Since the Maxwell time of the Earth's mantle is of the order of 10^3 years, on the time scales of PGR the whole Earth responds to surface loads both elastically and viscously. Post glacial sea–level curves are employed to constrain the history of deglaciation since the Last Glacial Maximum (LGM) and the rheological profile of the Earth (e.g. Mitrovica and Peltier, 1991; Peltier, 2004). In Section 1.2, the role of GIA will be examined in a larger detail. Indeed, GIA constitutes an important source of contamination of the instrumental sea–level observations obtained from tide gauges and of the satellite observations as well.

At even longer time scales (10^6 years), the geodynamic processes are dominated by plate tectonics and mantle dynamics (Harrison, 1990; Müller et al., 2008) that can cause sea–level changes in consequence of the change in shape of the ocean basins (Turcotte and Schubert, 2014). In Figure 1.1C, the most important tectonic processes are sketched: subduction and mid-oceanic ridge expansion. Sediment accumulations and

volcano emplacements would be also relevant at this time scale.

To quantify the sea–level change over time, I restrict the perspective to the period that goes from the LGM, $\sim 21,000$ years before present, to date. A realistic representation of the global sea–level variation during this period is given Figure 1.2. This results from model ICE-5G (VM2) of Peltier (2004) who interpolated a set of relative sea–level observations distributed worldwide. Figure 1.2 shows that the change since the

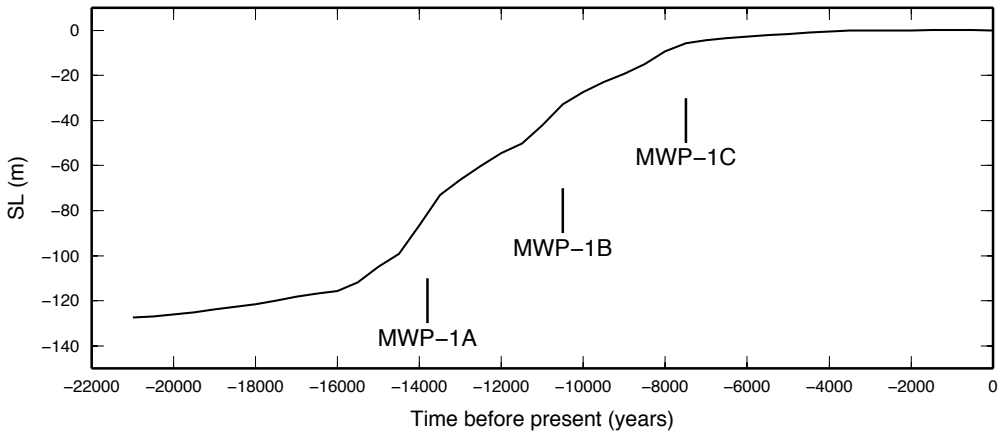

Figure 1.2: *Global sea level over time since the LGM. Time is indicated in years before present, present sea level is used as a reference level. Sea–level is in meters with 0 meters assigned to the present sea–level height. Labels MWP-NX mark the occurrence of the most relevant Melt Water Pulses.*

LGM has been ~ 130 m. We can recognize epochs of constant rate of change, steady accelerations and short lived pulses, the so-called Melt Water Pulses (MWP), which mark the rapid melting of large portions of the continental ice sheets (Fairbanks, 1989; Blanchon, 2011). Among the others, I mention MWP-1A, the largest one that occurred about 14,000 years ago when sea level rose ~ 20 m during a time span of about 500 years. The melting of the Laurentide ice sheet in North America, with the contribution of the Antarctica ice sheet, was the dominant source of this meltwater pulse (Clark et al., 2002). Figure 1.2 provides also the framework in which current models and future scenarios should be put while it should be remarked that, at time scale of millions of years, it is

realistic to think that variations almost 3 times larger ($\sim$450 m) occurred (Conrad, 2013).

The rate and acceleration variability since the LGM become more apparent if I plot the rate of sea–level change and its acceleration obtained by a five-point discrete derivative of the sea–level time history. From Figure 1.3a we observe that the sea–level rise ranged between 0 and $\sim$30 mm/yr with an average rate of $\sim$6 mm yr^{-1}, here the MWPs are more apparent. The acceleration (Figure 1.3b) ranged between about -3 and 3 myc[1] with an almost vanishing average that results from the comparable rates at the time series end points. Since the model is described at 500

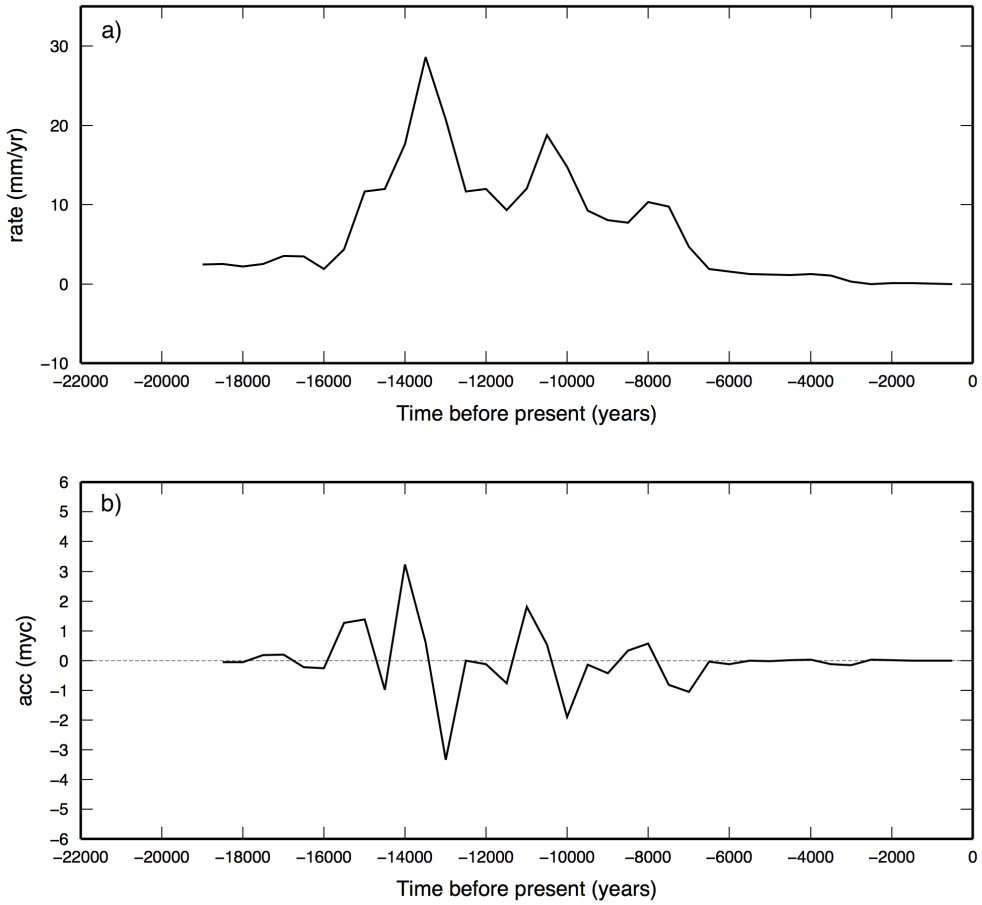

Figure 1.3: *a) rate of sea–level change and b) acceleration over time since the LGM, obtained by deriving the sea–level time history shown in Figure 1.2.*

[1] 1 myc = 1 mm year^{-1} century^{-1} = 0.01 mm yr^{-2}

years time steps, any sudden acceleration that lasted less than 500 years could not be caught but this would have been smeared along the time interval. Despite the low sampling rate of this model, these numbers will be useful in the following to put the sea–level rate and acceleration observed for the last decades and centuries in the framework of a longer time scale.

At shorter time scale (from decades to centuries) a variety of scientific works (e.g. Kalinin and Klige, 1978; Pirazzoli, 1986; Douglas, 1991; Cabanes et al., 2001; Cazenave and Nerem, 2004; Cazenave and Llovel, 2010; Spada and Galassi, 2012; Spada et al., 2015; Kopp et al., 2016) was aimed to provide rates of the sea–level variation at century and longer time scales that are dominated by the steric and the mass components. The first, steric, is related with density variations of the sea water consequence of changes in temperature (thermo-steric, Antonov et al., 2005) and in salinity (halo-steric, Jordà and Gomis, 2013). The second, the mass component, is consequence of the waning and waxing of the continental ice sheets (Farrell and Clark, 1976) plus glaciers and ice caps (Dyurgerov and Meier, 2005). Beside these, two other components complete the description of global sea–level change: one is the effect of the GIA and the other accounts for the remaining globally minor components, as the sediment compaction and anthropogenic factors. In this context, if I denote the sea–level change by S, I can write:

$$S_{TOT}(\theta, \lambda, t) = S_{STE} + S_{MASS} + S_{GIA} + S_{OTH}, \qquad (1.1)$$

where the left side of Equation (1.1) is the total sea–level change observed at a certain site of colatitude and longitude (θ, λ) and at a certain epoch t, while on the right side I have the "steric", the "mass", the "GIA" components mentioned above, and S_{OTH} that represents the remaining minor effects. The effect of each component results in what is called a "fingerprint", a map representing the spatial distribution of the corresponding sea–level change. If we consider the impact of the sea–level change at global and regional scale, the discrimination of the

effects originating from the different components in Equation (1.1) becomes even more important to make mitigation actions effective.

Many authors agree on the fact that global mean sea level has been rising during the last century at a rate of about 1–2 mm yr^{-1} (Church et al., 2013) with an acceleration of $\sim$1 myc (Spada et al., 2015, and references therein). Conversely, during the last two decades, the mean rate of sea–level rise was $\sim$3.4 mm yr^{-1} (see Nerem et al., 2010, and updates[2]). Recent works however have evidenced that global assessments loose their significance at the scale of one single basin (Church et al., 2004; Wöppelmann et al., 2014b) marking the existence, at different time scales, of a significant spatial variability. This heterogeneity at basin scale comes along with the ocean circulation effects and other local scale phenomena. A further complexity is given by the availability or lack of reliable data on which models can rely. This is, for example, the case of the Mediterranean Sea (Bonaduce et al., 2016) in which the southern border is not sampled by long-lasting sea–level time series: a strong limitation for any spatial reconstruction. Some other basins, conversely have good sampling along their coasts, e.g. the Adriatic Sea (Galassi and Spada, 2015) and the Baltic Sea (Olivieri and Spada, 2016). In this framework, as remarked in the conclusion by Olivieri and Spada (2016), the size of the basin is a crucial parameter that should be considered together with the density of observations along the coastlines.

Further contribution to the "mass" component of sea–level change is provided by contemporary glacial melting whose major sources are Greenland and Antarctica plus the glaciers and ice caps (Meier, 1984). Since in this case the characteristic time scale of melting is relatively short (from a few decades to one century), the rheological behavior of the Earth can be approximated to that of an elastic body (Slangen et al., 2012). For this reason, the corresponding fingerprints (Figure 3 in Spada, 2017) are not sensitive to mantle viscosity. Further characteristic of the

[2] *http://sealevel.colorado.edu/content/global-mean-sea-level-time-series-seasonal-signals-removed*

contemporary glacial melting is that the current mass rate is not null and consequently the average sea–level change does not vanish at global scale. Remarkably, the contribution of contemporary glacial melting is dominating the current sea–level rise and this would be even more dramatic if the persistent global warming would result in the total melting of Greenland or Antarctica in the near future (Stocker et al., 2013).

Besides the steric and mass effects mentioned above and the GIA effect to which a dedicated section will follow, we must consider some other phenomena whose effect on sea level is small but not negligible. One of the most relevant is related to the mass change in the amount of water stored inland by means of snow, permafrost, lakes and groundwater. This change can be natural, as for the case of increased evaporation in lakes, but also consequence of human activities, as for the case of groundwater extraction or water impoundment in reservoirs (Wada et al., 2012). Climate-related changes consequence of terrestrial water storage show fluctuations at interannual to decadal scale (Nerem et al., 2010) but significant trends during the recent decades were not observed (Church et al., 2013). Conversely, human made changes have been characterized by two activities with opposite effect on the sea–level change. The first, water segregation by means of dam constructions, contributed to a reduction of the sea–level rise at a rate of ~ 0.55 mm yr^{-1} between 1950 and 2000 (Chao et al., 2008). The second, groundwater extraction, adds an opposite effect that globally caused a sea–level rise with rate ~ 0.35 mm yr^{-1} at year 1900 and ~ 0.57 mm yr^{-1} at year 2000 (Wada et al., 2012). The combination of the two neatly resulted in a positive rate of sea–level rise at least at the end of the 20^{th} century.

Another important process that locally affects sea level is tectonics occurring at time scales shorter than those mentioned above. The possible effects of tectonic vertical deformations on locally observed sea-level are difficult to assess, since no global predictive models can be invoked on a secular or multidecadal time scale. However global models

for the earthquake-related component of tectonics have been proposed and these account for the co- and post-seismic deformation. One example is the work by Melini et al. (2004) in which the authors concluded that, globally, earthquakes contribute with ~ 0.1 mm yr^{-1} to long term sea–level change.

1.2 Glacial Isostatic Adjustment

The climatic history of the Earth has been characterized by glacial cycles with large temperature fluctuations that culminated in glaciations, epochs in which large portions of the continents were covered by thick layers of ice while large areas of the previous ocean basins were drained (Farrell, 1972; Farrell and Clark, 1976; Clark et al., 1978). Glaciations culminate in a glacial maximum, and, then an interglacial period starts, In this period, as it occurred since the LGM, temperature rose, ice started melting and the rearrangement of this load from continents to oceans started a consistent change in the shape of the Earth, as well as in its gravitational field.

The relaxation of the solid Earth in response to changes in the mass loading at the surface is a viscoelastic process, which is a combination of instantaneous (elastic) and delayed (viscous) behavior. The initial response to loading or unloading, as for the melting of present ice, can be considered purely elastic, and it results in a direct uplift or depression of the crust (Spada et al., 2013). On timescales of thousands of years, the viscous effects become dominant: this is the GIA process that represents the ongoing response of the viscoelastic Earth to the loading from the ice age.

Presently, the GIA is the process influencing sea–level change that is originated by the mass redistribution still caused by the melting of the late-Pleistocene ice sheets (Farrell and Clark, 1976). The GIA effects on relative sea–level average out to zero across the surface of the oceans in consequence of the presently null melting rate of late-Pleistocene ice

sheets (Spada, 2017), but they are the source of local and regional sea–level variations, both in the formerly glaciated areas at the LGM and in key-areas such as the Mediterranean Sea (Stocchi and Spada, 2009).

The GIA-induced sea–level variability ranges from positive (the rebound of previously ice covered areas) to neatly negative values. Large ice sheets forming during an ice age, locally increase the load, depressing the crust and making the mantle material flow away: the consequence is a downward movement below and an upward movement around the ice mass (the so-called peripheral bulges), as illustrated in Figure 1.1B. During the melting phase, the process acts in the opposite direction, causing an uplift at the former location of the ice sheets and a downward movement of the bulges (Slangen et al., 2012).

Since the work by Peltier and Andrews (1976), who only considered the deglaciation of the Northern hemisphere, different models have been proposed for the history of deglaciation and for its relative sea–level change. These models rely on proxy observations of relative sea–level change as well as on models of the size and thickness of the ice sheets during the last glaciation and on hypotheses about the rheological parameters for the mantle and the lithosphere: viscosity and thickness. Among others, I mention the most commonly used: ICE-3G (Tushingham and Peltier, 1991), ICE-5G (Peltier, 2004), the most recent ICE-6G (Peltier et al., 2015) and those produced at RSES (Australia, Fleming and Lambeck, 2004).

The GIA process induces a relative sea–level change whose spatial distribution for the rate (fingerprint) is computed by solving Equation 1.22 in Galassi (2015). The resulting map is displayed in Figure 1.4. Here we can observe that the largest rates of sea–level change are confined where the ice melting has occurred (negative values) in North America, Fennoscandia and Antartica while conversely, large positive rates are predicted in the surroundings.

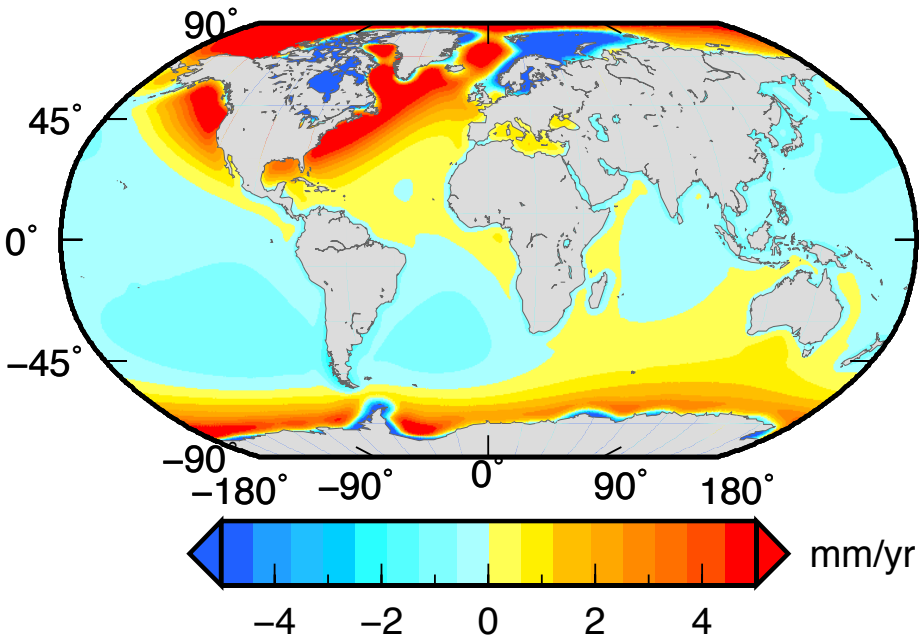

Figure 1.4: *GIA fingerprint for the case of ICE-5G (VM2) (Peltier, 2004). Color code represents the rate of present-day relative sea–level change.*

1.3 Sea–level change models

The study of the sea–level change and its formalism in the geodynamic context roots on the so-called Sea-Level Equation (SLE) that, in its simplest form, reads

$$S = N - U. \tag{1.2}$$

The SLE does not directly involve the sea level, rather it involves its variation, a quantity defined as sea-level change, relative to a previous time t_0 labeling an equilibrium reference state. The SLE results from combining the definition of the variation of relative sea level (S) with N, the sea surface variation in a geocentric reference frame, often referred to as absolute sea-level change (Farrell and Clark, 1976; Spada, 2017). In other words, S is the sea-level variation that would be measured by a meter stick attached to the solid boundary of the Earth while N defines the change in radius of the equipotential sea surface in the absence of winds, tides, and ocean currents (Spada and Stocchi, 2006) and U is vertical displacement of the solid surface of the Earth. It should be remarked

here that the term "Sea Level Equation" is not unique and that different perspectives (e.g. oceanography) led to different representations of the problem. An example is the work of Pinardi et al. (2014).

The three terms in Equation (1.2) are function of (θ, λ, t), i.e., colatitude, longitude and time, respectively. If the concept of SLE was based on the work of Woodward (1888), its theory and solution was discussed by different authors and a comprehensive review can be found in Spada (2017).

For the purpose of this work, I define:

$$H = H(\theta, \lambda, t) \tag{1.3}$$

as the sea level in a certain position (θ, λ) and at a certain epoch t. H differs from S and from N and it will be used to ease the comprehension of the problem, as it will become apparent in the following.

Equation (1.3) would need a reference frame that traditionally, for a TG, is local and referred to the ground from which the measurements of the sea level was taken, typically the pier of the harbor. This type of measurements and the corresponding data have been historically referred as "relative sea–level data" (hereinafter H_r). The subscription r also marks a distinction from those considered "absolute" (H_a) that, for example, result from the satellite altimetry. In the formalism of the SLE (Equation 1.2), $\Delta H_r = S$ and $\Delta H_a = N$.

Regardless the reference frame, it would be then natural to describe sea level change, and consequently its rate of rise, as the sea–level difference at two different epochs and as the difference quotient respectively. From Equation (1.3) these result in:

$$\begin{aligned} \Delta H(t_0, t_1) &= H(t_1) - H(t_0) \\ R(t_0, t_1) &= \frac{H(t_1) - H(t_0)}{t_1 - t_0}, \end{aligned} \tag{1.4}$$

where R represents the mean rate of the sea–level change over the time span (t_0, t_1) and where coordinates (θ, λ) have been omitted for simplicity. The above equations are valid either in the reference frame of the

mass center of the Earth or in a local one. In spite of the above definition, common practice led to a different approach for the routine determination of the rate of sea–level rise. This mainly results from the necessity of a simple analysis of complex data often contaminated with periodic oscillations in a broad range of frequencies. Given a time series $H(t_i)$, the rate of sea level rise ρ is commonly defined as the slope of the best-fitting first-order polynomial resulting from the solution of the Ordinary Least Square (OLS) problem:

$$H(t_i) = \rho^* \cdot t_i + h_0 + \epsilon_i, \quad t_i \in (t_a, t_b), \tag{1.5}$$

where ρ^* represents the slope of the preferred model that minimizes the residual ϵ. By definition, the result of an OLS problem is valid only within the time span covered by the data, in this case (t_a, t_b). From Equation (1.5), I retrieve the preferred model, H^*, defined as:

$$H^*(t_i) = \rho^* \cdot t_i + h_0. \tag{1.6}$$

To describe the caveats connected with using the best-fitting first order polynomial for estimating the rate corresponding to a certain sea–level time series, I applied it to the global mean sea–level since the LGM provided in Figure 1.2. The best-fitting linear model resulting from an OLS is plotted over the time series in Figure 1.5. The predicted rate ρ^* is ~ 7.8 mm yr^{-1}, 30% larger than the average rate resulting from the discrete derivative of the time series (see above). Most importantly, the total sea–level change since the LGM is $\sim$130 m but, if I use the rate ρ^*, this results in $\sim$165 m.

The validity of this approach was not a major topic in the recent literature dedicated to the assessment of sea level, however the strong motivation in support of it was the presence, in sea–level data, of short period patterns (tides) that could expose alternative approaches to the risk of biases or large associated error bars. Conversely, at time scales exceeding the dominant short period signals, Equation (1.5) can guarantee the independence of the results from to the chosen time span (details in Section

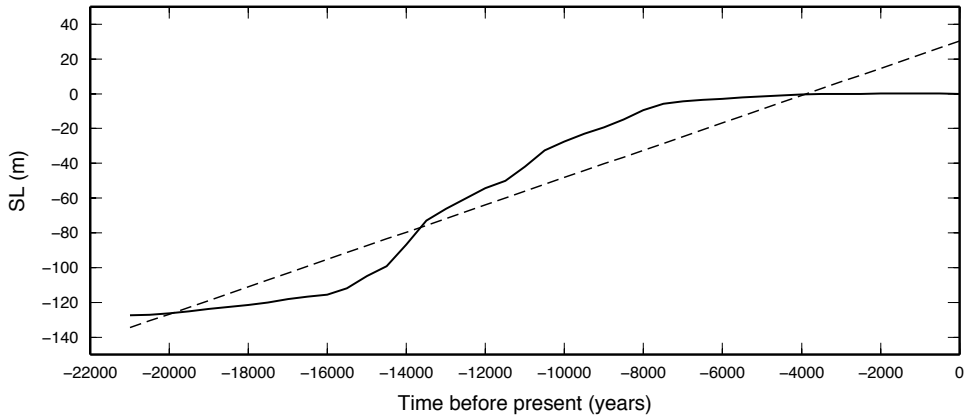

Figure 1.5: *Sea–level change since the LGM (thick line) superimposed to its best fitting linear model (dashed line) resulting from OLS.*

2.2). This could be considered an *a-posteriori* proof of the stability of the resulting rate of sea–level rise. The fact that $H^* \neq H$ remarks the difference between the true data and the model where $\epsilon_i = H(t_i) - H^*(t_i)$ represents the inaccuracy of the models over time and its variance σ_ϵ^2 its average value. The analysis of σ_ϵ^2 and of the other parameters resulting from the OLS solution provides information about the quality of the model, and of the data as for homoscedasticity and autocorrelation. The two topics will be discussed in Section 2.2.

In accordance with the above definition, Douglas (1992) introduced the concept of "apparent acceleration" (α) defined as twice the quadratic term of the best-fitting parabola (second order polynomial):

$$H(t_i) = \frac{1}{2}\alpha \cdot t_i^2 + \beta \cdot t_i + h_0 + \epsilon_i, \tag{1.7}$$

where again ϵ_i represents the error of the model. The name "apparent acceleration" marks the difference with respect to the true acceleration that is, indeed, the function of time $\ddot{H}$. It should be remarked at this stage that, given the complexity of sea level and given the above definitions for the rate and for the acceleration, any assessment for ρ or for α should be considered valid only for the time span of the input data set and at the location (θ, λ) where data were collected.

This observation rises the question: how can we extend in space and time the validity of results for any determined rate or acceleration? The question has not a trivial answer and it is strongly linked with the concept of "global mean sea level" for the epoch that preceded the "altimetry era" (1993 to present). This problem will be one of the main topics for the next chapters of this thesis with focus on sea–level reconstructions, i.e. those time series that, under some hypotheses, are presumed to represent the global sea–level change over time[3].

It should be also remarked, in the context of determining the preferred model by means of a best fitting relation, that the reduction of the variance can not be the unique parameter to be considered since it is implicitly reduces when further degrees of freedom are added. This is the case when parabolas are compared to linear models. Part of Section 2.2 will be dedicated to the discussion of this topic.

A different approach for the search of a possible acceleration in time series is to split the time span into two branches and then compare the resulting rates (e.g. Ray and Douglas, 2011). In this case, the hypothesis of constant acceleration (case of best-fitting parabola) is dropped and replaced by the possibility of a sudden but short lived one. Examples could be co- and post-seismic deformation (Olivieri et al., 2013), the industrial revolution that boosted the global warming and large volcanic eruptions that, by injecting aerosols in the stratosphere, reduced the amount of sunlight on the Earth's surface (Rampino and Self, 1984; Fasullo et al., 2016). To account for the above short-lived acceleration hypothesis, Equation (1.5) will be rewritten as:

$$H^*(t) = \begin{cases} \rho_1^* \cdot t + h_1, & \text{for } t > t_{cp} \\ \rho_2^* \cdot t + h_2, & \text{for } t > t_{cp}, \end{cases} \tag{1.8}$$

where cp stands for Change Point (CP). Equation (1.8), represents the case of a bi-linear model, and its definition requires two assignments:

[3] http://www.psmsl.org/products/reconstructions/ and references therein

the continuity of sea level at t_{cp} and the epoch at which the CP occurred. In some cases, the epoch of t_{cp} is known as for earthquakes, or it can be guessed by visually inspecting data. Conversely, when the epoch of the CP is unknown, it would be more appropriate, and statistically meaningful, to consider it as a variable. The problem, that includes one further degree of freedom with respect to Equation (1.8), was solved by Chow (1960) for the case of what Econometrics calls structural changes in time series. The Chow (1960) statistics allows for the detection of a CP whose timing is *a priori* unknown. In this testing procedure, the time series is split into two sub-periods, and for each of them a linear regression is performed. The misfit obtained for such bi-linear model is then compared, by means of a Fisher F-test (e.g. Winer, 1962), with that obtained by a linear model for the whole time series. In Section 2.4, we will implement the recipe by Hansen (2001) who, following an idea by Quandt (1960), described a methodology that overcomes the limitations caused by the unknown break date.

1.4 Sea–level observations

People living in coastal areas have been surveying tides and tidal currents since many centuries. This observation has been useful for scheduling the sailing of ships from and to the harbors. In the second half of 1800, the subject of ocean tides, attracted the interest of many scientists. Among the others, I mention Sir William Thomson (Lord Kelvin) who explored the harmonic nature of tides, as well as Laplace, and Sir George B. Airy[4]. At that epoch, the measurement and the archival of the daily sea level records became a routine practice. Historically, sea level has been measured at the pier of harbors by tide gauges, i.e. graduated bars (Figure 1.6) that were later replaced by mechanical or optical instruments. The main purpose was to monitor tides and to help the navigation of boats and ships. Meanwhile, the study of the harmonic components of

[4] https://www.tidesandcurrents.noaa.gov/predhist.html

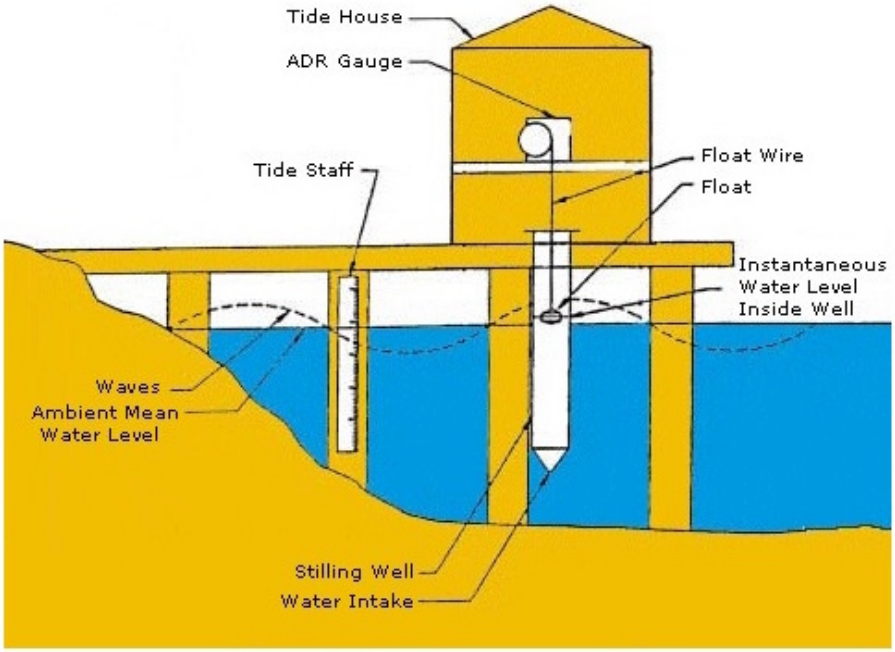

Figure 1.6: *Sketch of an ancient shelter for tide observation by means of a float and an analog data recorder. Reproduced under permission from NOAA website http://oceanservice.noaa.gov/education/kits/tides/media/supp_tide10b.html.*

tides led to very accurate models and single ships could just read the tabulated tides at specific harbors worldwide in advance. In the second half of last century, navigation-related interest for tides decreased although the tide observation continued in most of the harbors for different reasons. The first was to detect anomalous phenomena like exceptional sea–level heights in consequence of surge storms or tsunamis, and the second was the mere scientific purpose. All these observations, whose first one dates back to the early decades of 1700, nowadays constitute a unique data set of relative sea level heights around the world that covers, with different spatial distribution over the decades, 300 years (details in Section 2.1). Some recent projects remarked the importance of tide gauge data. Some have been focused on the reconstruction, digitalization and distribution of data for sites that where previously unavailable. These efforts contribute to a more complete coverage of the coastal regions. Among the others I mention the work about Mazara del Vallo

(Italy) and the one about Marseille (France) by Olivieri et al. (2013) and Wöppelmann et al. (2014a), respectively.

As introduced above, the relative sea level $H_r(\theta, \lambda, t)$ is the sea level observed in the local reference frame of the pier where the tide gauge is attached or of the ground from which paleo sea–level proxies are observed. From the above consideration I can write:

$$H_r(\theta, \lambda, t) = H(\theta, \lambda, t) + \int_{t_0}^{t} \dot{H}_{ground}(\theta, \lambda, t')dt', \tag{1.9}$$

where $\dot{H}_{ground}$ is meant to account for total ground deformation whose origin can be local, as for the case of the compaction of sediments, or global as for the deformation consequence of GIA. An important limitation of using tide gauges data is that these are contaminated by vertical land movement that, in the absence of independent observations, cannot be removed. As shown by some sites, this is not just one of the errors associated to the sea–level measurements but a dominant component of the signal. An example is the case of Venezia (North Adriatic coast, Italy), at which the long term rate of sea–level rise is larger than the one observed at Trieste (Tsimplis et al., 2012) although the variability of the Adriatic sea is dominated by basin-scale components (Galassi and Spada, 2015). In this case, the discrepancy is a consequence of the large subsidence occurring in Venezia (Tsimplis et al., 2012) but in other sites this could be a consequence of earthquakes (Messina 1908, Olivieri et al., 2013) or volcanic inflation (Miyakejima eruption, Nerem and Mitchum, 2002). This observation clearly marks the distinction between local models, where the ground deformation can be important, and global ones in which, conversely, this introduces a bias that requires to be modeled and corrected.

The global sea–level change is a central research topic, mainly because it is a key indicator for the ongoing climate change. However, a definition for the Global Mean Sea Level (GMSL), for its rate and for its acceleration was never formally introduced. On the contrary, most of the works published so far, the definition adopted reflects what can be

calculated from data[5]. If I define the "mean sea level" as the mean height of the sea over a given domain, in the formalism of Equation (1.3), I can define global mean sea level at a certain epoch t by the integral mean value:

$$\overline{H}(t) = \frac{1}{A_0} \int_{A_0} H(\theta, \lambda, t) dA, \tag{1.10}$$

where A_0 represents the area of the oceans and $dA = a^2 \sin\theta d\theta d\lambda$ the area element on the sphere. The limit of this definition stems from the fact that sea-level observations are limited in space at TG sites.

Since the early 90s, a breakthrough methodology for the observation of the ocean provided a new, almost global, perspective to scientists. This is the satellite altimetry that, by means of radar altimeters mounted on satellites (Figure 1.7), provided for the first time a simultaneous and comprehensive picture of the oceans topography. Different scientific projects (Le Traon and Morrow, 2001), aimed at providing global pictures of the sea level launched a group of radar altimeters on board on a constellation of satellites (Fu et al., 1994). The production of reliable sea–level images started at the end of 1992 and nowadays the longest time series cover almost a quarter of a century. If TGs provide measurement for the relative sea level, satellite altimetry provides absolute measurements of the sea–level height. This innovative approach changed the perspective for the study of the global sea level. Reconstructions from sparse and almost coastal observations have been replaced with direct observations for the entire surface of the oceans. For the purpose of global assessment of sea–level change, this new methodology makes available global maps (an example is shown in Figure 1.8) of the sea–level change over time, and a time history representative for the global mean sea level (Figure 1.9a) resulting from Equation (1.10). A further important outcome of this approach is the possibility to establish the spatial sea–level variability (Figure 1.8 and 1.9b), as it will be discussed in

[5]http://sealevel.colorado.edu/content/what-definition-global-mean-sea-level-gmsl-and-its-rate

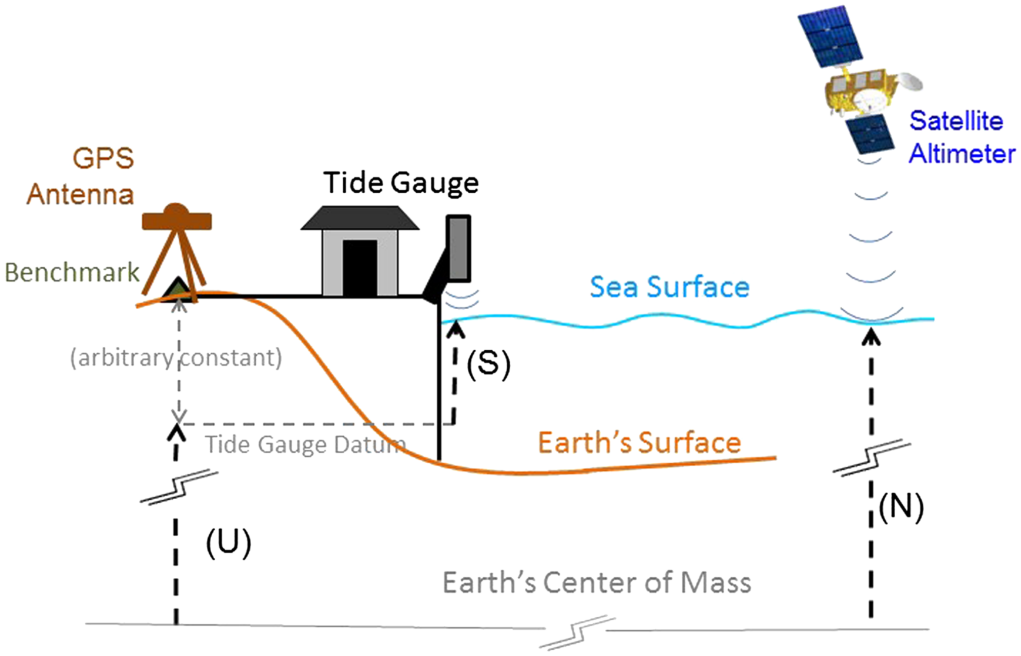

Figure 1.7: *Sketch showing basic differences in the observation of relative and absolute sea–level change. S, N, and U are the quantities described by Equation (1.2). Reproduced with permission from Wöppelmann and Marcos (2016).*

Chapter 3.

If global mean sea level results from averaging the observation over the entire surface of the ocean (satellite altimetry era), this would not be possible for the antecedent epoch when a limited number of sparse observations was available. The problem, which will be discussed in detail in Chapter 2, implies that Equation (1.10) should be downgraded from a integral mean over the entire surface to a summation (stacking) over the available data:

$$\overline{H}'(t) = \frac{1}{M} \sum_{k=1}^{M} w_k H_k(t) - c_k(t), \tag{1.11}$$

where the "prime" denotes that $\overline{H}'$ can differ for the $\overline{H}$ defined in Equation (1.10), M is the number of available observations, $H_k(t)$ is the sea level observed at the specific site k, w_k is the weight assigned to site k and c_k is the correction applied to site k (e.g. GIA, ground deformation or atmospheric pressure). Equation (1.11) is derived from seismology

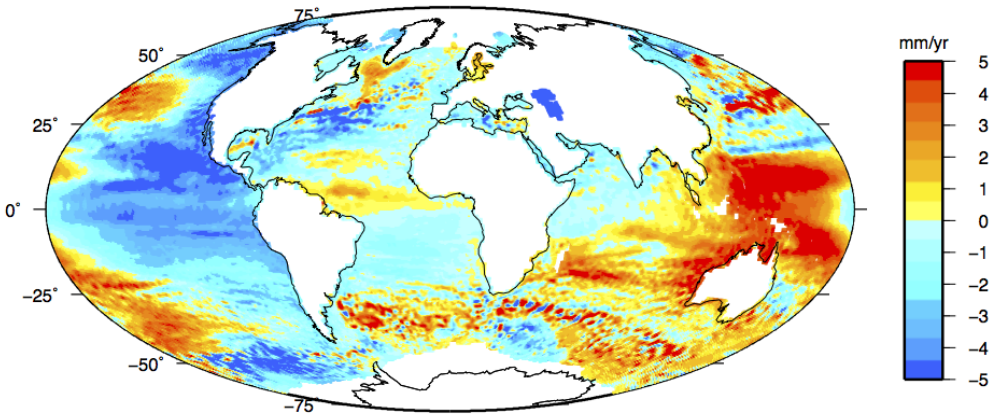

Figure 1.8: *Distribution of the rate of sea–level rise as resulting from the CSIRO model. For each pixel of the grid, the color code represents the rate resulting from the best-fitting linear regression over the time span (1993–2012).*

that commonly stacks seismograms to enhance the signal and to remove the undesired incoherent noise from data (Gilbert and Dziewonski, 1975; Olivieri et al., 2013). The hypotheses undergoing the stacking of TGs time series, as well as any type of signal, is that the coherent signal is the combination of thermosteric and mass-change effects, while the noise are ocean circulation, tides and local ground effects (Olivieri and Spada, 2013). This assumption, strong and for some cases unverifiable, is the ”dogma” that sustains, in different flavors, all the sea–level reconstructions from tide gauges that do not use sophisticated approaches: a single observation of sea level is the combination of the global mean sea level plus local effects. If local effects are not coherent, they cancel out while the coherent signal emerges (see Section 2.4 for details).

A completely different approach to the sea–level reconstruction before the altimetry era is based on the Reduced Space Optimal Interpolation (RSOI) technique, first introduced by Kaplan et al. (1997) to reconstruct atmospheric pressure from data. For the case of sea level (Church et al., 2004), altimetry data are decomposed in a set of Empirical Orthogonal Functions (EOFs) that allow to study quantitatively the sea–level variability at different spatial wavelengths (Navarra and Si-

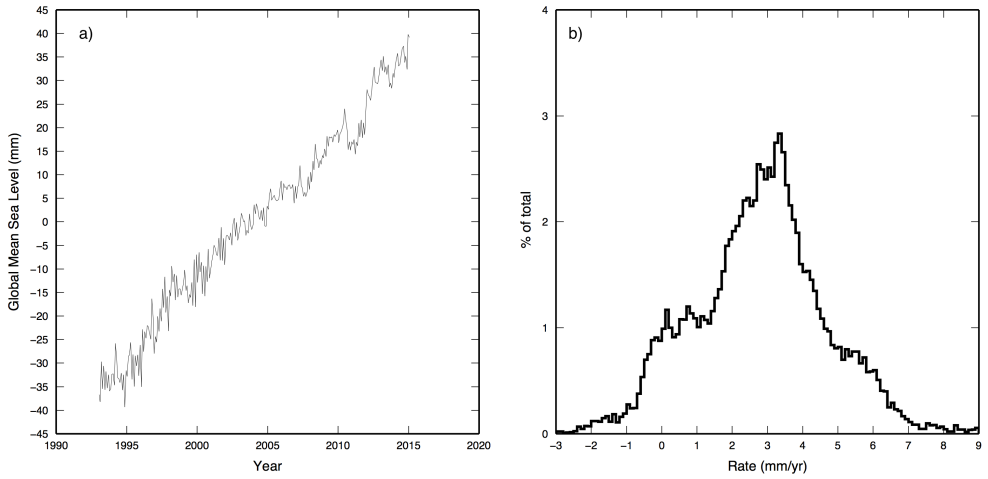

Figure 1.9: *Time history of the global mean sea level as computed from CSIRO altimetry data.*

moncini, 2010). These, or a subset of them, are then fitted in a weighted least square sense, to a set of tide-gauge records to reconstruct the spatial variability of the past sea level. Equation (1.10) can be than applied to a longer time span by replacing $H(\theta, \lambda, t)$, the true sea level height, with the resulting $H_{rsoi}(\theta, \lambda, t)$:

$$\overline{H}'(t) = \frac{1}{A} \begin{cases} \int_A H(\theta, \lambda, t) dA & \text{for } t \in [T_{\text{ALT}}] \\ \int_A H_{RSOI}(\theta, \lambda, t) dA & \text{for } t \in [T_{\text{RSOI}}], \end{cases} \tag{1.12}$$

where T_{ALT} is the time span covered by altimetry, T_{RSOI} is the time span during which sea–level height H_{RSOI} is reconstructed from TGs and A is the surface of the oceans sampled by satellite altimetry. The strong assumption that undergoes this approach is that the spatial variability of sea level for $t \in [T_{ALT}]$ is representative also for the time $t \in [T_{RSOI}]$.

The need of improving the quality of the data and their usability for the purpose of GMSL assessments stimulated some important works in the last decade (e.g. Wöppelmann et al., 2007; Santamaría-Gómez et al., 2012), aimed at providing a simultaneous correction for ground deformation occurring at the site where the tide gauge is deployed. This was

possible by co-locating Global Positioning System (GPS) antennas in combination with TGs. The main goal of these work is to solve the trade off between "relative" and "absolute" sea level or, in other words, to provide the true instantaneous correction for the effect of vertical land movement on sea–level observations and then to measure, simultaneously, S, N and U.

A third "family" of sea–level observations that span from decades to millennia is composed of proxy data. These consist of indirect measurements of the paleo elevation of sea level relative to the solid Earth. Mainly these consist of pale-shorelines (Peltier, 1998, 1994), but also salt marshes (Barlow et al., 2013; Kopp et al., 2016) buildings (e.g. Florido et al., 2011), or pictures from the past (e.g. Camuffo et al., 2005). An example for the latter case is provided in Figure 1.10 in which we display the case study dedicated to the harbor of Cesenatico (Delvecchio, 2016), a small town facing the Italian side of the North Adriatic Sea. By means of two repeated pictures of the same location it was possible to determine the difference between the height of the sea over a 62 years time span (1943–2015).

Furthermore, I consider another class of data for the study of sea level, that consists of "ocean reanalysis". Ocean reanalysis is a method of combining observations of the ocean parameters with a general ocean model (typically a computational model) driven by historical estimates of surface winds, heat, and freshwater. By way of a data assimilation algorithms it reconstructs the changes in the state of the ocean (Sivareddy, 2015). The use of ocean reanalysis derives from the fact that historical observations are sparse and insufficient for depicting the history of the ocean and its circulation. By utilizing data assimilation techniques in combination with advanced computational models of the global ocean, researchers can interpolate the historical observations to all points in the ocean. This process is analog to the construction of atmospheric reanalyses and is closely related to ocean state estimation. Ocean reanalysis are

Figure 1.10: *The sea–level change at the harbor of Cesenatico recognizable by comparing the pictures of the same bridge photographed in 2015 (top) and in 1943 (bottom). The size of the buildings (red segments) was used to determine the sea level at 1943.*

not data, in the sense that these are not the result of a direct observation, but they are the result of the processing of a set of data into a model. However, these provide a unique opportunity to fill the gap for the ocean variability description during the epoch that preceded altimetry (for the case of sea level height). It should be remarked here that presently a large set of ocean reanalyses exists, with different spatial resolution, temporal coverage and different capability of reproducing short to long term climate related phenomena[6]. I do not enter into the details, since these go beyond the purpose of this work but, in Section 3.2, I will discuss the

[6]A comprehensive list of the available ocean reanalyses can be found at *http://icdc.cen.uni-hamburg.de/projekte/easy-init/easy-init-ocean.html* with references therein.

reliability and realisticness of one of them.

1.5 The rate of sea–level rise

Satellite altimetry provides a clear picture of sea–level change over time for the last 24 years with good accuracy but some limitations in the vicinity of the coastlines and at high latitudes (Passaro et al., 2014). From it, different authors (see Chambers et al., 2016, and references therein) coherently reported that during the last 24 years sea level has been rising at a rate of (3.4 ± 0.3) mm yr^{-1}. This rate, which represents the average over the surface of the oceans sampled by altimetry, results from the linear regression of the GMSL time series in Figure 1.9a or similar ones obtained by different agencies[7].

As mentioned above, during the pre-satellite era, a different approach was necessary since the only available data were the sparse TG observations at coastlines. The problem, i.e. the determination of the past rate of GMSL, has been the subject of extensive research since the seminal work of Gutenberg (1941) who first estimated the global sea-level rise and its uncertainty from instrumental records (1.1 ± 0.8 mm yr^{-1} for the period 1907–1937). There is now a general consensus about the rate for GMSL during the 20^{th} century, which realistically could be in the range 1–2 mm yr^{-1}. A summary of the existing assessments for the global rate was recently published by Spada et al. (2015) where time span and GIA correction are also listed. All the works considered in Spada et al. (2015) rely on TG time series, selected and processed in different manners by the different authors. The aim is always that of representing the global nature of the entire oceans from sparse observations confined at coasts. The topic will be discussed extensively in Chapter 2 with focus on how TG data can and cannot be processed to reconstruct the sea level, and in Chapter 3 with a focus on the capability of coastal data to cap-

[7]Updated estimates for the rate of GMSL as computed by different agencies are listed at *http://sealevel.colorado.edu.*

ture the global sea level. I mention here the work by Thompson et al. (2016), in which the authors determine the impact of the TG distribution by following an innovative approach to the problem of long-term GMSL assessment. In their conclusions, the authors could verify that TGs are poorly located to capture the global nature of sea level at century scale. This observation will be considered and discussed in Section 3.9.

1.6 Sea–level acceleration

The Intergovernmental Panel on Climate Change, Fifth Assessment Report (IPCC AR5) report concludes that, at global scale, a positive sea–level acceleration exists although a realistic range is not given (Stocker et al., 2013). The main reason appears to be the contamination of multi-decadal oscillations in the TG time series (Chambers et al., 2012) and the subsequent dependency of the acceleration to the selected time span.

In his seminal work, Douglas (1992) estimated the Global Mean Sea Level Acceleration (GMSLA) by averaging the sea–level accelerations obtained from individual records of globally distributed TGs. His approach only provided weak evidence in support to a positive acceleration, even for the longest period considered (namely $\alpha \pm \Delta\alpha = 0.1 \pm 0.8$ myc during 1850–1991). This contrasted with the significant acceleration expected to accompany greenhouse warming. The negative result of Douglas (1992) confirmed that of Woodworth (1990), who limited his attention to European records.

More recent studies, either based on the "virtual station" method (Jevrejeva et al., 2006, 2008) or on a sea–level reconstruction of long TG records (Church and White, 2006, 2011), point to the existence of an acceleration, but propose quantitatively contrasting results. Based on a 300 years long time series (1700–2002) obtained by combining short and long TG records, Jevrejeva et al. (2008) reported an acceleration $\alpha = \sim 1$ myc (the uncertainty was not quantified), which apparently started at the end of the 18^{th} century. The EOF approach by Church and White (2006),

combined with polynomial regression, suggested $\alpha = (1.3 \pm 0.6)$ myc in the period 1870–2001 that reduces to $\alpha = (0.8 \pm 0.8)$ myc when the 20^{th} century only is considered. In their follow-up paper, Church and White (2011), proposed an acceleration $\alpha = (0.9 \pm 0.3)$ myc for the time period 1880–2009. The spread of proposed estimates for α based on TG records (summarized in Figure S1 of Spada et al., 2015) is significant. The large energy of decadal sea–level fluctuations (Jevrejeva et al., 2006; Chambers et al., 2012), the poor geographical coverage of TGs and the limited number of TGs facing the open seas (hence potentially less affected by coastal processes), are causes of uncertainty and of misinterpretation (see also the discussion in Douglas, 1992; Sturges and Hong, 2001). As recently evidenced by Gehrels and Woodworth (2013) and by a number of previous studies, the proposed value is strongly sensitive to the time span of the instrumental record considered and to additional selection criteria based on the quality of the data set. Spurious effects from gappy time series, contaminating tectonic (e.g. Larsen et al., 2003; Olivieri et al., 2013) or anthropic factors (Carbognin et al., 2010) may act to further complicate the estimate of the acceleration.

The constant acceleration model for sea–level rise is appealingly simple and constitutes the most obvious generalization of linear models ($\alpha = 0$) extensively employed to estimate ρ since the early stages of sea–level rise determination (Gutenberg, 1941). Inspection of sea–level compilations, however, also reveal short-lived accelerations and abrupt steepness variations (Gehrels and Woodworth, 2013). These can be modeled, to a first approximation, as CPs separating periods of constant rate and/or of constant acceleration. As pointed by Church and White (2006), a bi-linear model incorporating an abrupt slope change at year ~ 1930, unexpectedly during a period of little volcanic activity, can indeed be invoked as a possible alternative to a constant acceleration model for the time period 1870–2001. Inflections in global and regional compilations of instrumental records at year ~ 1930 have also been proposed

by Jevrejeva et al. (2008), Woodworth et al. (2009) and Church and White (2011). Based on proxy and instrumental observations from seven sites, Gehrels and Woodworth (2013) have recently proposed that year 1925 ± 20 could mark the date when sea–level rise started to exceed the long-term Holocene background rate. Inflections or CPs occurring during the 19^{th} century could be more difficult to ascertain, especially in view of the limited amount and sparsity of instrumental data available for that epoch. However, a major acceleration episode has been evidenced by Jevrejeva et al. (2006) during 1850–1870, although its significance was disputed.

In consideration of the evidence, it is realistic that the sea level has been rising at an average rate between 1 and 2 mm yr^{-1} during the last century, it remains difficult to provide a figure for the acceleration. Figure S1 in Spada et al. (2015) suggests that it could be restricted between 0 (no acceleration) and 2 myc over the last century. Evidence in support to the existence of an acceleration at global scale could be also considered the fact that during the altimetry era the sea level is rising at a rate of about (3.4 ± 0.3) mm yr^{-1}(Nerem et al., 2010), as it results from satellite altimetry, almost the double of what observed, on average, during the last century.

1.7 Open questions and goals

This work is focused on the epoch covered by TG data, namely from 1805 to present, and on the capability of TGs to provide a realistic assessment for the global mean sea level in terms of acceleration. In particular, some of the analysis will be restricted to the last century (1900–2000) to ease the comparison with other results and to exploit the larger data set covering that epoch. The main goal of this work was to prove the existence of not null long-term global sea–level acceleration and to confirm or deny if TGs are capable to provide robust proofs for it.

Chapter 2 is devoted to the data availability and to the methodolo-

gies that can and cannot be used in order to establish the long-term sea–level change and on how periodic contaminations can perturb or bias it. A special attention is dedicated to the influential work by Chambers et al. (2012) entitled *"Is there a 60-year oscillation in global mean sea level?"* since it had a significant impact on the recent IPCC AR5 report. Here, a different approach to the problem posed by the authors leads to different results that could influence the validity of the current GMSL acceleration estimates. In the same Chapter, results from the work by Olivieri and Spada (2013) are presented to provide the proper framework for the open issues discussed in Chapter 3. These are: the extent to which coastal sea level is representative of GMSL, and the extent to which the limited sampling of TG records allows for robust estimates of the global sea–level rate and acceleration. The findings, observations and results are gathered in Chapter 4 where a tentative approach to a new model is drawn. The final conclusions and open issues are then summarized in Chapter 5.

CHAPTER 2

Tide gauges: data and analysis

2.1 Tide gauges: history and observations

Systematic observation of sea level and of its changes started in the 17^{th} century with the function of monitoring, and predicting, the tide in harbors in order to help the entrance and exit of commercial ships. As introduced in Section 1.4, sea–level measurements were done, and still are, by means of Tide Gauges (TGs), graduated staffs or floats that determine the height of the sea with respect to the pier to which these are fixed (Figure 1.6). Since 1933, these locally recorded sea–level heights have been gathered and harmonized to form the archive currently kept, maintained and validated by Permanent Service for Mean Sea Level (PSMSL)[1]. In its current version, this archive counts more than $600,000$ quality-checked observations since 1807 of monthly sea–level heights from about 1450 sites (PSMSL, 2015; Holgate et al., 2013) spread all along the world coastlines (Figure 2.1). Data are available in their raw form (called "met-

[1] http://www.psmsl.org

ric") as provided by the contributors as well as in a quality controlled and validated version that is labelled Revised Local Reference (RLR)[2]. As the label tells, these are also put in a proper reference frame to make data comparable with neighboring sites. Since PSMSL discourages the use of "metric" data because of their potential inaccuracy, in the following I will focus only on RLR data from RLR TG sites.

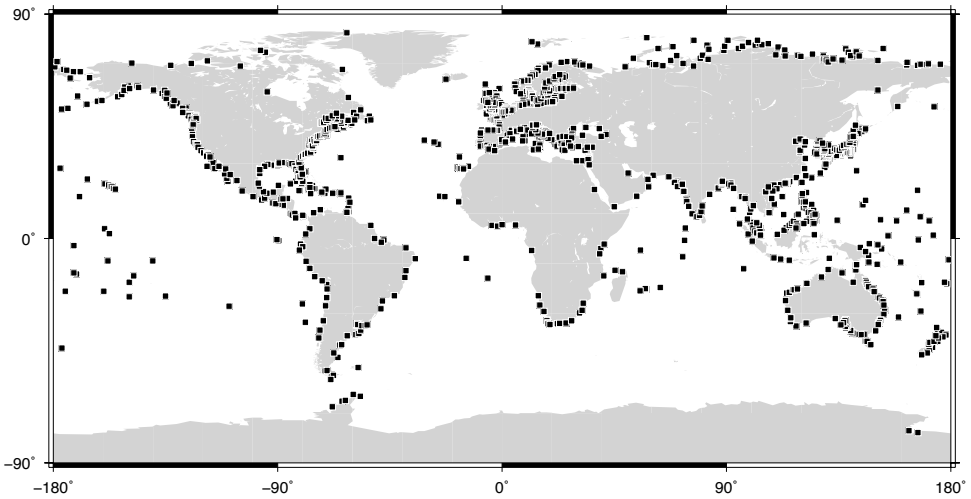

Figure 2.1: *Distribution of the 1466 sites for which validated RLR sea–level data are archived at PSMSL as of June 13, 2016.*

The main weaknesses of TG data sets are the uneven distribution of the sites along the coastlines, recognizable in Figure 2.1, and the heterogeneous time spans covered by the different sites. The latter, worsened by the different levels of completeness, leads to a strong time dependency of the number of available RLR observations. Globally, RLR observations range between few observations in the early years and several hundreds some years ago (Figure 2.2). The peculiar time distribution for the last decades is motivated by the latency existing between the data collection by local authorities and the dissemination by PSMSL. What cannot be appreciated from Figure 2.2, but it will be discussed in Section 2.4, is the fact that the limited number of available sites in the early

[2]see http://www.psmsl.org/data/obtaing/psmsl.hel for RLR description.

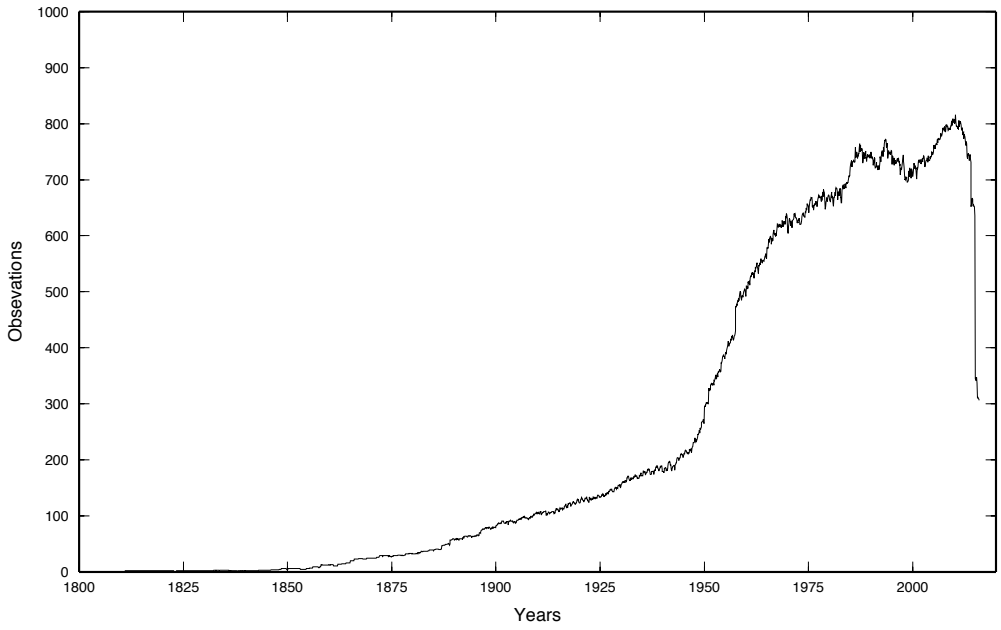

Figure 2.2: *Number of monthly RLR sea–level observations archived at PSMSL as a function of time.*

decades clusters in northern Europe and North America, enhancing TGs uneven spatial distribution.

An example of TG time series is given in Figure 2.3a in which the sea level observed at San Francisco (USA, time span: 1854–2016, duration 161 year, completeness 100%) is displayed in terms of monthly mean heights. From this figure, we can recognize a long-term rise and the oscillations with different frequencies in consequence of the different phenomena that contribute to the rise and fluctuation of the sea. This observation is confirmed by the spectrum (Figure 2.3b) computed over the same time series by means of a Discrete Fourier Transform (DFT) implemented in SAC (Goldstein et al., 2003). It is apparent from Figure 2.3 that the spectrum is dominated by two periodicities at 1 and 0.5 years, which mark the annual and the semi-annual tide, respectively.

We can also notice the presence of energy at all frequencies from months to half the length of the time series ($\sim$81 years). Longer oscillations (in excess to half the length of the time series) and shorter ones (less than the twice the sampling rate of the time series) are out of the

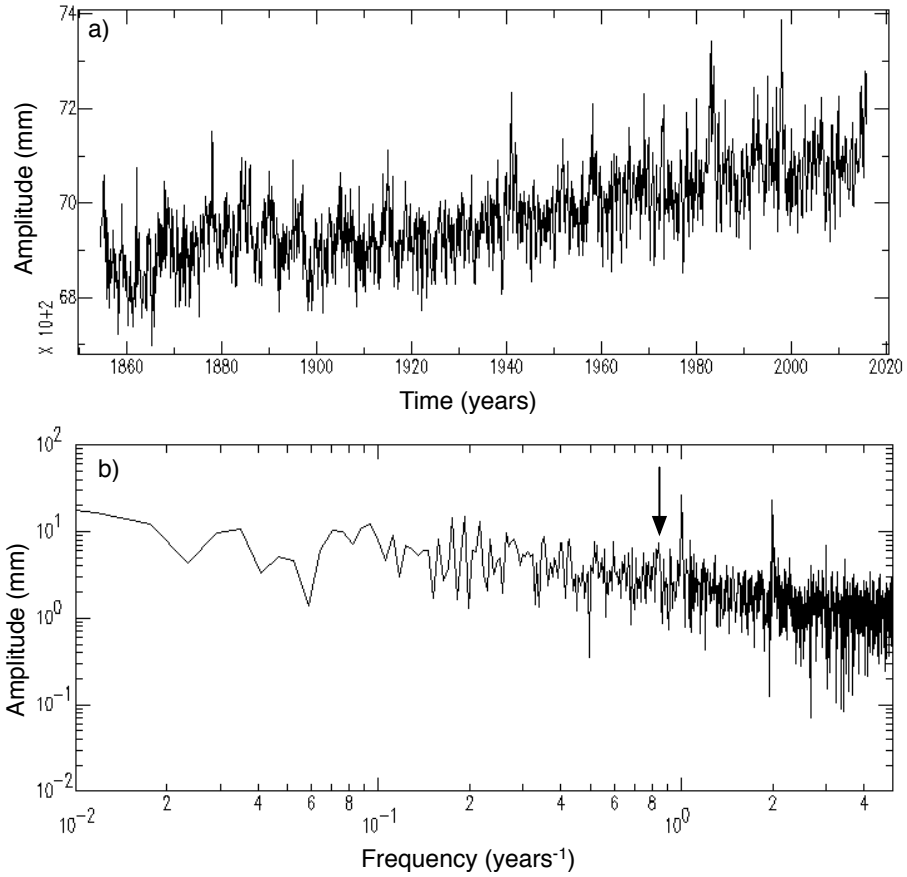

Figure 2.3: *a): monthly mean sea level as recorded at the San Francisco (USA) tide gauge. The arbitrary offset corresponds to the reference frame in which RLR data are put by PSMSL. b): frequency content for the San Francisco (USA) sea–level time series, fromDFT analysis. The black arrow marks the weak signal in correspondence of the expected pole tide frequency.*

frequency range for the DFT. When considering long-lasting time series and possible contaminating oscillations, signals not directly related to the ocean should also be considered. Here I refer to the seminal work by Trupin and Wahr (1990), in which TG time series have been explored in search for two of the prominent signals, the Chandler wobble (Smith and Dahlen, 1981) that reflects in the 14 months pole tide and the 18.6 year lunar tide (Lambeck and Nakiboglu, 1983). As the authors concluded, these signals are difficult to be caught in data. However weak evidence for the pole tide can be recognized in the spectrum for some of the TG time series. An example is again the site of San Francisco (USA), whose

spectrum (Figure 2.3b) shows some energy at ~ 0.85 yr^{-1} (14 months).

These observations: energy at all frequencies in time series spectra and unavailable models to predict multidecadal oscillations, should be taken into consideration in the following while discussing long term results. In particular, this is pertinent to the search for the apparent acceleration and it can lead to biases or misinterpretation of the results. A dedicated focus on this issue can be found in Section 2.2. It is important to remark, at this stage, how DFT is defined and the physical meaning of the displayed spectrum. When decomposing a function by means of a Fourier transform, it is assumed that this can be represented by a series of sines and cosines, i.e. by functions having constant frequency and amplitude over time. If, from a mathematical point of view, this always applies, the physics of the problem suggests that this approach is too restrictive since the origin of such fluctuations has not been completely discerned.

In the recent past, more sophisticated approaches to the extrapolation of the periodic signals contained in time series have been suggested in replacement of standard DFT. Here I focus on the Empirical Mode Decomposition (EMD) that, since its introduction by Huang et al. (1998b), has found a large number of applications in different fields of physics and geophysics (Huang and Shen, 2005; Huang and Wu, 2008). EMD is an adaptive method with which any arbitrary data set can be decomposed into a finite and often small number of oscillatory Intrinsic Mode Functions (IMFs) with increasing instantaneous frequency, plus a residual RES which can be a monotonic or a single-extremum function (Huang et al., 1998b). Details on the method and on its application will be given in Section 2.3. An example of the application of the EMD analysis to TG data is given by Figure 2.4 for the case of San Francisco (USA). The frequency content for each IMF was gathered and displayed in Figure 2.5.

To mention some of the benefits of using EMD in sea–level analysis from TG observations, I remark that IMFs are mutually orthogonal func-

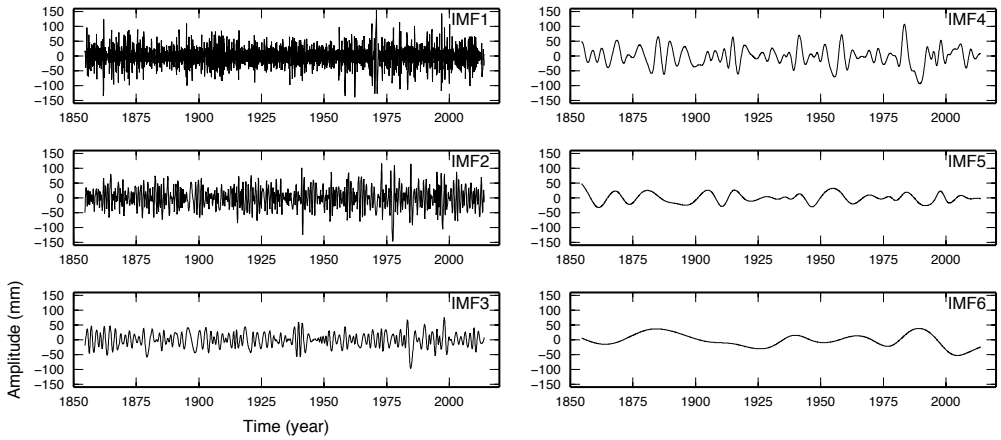

Figure 2.4: *IMFs time series resulting from the EMD analysis for the San Francisco (USA) tide gauge.*

tions and their nature, i.e. the variable period and amplitude, can better reproduce those non stationary and non linear phenomena characterizing the sea–level variability (Galassi and Spada, 2015). The EMD approach has found several applications also on sea–level data. Among the others, I mention the work by Ezer (2013) who found a Gulf Stream related latitudinal pattern in sea level along the U.S. East Coast, and the work by Galassi and Spada (2015) who explored the nonlinear variability of sea level in the Adriatic. Conversely, some skepticism about EMD usability was risen by Chambers (2015), who suggested caution when searching for multidecadal signals and acceleration.

2.2 Long term rate and acceleration

The concept of the rate of sea–level rise ρ as the slope of the best fitting first order polynomial was introduced in Section 1.3 and defined by Equation (1.5). I remark here that the presence of long period sinusoids (or oscillations) with significant amplitudes can introduce a bias when the rate is determined by means of Ordinary Least Square (OLS) for a first order polynomial. This concern, mentioned by different authors (Jevrejeva et al., 2006, 2008; Chambers et al., 2012; Carson et al., 2015; Chambers, 2015) was not explored exhaustively and a common

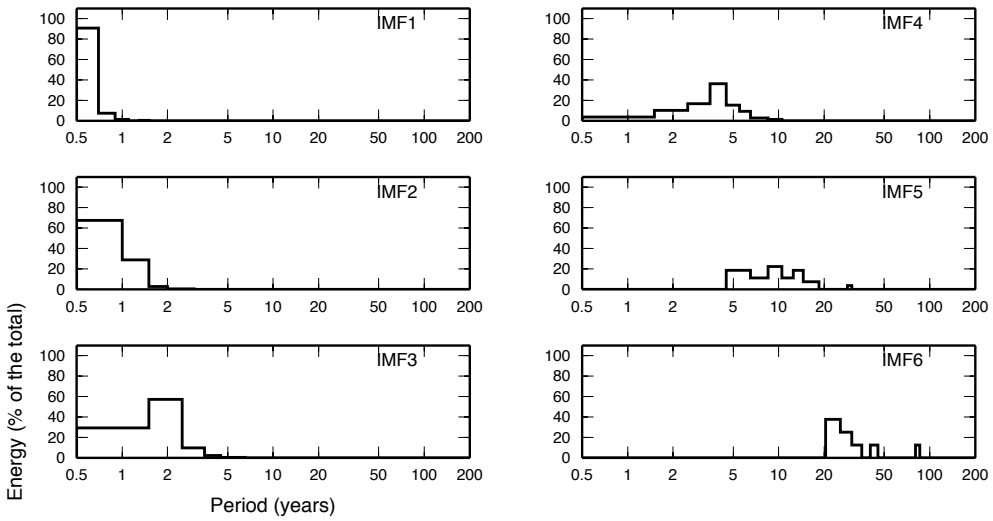

Figure 2.5: *Periodicities observed in each of the IMFs plotted in Figure 2.4, San Francisco (USA).*

approach to prevent possible biases or misinterpretations of the results does not exist.

To provide an example of the impact of long-period oscillations, I have defined a time series at annual sample rate that combines a constant trend ρ^* and a sinusoidal term of period T, phase ϕ, and amplitude A:

$$H(t_k) = H_0 + \rho' \cdot t_k + A \cdot \sin\left(\frac{2\pi t_k}{T} + \phi\right). \tag{2.1}$$

A set of synthetic TG time series has been then produced by varying the rate ρ' (1.0, 1.5 and 2.0 mm yr^{-1}), the amplitude A (range: 0.5–25 mm) consistent with what predicted by Chambers et al. (2012), the period T (range: 5–100 years) and the phase ϕ (range: 0–2π). According to the definition in Equation (1.5), the rate of rise for each of the synthetic time series has been computed. The results are displayed in Figure 2.6, where the different frames refer to the different combinations of rate ρ' and period T. In each frame, the resulting rate ρ is displayed as a function of the input amplitude A. The first remarkable observation from Figure 2.6 is that, as expected, the larger is the input amplitude A, the larger is the variability of the resulting rate ρ, which also depends on the input phase ϕ. Since ϕ is difficult to constrain in data, rates ρ have

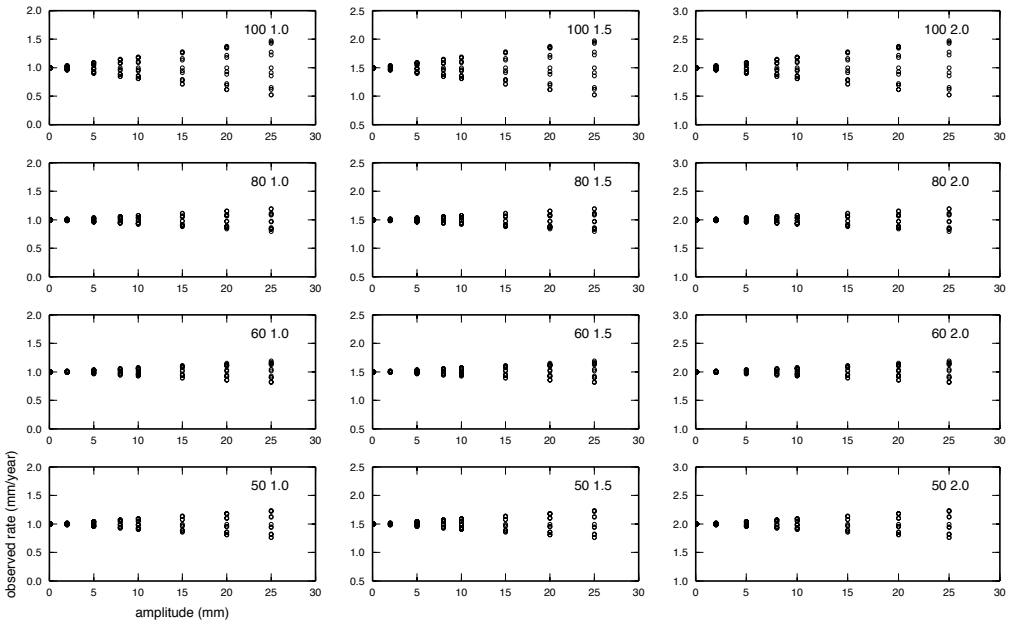

Figure 2.6: *Each frame show the observed rate as a function of the amplitude of the input sinusoid described by Equation (2.1), Different circles for the same amplitude describe the effect of varying the phase of the sinusoid over the entire range* $(0-360)$*. The two numbers in the top right angle of each frame refers to the period* T *of the input sinusoid (left), and to the input rate* ρ *(left).*

been gathered for the different input phases to represent the variability at each amplitude. From Figure 2.6 we can also note that, at fixed values of A and ϕ, the longer the period the larger the rate. This occurs in consequence of the comparatively lower number of complete cycles included in the time series. For the case of contaminating signals with period longer than 50 years, two cycles are not completed in 100 years, and this results in rate biases as large as 50% of the input one. This is connected with leverage[3]: the effect of outliers positioned at the extremes of a time series. Conversely, those periodic signals that complete more than 5 cycles lead to an almost negligible effect.

To explore the effect of long period oscillations on the apparent acceleration, I repeated the above test on the same set of synthetic time series described above, but using a second order polynomial (Equation 1.7) to

[3]http://pages.stern.nyu.edu/ churvich/Undergrad/Handouts2/31-Reg6.pdf

search for the best fitting parabola. The results for α are presented in Figure 2.7, where the apparent acceleration is displayed as a function of the input amplitude. Given the fact that the input acceleration is supposed to be null, the biasing effect of the sinusoid becomes even more evident.

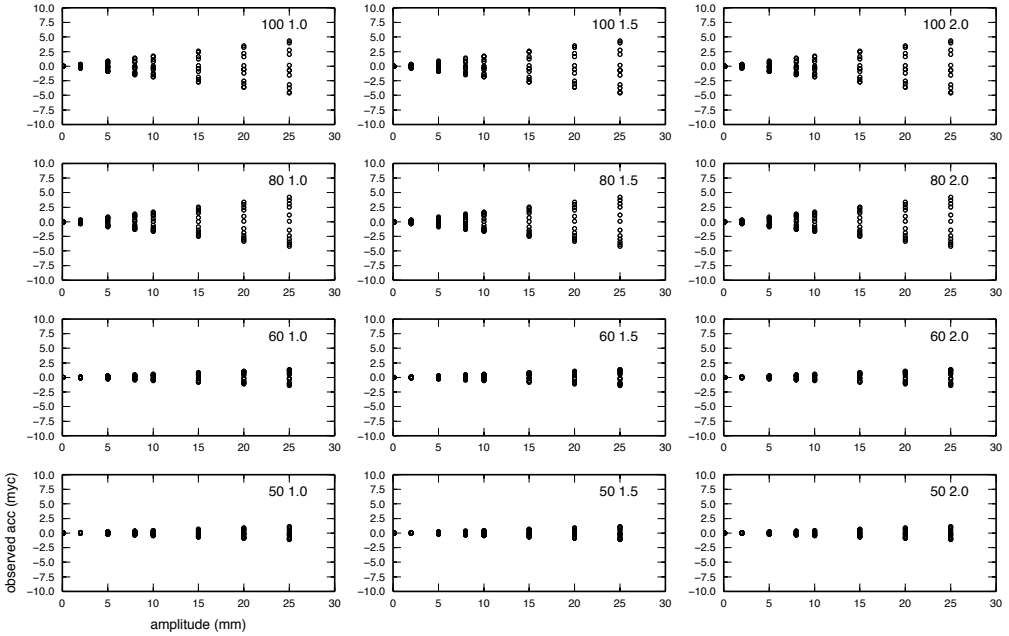

Figure 2.7: *Each frame show the observed apparent acceleration in myc as a function of the amplitude of the input sinusoid described by Equation (2.1). Different circles for the same amplitude describe the effect of varying the phase of the sinusoid over the entire range (*0-360*). The two numbers in the top right angle of each frame refers to the period T of the input sinusoid (left), and to the input rate ρ (left).*

To further show the effect of harmonic signals on trends, I now consider two 100 year long time series that consists of a constant rate equal to 1.5 mm yr^{-1} and a sinusoid with period $T = 100$ years, amplitude $A = 10$ mm and phase $\phi = 0$ and $\frac{\pi}{2}$ to represent a sine and a cosine with same amplitude, respectively (Figure 2.8). The rate is then evaluated by means of different approaches.

From Equation (2.1), the result is $\rho = (1.4 \pm 0.2)$ mm yr^{-1} ($\phi = 0$) and $\rho = (1.54 \pm 0.2)$ mm yr^{-1} ($\phi = \frac{\pi}{2}$), while from Equation (1.4) I obtain $R = 0.73$ and 1.08 mm yr^{-1} respectively. Then, I apply a first-difference derivative to the input time series and compute the average.

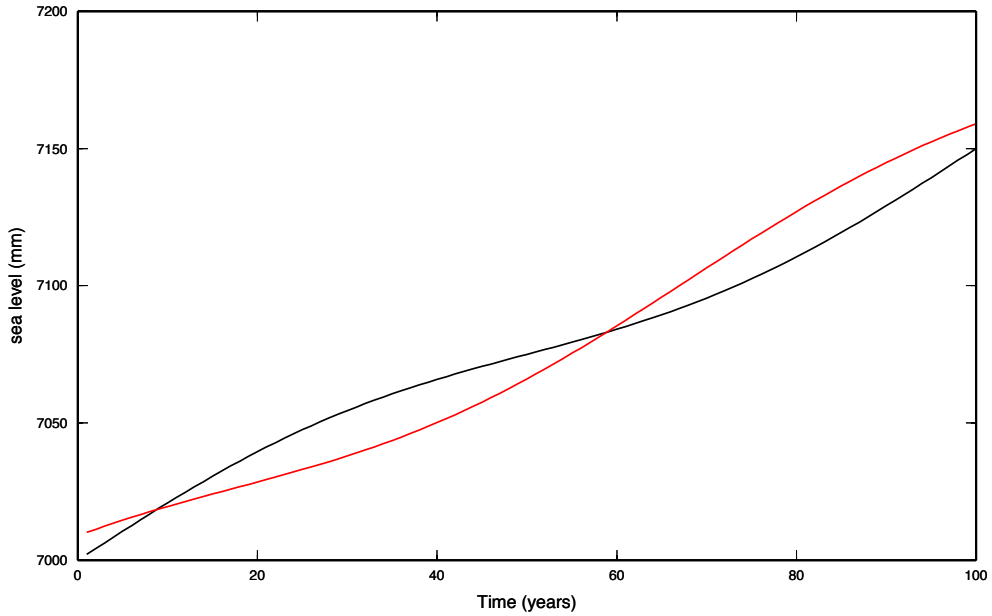

Figure 2.8: *Synthetic time series composed by a straight line with trend equal to 1.5 mm yr^{-1}superimposed to a sinusoid with $T = 100$ years and $A = 10$ mm. One (black line) is characterized by $\phi = 0$ while to the other (red line) by $\phi = \frac{\pi}{2}$ was assigned.*

The rate results in 1.49 and 1.51 mm/yr respectively but, when searching for the acceleration, this results in $\alpha = 0.0$ and 1.0 myc, respectively.

The above exercise could sound speculative, but this shows that, if we consider a time series like Equation (2.1) defined on a limited time span (100 years, $k \in [1, 100]$ in the formalism of Equation 2.1), it could be misleading to say that its rate is ρ and its acceleration is null. The two (ρ and α) vanish only for the limit of k tending to infinity and their value depends also on the selected approach for estimating the rate and the acceleration. This consideration becomes more apparent by considering the Taylor series for $\sin(x)$ that, around the point $x = 0$, gives $\sin(x) = x + O(x^3)$ while $\sin(x + \frac{\pi}{2}) = 1 - x^2 + O(x^4)$ introducing a rate an acceleration respectively. The lesson that should be taken from above is that, the presence of a sinusoid in a time series whose long term acceleration is null, can result in non null estimates for the rate or the acceleration. This is noise in a long term perspective but, since the model

is valid only within the time span covered by the time series, it would be difficult to distinguish the noise from the signal (Silver, 2012).

The problem outlined above was first evidenced by Douglas (1992), who first determined the "apparent acceleration" for all of the RLR TG time series available at PSMSL with record > 10 years in length. The plot of α as a function of the length of the record unveiled that the shorter the time series the larger the variability for the resulting acceleration. From this observation, Douglas (1992) concluded that those time series shorter than 50 years should be excluded when assessing the long period acceleration. I have repeated this analysis with the same approach but with the current PSMSL dataset that, 24 years later, counts a larger number of sites and longer time series. The results for α as a function of

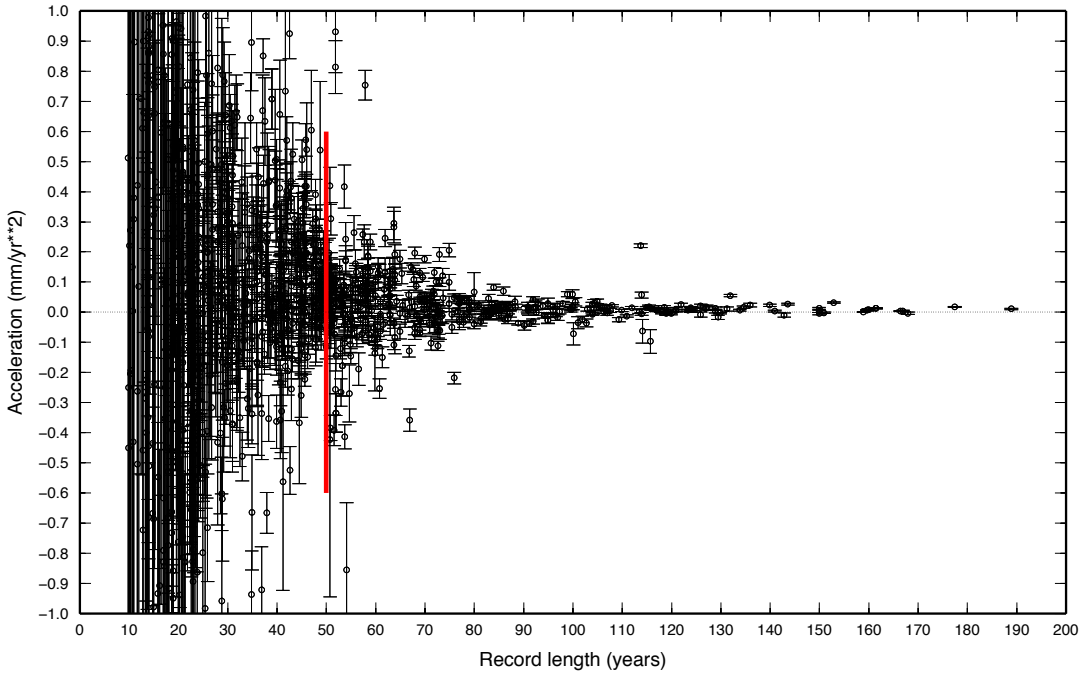

Figure 2.9: *Apparent acceleration of sea level for sites with records length >10 years. The red bar marks the 50 years threshold.*

the record length are displayed in Figure 2.9. This updated figure confirms the stability, in terms of reduced range of values, for those sites with long record length. It also confirms that the majority of the α values are positive thus suggesting the existence of a positive global acceler-

ation or a bad sampling of the global sea level by TG sites. However, from the comparison between Figure 2.9 and Figure 3 in Douglas (1992) we can notice a larger scattering for α at the record length of 50 years, the threshold chosen by Douglas (1992). It could be argued that it is a consequence of the larger number of sites with record length similar to the selected threshold or that contemporary sea–level variability is larger than previous.

2.3 The $\sim$60 year oscillation in tide gauge records

An influential work about the contamination of long time series by multi-decadal periodic signal is the one by Chambers et al. (2012). The authors explored a subset of long-lasting TGs ($T > 100$ years, with few exceptions) and, in each time series, found a significant $\sim$60 years periodic signal whose presence can influence the acceleration assessment. In the IPCC AR5 report, this work is pivotal for weakening the reliability of existing time-dependent global acceleration assessments (Church et al., 2013). The approach chosen by Chambers et al. (2012) was simple: they compared the fit for a first order polynomial with the fit for the combination of a straight line and a sinusoid with period assigned to 55 years. The second model includes two further regressors: the sinusoid amplitude and its phase. The significant variance reduction for each of the time series was considered as evidence for the presence of this oscillation in the signal. The different phases observed at different sites show some coherency at basin scale. However, the authors were quite conservative in drawing conclusions leaving some room for doubts. One of the conclusion drawn by the authors was that, despite data records are too limited in space and time, the possible existence of a 60 year oscillation should be considered when searching for the global mean sea–level acceleration.

I first note that the authors did not consider that, when regressing a data set with two models in which the second includes two further degrees of freedom (in this case sinusoid amplitude and phase), necessarily

the more complex model will result in a smaller variance with respect to the simpler one. The variance reduction cannot be considered, indeed, an evidence of the quality of the model. A second consideration that could further reduce the strength of their results, is the absence of any test to compare the selected period (55 years) with other possible values that could, in principle, provide a better model. Moreover, they did not consider that, in some cases, the selected period (55 years) is comparable with the duration of the time series itself. Besides the above considerations, the possibility of an "aliasing effect", i.e. the effect of undersampling that makes two different signals undistinguishable, should be also considered.

For these reasons, I re-evaluated the work of Chambers et al. (2012) using the same set of tide gauges but following a different approach and using the longer records presently available at PSMSL. My idea was to evaluate the frequency content of the time series by applying the EMD analysis. As introduced in Section 2.1, EMD is a fully adaptive time-domain method that should be preferred for the case of non-stationary and non-linear signals, as TG time series are. The subset of TG records used by Chambers et al. (2012) has been extracted from the current version of PSMSL archive to improve their length. Then, these were GIA corrected by adopting model ICE-5G(VM2) of Peltier (2004) and an improved version of program SELEN[4] (Spada et al., 2012), originally proposed by Spada and Stocchi (2007). These TG time series will be labelled "nogia" in the following. In this case, GIA correction is a mere constant rate added or removed to the time series despite the observation by Spada et al. (2014) who suggested a marginal acceleration effect in GIA at time scales longer than 100 years. The extraction of periodic signals is then performed by applying a modified implementation of the EMD proposed by Huang et al. (1998a), in which border effects for the IMFs and for the residual function RES are prevented by mirroring, at

[4]SELEN: a Sea levEL EquatioN solver.

each step, the last minimum and maximum at each extremum of the same time series. This mirroring approach, that modifies the one proposed by Rato et al. (2008) was preferred because it minimizes the impact of the added portion of the time series on the results. The analysis can be summarized by:

$$S_{nogia}(t_k) = S(t_k) - \rho_{gia} \cdot t_k + \sum_{i=1}^{n} IMF_i(t_k) + RES(t_k), \qquad (2.2)$$

where S_{nogia} and S are the GIA-corrected and raw sea level time series at a given TG site respectively, ρ_{gia} is the GIA rate, IMF_i ($i \in [1, n]$) and RES are the cyclic and non cyclic time series from the EMD analysis.

As introduced above, IMFs are not stationary, so a specific periodic signal can move from one IMF to another in different epochs. Standard DFT is then dropped and replaced by a simpler method to determine the frequency content of one IMF. The idea roots on the definition of IMF: *"in the whole data set, the number of extrema and the number of zero crossings must either equal or differ at most by one"* (Huang et al., 1998b). I then determined the semi-period as the portion of each IMF comprised between two consecutive extrema as the time span between them. The overall "periodic content" is then gathered by merging the results for each IMF. This "periodic content" is then used to evaluate if, in accordance with Chambers et al. (2012), any signals with period around 55 years, could emerge for any of the selected TGs. The results are summarized in Table (2.1) in which the number of expected extrema, function of the duration of the time series is also reported for comparison. The expected extrema were determined as twice the number of cycles for sinusoids with period $T = 50$ and $T = 60$ years contained in the time span covered by each time series. The low number of observed cycles at periods comparable with 55 years for the majority of the TGs is not supporting the hypothesis that a sinusoid with period $T = 55$ years is present in the selected subset.

I would remark here that EMD does not require trend-removed time

series as it applies to DFT. This could mask small amplitude periodic signals whose extrema are not large enough for being recognized by the EMD sifting process. For this reason, I repeated the above analysis on the detrended time series (labelled "notrend" in the following) to improve the consistency with the experiment conducted by Chambers et al. (2012), regardless the appropriateness of this choice. This test (Table 2.1) confirms the conclusion outlined above, i.e. that for all but one (St Georges, Bermuda) of the selected sites, there is no evidence for the presence of periodic signals with period of about ~ 55 years. This suggests

PSMSL ID	TG location	duration (years)	expected [min-max]	observed nogia	observed notrend
1	Brest	206.9	[6.9–8.3]	3	3
10	San Francisco	159.4	[5.3–6.4]	1	1
111	Freemantle	116.9	[3.9–4.7]	0	3
112	Fernandina Beach	116.5	[3.9–4.7]	3	2
12	New York (The Battery)	157.9	[5.3–6.3]	4	4
130	Aburatsubo	83.9	[2.8–3.4]	1	0
132	Wajima	83.9	[2.8–3.4]	0	0
133	Hosojima	83.9	[2.8–3.4]	2	2
136	Dudenin II	113.9	[3.8–4.6]	1	1
148	Baltimore	111.4	[3.7–4.5]	0	2
150	Auckland II	96.5	[3.2–3.9]	0	2
154	Trieste	138.9	[4.6–5.6]	0	3
155	Honolulu	108.9	[3.6–4.4]	0	1
157	Buenos Aires	82.9	[2.8–3.3]	0	0
158	San Diego (Quarantine Station)	107.9	[3.6–4.3]	2	0
163	Balboa	105.9	[3.5–4.2]	1	0
188	Key West	100.9	[3.4–4.0]	0	1
368	St. Geogres (Bermuda)	81.1	[2.7–3.2]	2	3
43	Mumbai (Apollo Bandar)	132.9	[4.4–5.3]	2	1
52	Cascais	111.9	[3.7–4.5]	1	1
61	Marseille	128.8	[4.3–5.2]	2	2
65	Sydney (Fort Denison)	107.9	[3.6–4.3]	2	3
85	Reposaari	13.9	[0.5–0.6]	0	0
94	Tonoura	90.2	[3.0–3.6]	0	0

Table 2.1: *Expected and observed extrema for the subset of sites selected by Chambers et al. (2012) for the case of a sinusoidal signal with period between $T = 50$ and $T = 60$ years. Observed values, resulting from the EMD analysis, are displayed for the two cases of GIA-corrected and detrended time series.*

that the improved fit observed by Chambers et al. (2012) when incorporating a 55 year sinusoid was an artifact consequence of the addition of two degrees of freedom in the regressing function. To emphasize the meaning of the above results I have plotted, for each time series and for the two cases "nogia" (Figure 2.10) and "notrend" (Figure 2.11) the amplitude of each oscillation from all the resulting IMFs.

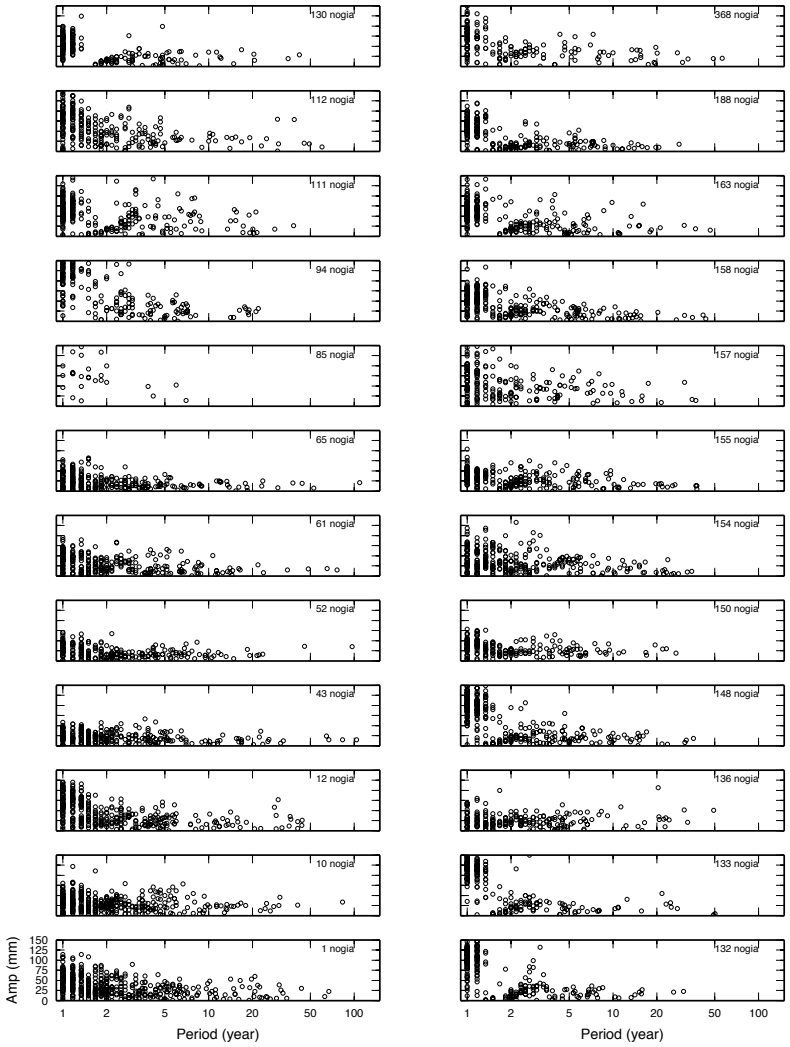

Figure 2.10: *Amplitude in mm as a function of the corresponding period for all the oscillations resulting from the IMFs at each site listed in Table 2.1 for the case of GIA-corrected time series.*

As a further test, I evaluated the significance of the model that combines a straight line plus a 55 year sinusoid with respect to the one that

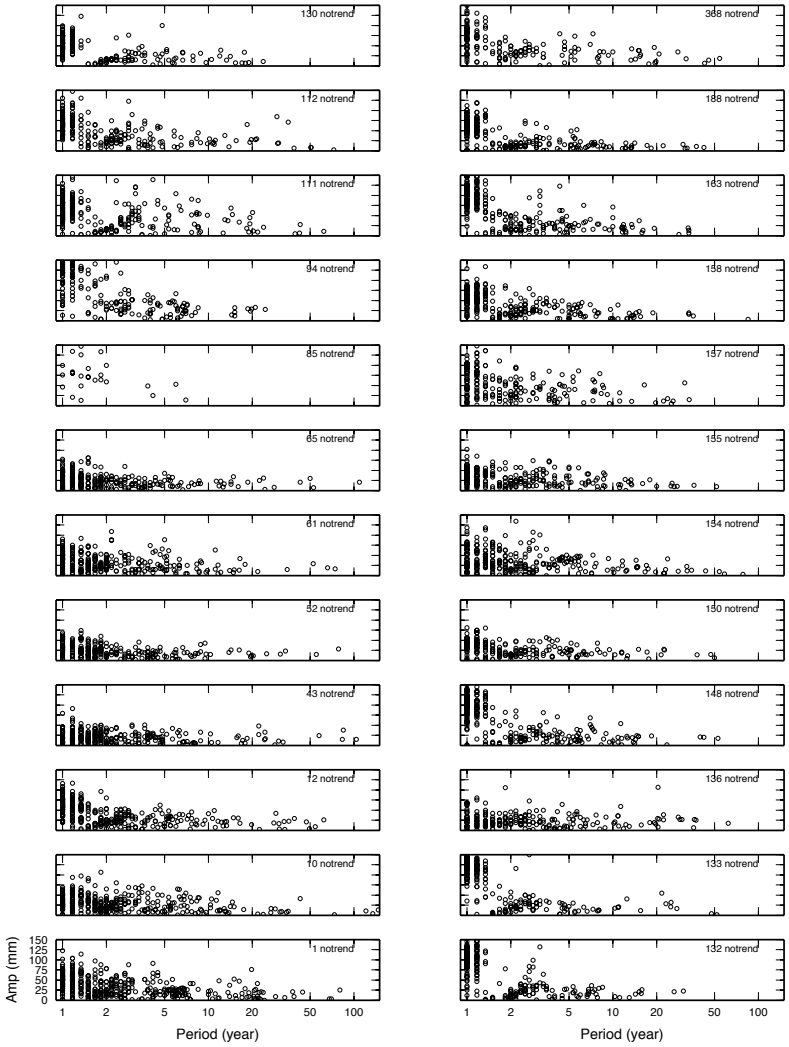

Figure 2.11: *As in Figure 2.10 for the case of detrended time series.*

includes only a straight line by accounting for the different number of degrees of freedom. The mere comparison of the variances is valid only for the cases in which the two models have the same degrees of freedom while, in this case the proposed model includes two further variables: the phase and the amplitude of the sinusoid. The appropriate approach is then to perform a Fisher F-test that accounts for the number of degrees of freedom and of the number of samples in the data set. The results are not encouraging since for only 7 out of 23 sites the new model (linear trend plus 55 year sinusoid) improves (95% significance) the linear model. For the large majority of the sites selected by Chambers et al. (2012), the

more complex model does not significantly improve the variance (95% significance) and, indeed, this test does not confirm the presence of this sinusoid in selected data.

To complete the discussion about the work by Chambers et al. (2012), I have reconsidered the sea–level reconstruction by Jevrejeva et al. (2008) for which the authors suggested the presence of a sinusoidal oscillation with period 54 years and amplitude 14 mm during the time interval 1900-2003 (see Table 1 in Chambers et al., 2012). Following the methodology applied to the single TG time series, I removed the trend and than applied the EMD analysis to the reconstruction by Jevrejeva et al. (2008) restricted to the time interval 1900-2003. I then considered the IMFmax, i.e. the higher degree IMF that contains the longer period cyclic components, as a representation of its long period signal and plotted it in Figure 2.12 along with the proposed sinusoid and the sea–level reconstruction itself. Visual inspection suggests that the IMFmax better follows the long term component of this sea–level reconstruction, which is also confirmed by the larger variance reduction with respect to the one resulting from the 54 year sinusoid. I note that the IMFmax is composed by a first portion with amplitude 17 mm and period 64 years and a second one with amplitude 10 mm and period 46 years whose average period (55 years) and average amplitude (13.5 mm) are consistent with what proposed by Chambers et al. (2012). However, this result again confutes the idea of a constant-period oscillation.

In my opinion, and according to the above results, sinusoidal oscillations in sea–level time series are an artifact resulting from the approach chosen by the authors, although multidecadal oscillations exist. The above analysis confirms also that it is more realistic to represent the long period signals contained in sea–level reconstruction, as well as in single tide gauge time series, by means of cyclic functions whose amplitude, period and phase can vary over time. This observation will support the use of IMFmax in Section 4.2 and 4.3.

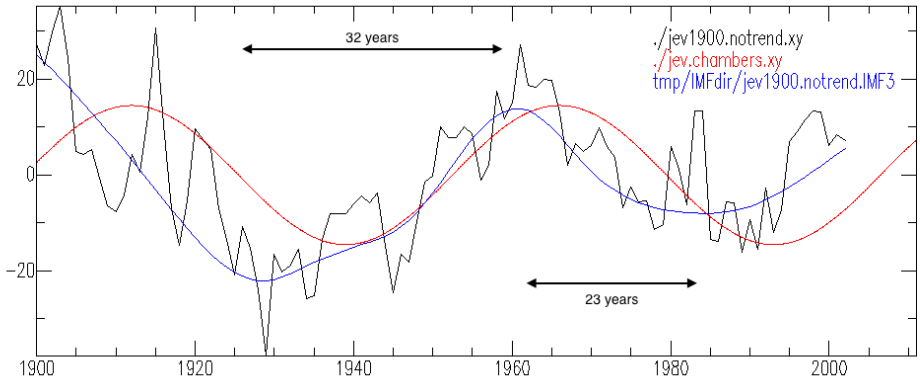

Figure 2.12: *Black line: trend removed sea level reconstruction by Jevrejeva et al. (2008). Red line: 54 year sinusoid proposed by Chambers et al. (2012). Blue line: the IMFmax computed in this work. The two arrows mark the distance between the extrema for the IMFmax used to determine the period of the two oscillations.*

2.4 An example of sea-level reconstruction

A global sea–level reconstruction is a time series representative for the global sea–level change, that results from the combination of different sea–level observations. Here, I will only consider those reconstructions derived from TG time series. As discussed in Chapter 1, the sea–level change observed at a TG site combines the global sea–level change with the GIA deformation as well as local and regional components that can affect the sea but also the ground in the surroundings. For this reason, the move from TG time series to a sea–level reconstruction is not a simple task and different recipes have been implemented during the last decades by different authors. Some of them (e.g. Douglas, 1991; Spada and Galassi, 2012) restricted the data-set to a small reliable number of TGs, by applying specific selection criteria. Others have preferred to keep the dataset as wide as possible (e.g. Olivieri and Spada, 2013) with the idea that the larger the number of observations, the better the representation of the global signal. Indeed, a larger set of observations should be less affected, on average, from local disturbances that may appear in individual time series. The methodology to move from single TG time series to global reconstructions is not yet standardized, with some au-

thors using combinations of pre-selected time series (e.g. Douglas, 1991; Spada and Galassi, 2012; Olivieri and Spada, 2013), others introducing more sophisticated approaches (e.g. the virtual station method, Jevrejeva et al., 2008) designed to mitigate the uneven distribution of TGs along the coastlines. Furthermore, the application of the Reduced Space Optimal Interpolation (RSOI) approach (e.g. Church and White, 2006; Calafat et al., 2014) leads to century long sea–level reconstructions that account for the sea–level spatial variability observed by satellite altimetry. This concept will be discussed in details in Section 3.1.

Our preferred approach (Olivieri and Spada, 2013) was to select all the TG time series whose time span exceeded 50 years, and to apply a standard stacking (Equation 1.11) on GIA corrected time series. This approach led to the creation of a sea–level reconstruction based on 315 RLR time series whose distribution is displayed in Figure 2.13. The

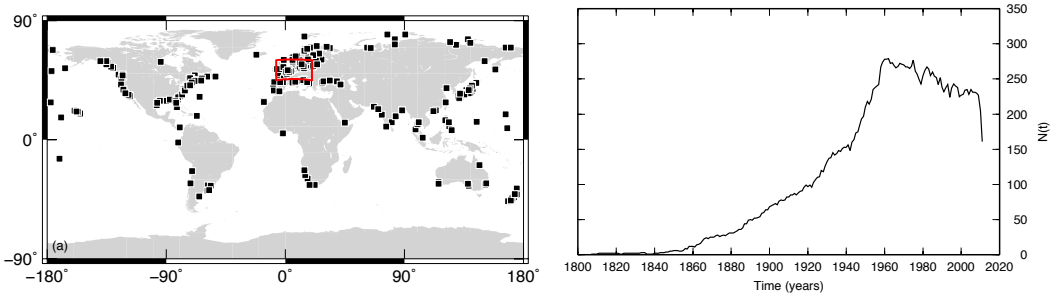

Figure 2.13: *Left: distribution of the 315 selected TG sites contributing to the sea–level reconstruction. Right: number of sites providing data for the stacking over time. Modified with permission from the work by Olivieri and Spada (2013).*

choice of setting the time span threshold at 50 years, in accordance to minimum threshold suggested by Douglas (1992) was also motivated by the resulting larger dataset and better spatial coverage. Specific tests in which the threshold was changed to 60 and 75 years, confirmed that this choice would not affect the results. Each of the TG time series covers a specific time span (with gaps) and this produced a time varying number of observations contributing to the stacking (Figure 2.13) that reaches its maximum ($\sim$60) around year 1960. Conversely, in the early decades this

number is reduced to a few units confined in northern Europe. The early portion of the sea–level reconstruction was then dropped and we limited its time span to the period 1840–2008 (see Figure 2.14).

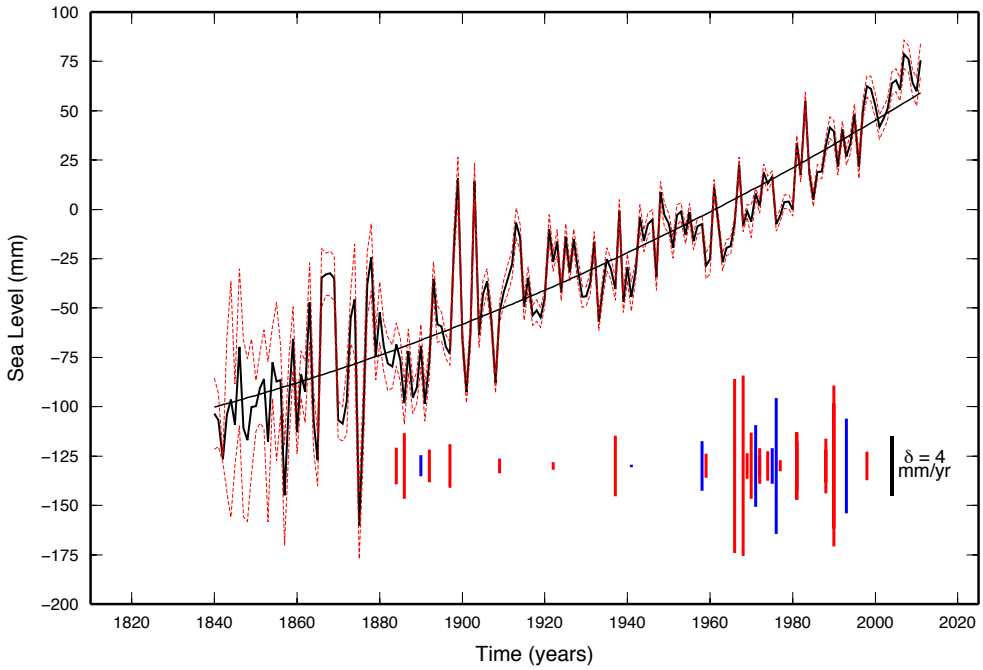

Figure 2.14: *The black curve shows the best fitting quadratic polynomial. The plot at the bottom shows the sequence of CPs found for each of the time series in the TG-B set. Red and blue segments indicate CPs for which the variation in the rate of sea–level change, denoted by δ, is positive and negative, respectively. Modified with permission from the work by Olivieri and Spada (2013).*

Three separate analyses have been then performed to search for the best fitting polynomial of the first and of the second order and for a bi-linear function. The latter was motivated by the possibility that the acceleration is not a steady process that covers the entire time span but, on the contrary, a sudden process occurring in a limited time interval (see Equation 1.8). An F-test that accounts for the different number of degrees of freedom between the three models was used to choose the preferred one that is, at 95% significance, the quadratic one. This means that the model that better represents the sea–level reconstruction displayed in Figure 2.14 is a parabola and the apparent acceleration is $\alpha = (0.4 \pm 0.1)$

myc for the period (1840–2010). The associated error, 2σ, is the result of a bootstrap that considered the distribution around the mean, at each time step, resulting from the stacking.

Conscious that the acceleration is small and possibly difficult to be recognized on single tide gauge time series, we have repeated the above analysis, i.e. the search for the preferred model among linear, quadratic and bi-linear, for each of the 315 selected time series. This was aimed to explore, if possible, the origin of the observed acceleration. The results, summarized in Figure 2.15, evidence that for the majority of the sites (subset TG-L, 75 % of the total), the preferred model is a linear one that does not include any acceleration. In this case, remarkably, it is

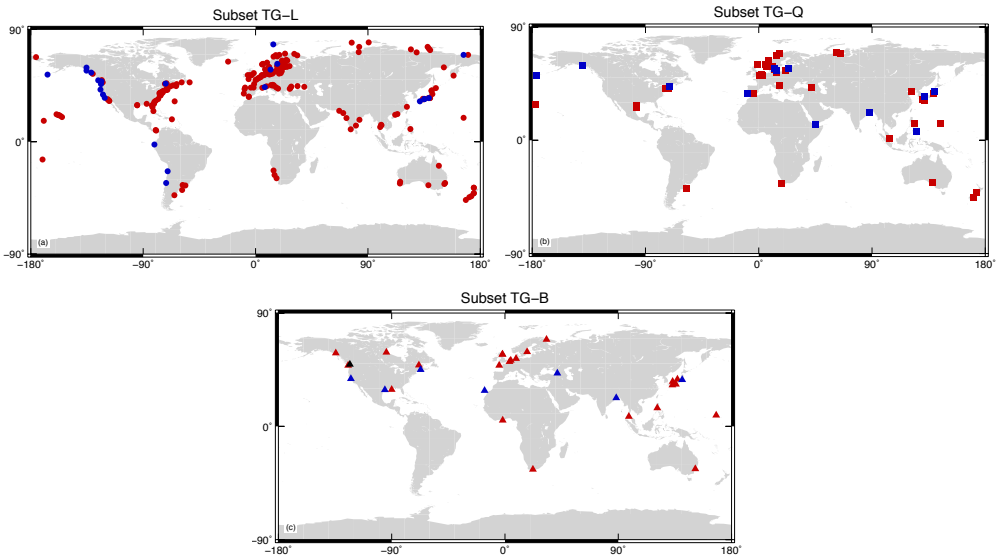

Figure 2.15: *Locations of TGs according to the preferred best-fitting model. Subset TG-L, linear model, red and blue symbols denote positive and negative trends, respectively; subset TG-Q, quadratic model, the red color indicates a positive quadratic term, the blue a negative one; TG-B, bi-linear model, red and blue colors indicate positive and negative rate change. Reproduced with permission from the work by Olivieri and Spada (2013).*

not possible to discriminate between absent and not emerging acceleration. However the stacking of this subset of "linear" TGs led to a time series whose preferred model is a linear function, pointing to a vanishing acceleration. The remaining sites are divided in about 15% of the

total (subset TG-Q) whose preferred model is a parabola with constant acceleration, and the remaining, subset TG-B (10% of the total), whose preferred model is a bi-linear function. While stacking the two subsets (TG-Q and TG-B) we obtain, in both case, a time series whose preferred model is a parabola. If this was expected for subset TG-Q, the result for subset TG-B can be surprising. However, by plotting the epoch of the change points over time (bottom part of Figure 2.14) we notice that their occurrence distributes over the entire period 1840-2008, motivating why the combination of many sudden accelerations results is a constant one when averaging those data. It should be also remarked that the spatial distribution of the three subsets does not show any apparent pattern suggesting that quadratic or bi-linear models do not cluster.

Author(s) year	$\alpha \pm \Delta\alpha$ (myc)	Period (year–year)	Input dataset	Methods
Douglas (1992)	-1.1 ± 1.2	1905–1985	23 TGs	Regional
” "	$+0.1 \pm 0.8$	1850–1991	37 TGs	"
Church and White (2006)	1.3 ± 0.6	1870–2001	TGs	EOFs
" "	0.8 ± 0.8	20^{th} century	"	"
Jevrejeva et al. (2008)	~ 1	1700–2002	1023 TGs	Virtual station
Church et al. (2011)	0.9 ± 0.3	1880–2009	TGs and altimetry	RSOI
This study	0.42 ± 0.12	1840–2010	315 TGs	Stacking

Table 2.2: *Global mean sea–level acceleration estimates based on global analyses of instrumental records, for which a quadratic term in a polynomial regression is evaluated.*

In conclusion, our sea–level reconstruction suggests that an acceleration exists for the global mean sea level. Its value (~ 0.4 myc) turns out to be smaller than those obtained by some of the most credited works listed in Table 2.2 and displayed in Figure 2.16. The time span covered by the different reconstructions is not the same and this could indicate that the acceleration has not been constant over the last two centuries. We also observe that the cumulus of sudden accelerations occurring at different epochs at sparse TG sites leads to a model with constant acceleration. This suggests caution in concluding that the process underlying

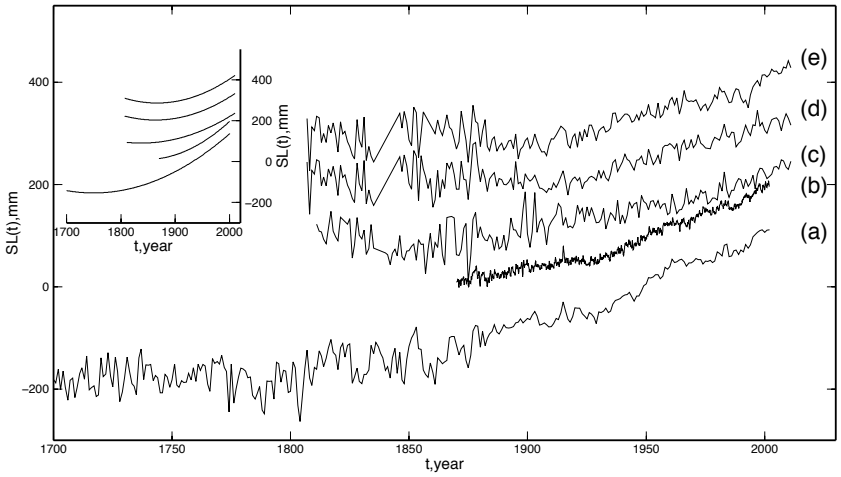

Figure 2.16: *Various sea-level curves. Curves (a) and (b) show the reconstructions by Jevrejeva et al. (2008) (the standard errors are not reproduced from the original work) and Church and White (2006), respectively. Curve (c) is the ST time series obtained in this work. Curves (d) and (e) result from the stacking of the TGs selected by Douglas (1992) and by Spada and Galassi (2012). The best-fitting quadratic polynomials to curves (a-e) are shown in the inset (numerical values of the corresponding accelerations are given in Table 2.2. Reproduced with permission from the work byOlivieri and Spada (2013).*

the observed global mean sea level acceleration is the spatially uniform constant acceleration. Finally, it could be argued that TG only observed "coastal" sea level but this topic and how coastal observations are representative of the global sea level will be one of the subjects of the next chapter.

CHAPTER 3

Coastal versus Global models

3.1 Introduction

TG records are the only set of instrumental observations that covers the last $\sim$200 years and more. Their uneven distribution in space and time (Holgate et al., 2013; PSMSL, 2015) hinders the robustness of any assessment for the rate of Global Mean Sea Level Rise (GMSLR) and for its acceleration (GMSLA) at century scale. Therefore, it is not surprising that different selections of TG records and different methodologies come to distinctly different clues for GMSLR and GMSLA (Spada and Galassi, 2012; Hamlington and Thompson, 2015; Spada et al., 2015; Visser et al., 2015). To illustrate this point, we have restricted some of the recent GMSL reconstructions to the common period 1900-2000 and estimated GMSLR and GMSLA, as shown in table Table 3.1, by means of Ordinary Least Square (OLS).

In details, from the reconstruction of Olivieri and Spada (2013) who stacked the longest TG time series, we find a GMSLR of (0.94 ± 0.06)

Authors	Method	ρ mm yr^{-1}	α myc
Calafat et al. (2014)	RSOI	1.91 ± 0.01	0.76 ± 0.09
Church and White (2011)	RSOI	1.67 ± 0.01	1.47 ± 0.06
Jevrejeva et al. (2014)	Virtual Station	1.91 ± 0.05	0.92 ± 0.35
Olivieri and Spada (2013)	TG Stacking	0.93 ± 0.06	1.33 ± 0.44

Table 3.1: *Values of GMSLR and GMSLA from a selection of published global sea–level reconstructions reduced to the common period* 1900-2000.

mm yr^{-1} and a GMSLA of (1.78 ± 0.41) myc. From Jevrejeva et al. (2014), who used the "virtual station method", we find a GMSLR of (1.91 ± 0.05) mm yr^{-1} and a GMSLA of (0.92 ± 0.35) myc. Church and White (2006) applied a Reduced Space Optimal Interpolation (RSOI) to an Empirical Orthogonal Function (EOF) decomposition of altimetry data, resulting in a GMSLR of (1.67 ± 0.01) mm yr^{-1} and a GMSLA of (1.47 ± 0.06) myc. Finally, from Calafat et al. (2014), using a different RSOI-based approach, we obtain a GMSLR and a GMSLA of (1.91 ± 0.01) mm yr^{-1} and (0.76 ± 0.09) myc, respectively. In all cases, the associated error reflects solely the uncertainty of the regression.

The apparent discordance between the values listed in Table 3.1 raises two fundamental issues, i.e.: *i)* the extent to which coastal sea level is representative of GMSL, and *ii)* the extent to which the limited sampling of TG records allows for a robust estimate of GMSLR and GMSLA. Here, these issues are addressed taking advantage of recent developments in sea–level observation and modelling.

3.2 Data

Since 1992, satellite altimetry has opened new perspectives on the study of sea–level variability providing, for the first time, an "instantaneous global picture" of sea level, with the exception of high latitudes ($> 60^{\circ}$). One of the benefits introduced by altimetry is the possibility of comparing coastal sea level to GMSL (Cabanes et al., 2001; Prandi et al., 2009;

Dean and Houston, 2013), though major limitations are the as yet short observation period and the reduced accuracy in shallow water (Passaro et al., 2014). These drawbacks can be alleviated using RSOI techniques that merge long-lasting coastal TG data with altimetric maps (see e.g. Church and White, 2006; Calafat et al., 2014). The main benefit of RSOI is the possibility of projecting the spatial distribution of sea level backward in time, as long as a sufficient number of TG records is available.

The concurrent development of accurate global oceanic models has also permitted a significant step forward in GMSLA studies as discussed by Cazenave and Llovel (2010). Provided that the model outputs are successfully validated against sea–level observations, they can be used to study possible biases between coastal and global sea level and to test the representativity of a given spatio-temporal sampling. The advantage of model simulations with respect to altimetry data is that the former can span longer periods, which is essential to unveil the long-term rate of sea level (Douglas, 1991) and its acceleration (Douglas, 1992).

We used two sets of data with quasi-global coverage. The first is the CSIRO [1] multi-satellite gridded altimetry that maps the oceans surface at a spatial resolution of 1° with a temporal resolution of one month during the period $01/1993$-$12/2014$ (see Church et al., 2011, for details). This dataset, simply referred to as CSIRO in the following, is preferred to other similar products since it is released with options for relevant corrections. These include the Inverted Barometer (IB) response (Wunsch and Stammer, 1997), the GIA (Farrell and Clark, 1976), and the seasonal cycle correction (Tsimplis and Woodworth, 1994). Figure 1.8 displays the spatial variability of the rate of sea–level change from CSIRO, with the global mean rate subtracted and all corrections applied. In Figure 1.9b, this spatial variability is gathered in terms of frequency for the different rates observed at each cell of the grid. It is apparent that the distribution is not normal but more likely bimodal, reflecting different

[1] Commonwealth Scientific and Industrial Research Organisation http://www.cmar.csiro.au/sealevel/sl_hist_last_decades.html

concurring phenomena contributing to the global sea–level rise.

The second dataset consists of Sea Surface Heights (SSH) from the global ocean reanalysis Simple Ocean Data Assimilation (SODA)v2 (Carton and Giese, 2008; Giese and Ray, 2011), which consists of 138 years (01/1871-12/2008) of monthly data with a spatial resolution of 0.5° (Figure 3.1). This dataset will be referred to as SODAv2 in the following. SODAv2 was obtained by means of a Boussinesq ocean circulation model assimilating temperature and salinity data. It must be noted that SODAv2 itself does not reflect total sea–level change. In fact, SODAv2 accounts neither for the global ocean expansion/contraction due to warming/cooling (Boussinesq models conserve volume), nor for the mass change due to the waning and waxing of continental ice sheets. As a consequence, the spatial average for SSH in SODAv2, *i.e.* the GMSL, does not vary with time.

We focus on SODAv2 for two reasons: first it is a global model; second, the time span of current version covers the period 1871–2008 (Figure 3.1) and its duration is comparable with that of the longest TGs and well longer than the 50 years threshold suggested by Douglas (1992).

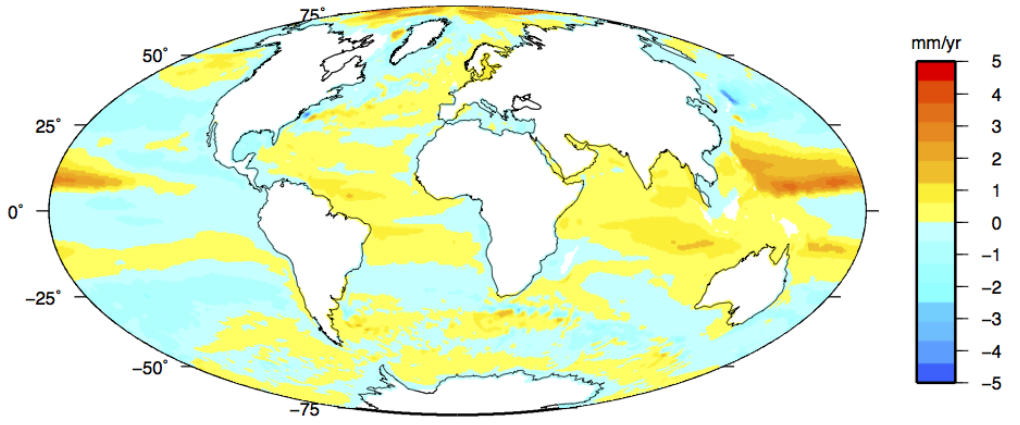

Figure 3.1: *Rate of sea–level rise resulting from the SODAv2 ocean reanalysis. This was computed by determining, for each cell of the grid, ρ from best-fitting over the entire time span of the model* (1871-2008).

3.3 On the validity of the ocean reanalysis SODAv2

The correlation between altimetry and ocean reanalyses data has been studied by Carton et al. (2005). They found strong similarities between the spatial distributions of SODAv2 and TOPEX/POSEIDON altimetry data (1993–2001). Furthermore, they computed the correlation between an earlier version of SODA (v1.42) and a selection of representative TG records for the period 1958-2001, obtaining moderate correlation with an average value of 0.70. Even though we are aware that the evaluation of an ocean reanalysis is a complex task (Storto and Masina, 2017), for the purpose of this work and to validate the entire period covered by SODAv2 (1871–2008), we have repeated the above correlation test with different subsets of TG time series that cover the entire period.

For the purpose of this test and, as for the data analysis that will follow, we created a synthetic version of the RLR monthly archive hosted at the PSMSL by associating to each TG site the closest wet point in SODAv2 (PSMSL-SODA in the following). Each of the TG time series will be then replaced by that of the paired SODAv2 point. The time span of the synthetic time series will match that of SODAv2 (1871-2008) and gaps existing in the TG time series will be replicated.

Carton et al. (2005) compared the real TG time series to their corresponding synthetic ones extracted from SODA. The authors selected 20 TGs with "proper quality and spatial distribution" and claimed an average correlation $R = 0.70$ for the 20 stations. We repeated the analysis, nearly following their recipe but extending backward in time the dataset to reach, at 10 years steps, the complete time span (1871–2008). To be consistent with Carton et al. (2005), the IB correction has been applied to TG time series. Furthermore, both datasets (the true data from PSMSL and the synthetic ones form PSMLS-SODA) have been downsampled from monthly to annual by averaging the twelve monthly data of each natural year (Carton et al. (2005) applied a 1 year running average). The correlation between time series has been computed by defining

the correlation coefficient r as:

$$r = \frac{\sum_{i=1}^{n}(x_i - \overline{x})(y_i - \overline{y})}{\sqrt{\sum_{i=1}^{n}(x_i - \overline{x})}\sqrt{\sum_{i=1}^{n}(x_i - \overline{x})}}, \tag{3.1}$$

where x_i and y_i denote the two time series for a given TG location and n is the number of data. The significance of the correlation is evaluated by a Pearson test. Consequently, the average correlation coefficient used by Carton et al. (2005) is:

$$R = \frac{1}{N}\sum_{n=1}^{N} r_n, \tag{3.2}$$

where n labels one single site and N represents the number of selected TG sites that, according to the different completeness and to the different time span covered by the different time series, will be time dependent. Figure 3.2 shows the correlation R for the 20 TG sites selected by Carton et al. (2005) plotted as a function of the starting epoch at each time span. The number of TGs for which data were available is displayed by a thin line. The red line marks the correlation reported in Carton and Giese

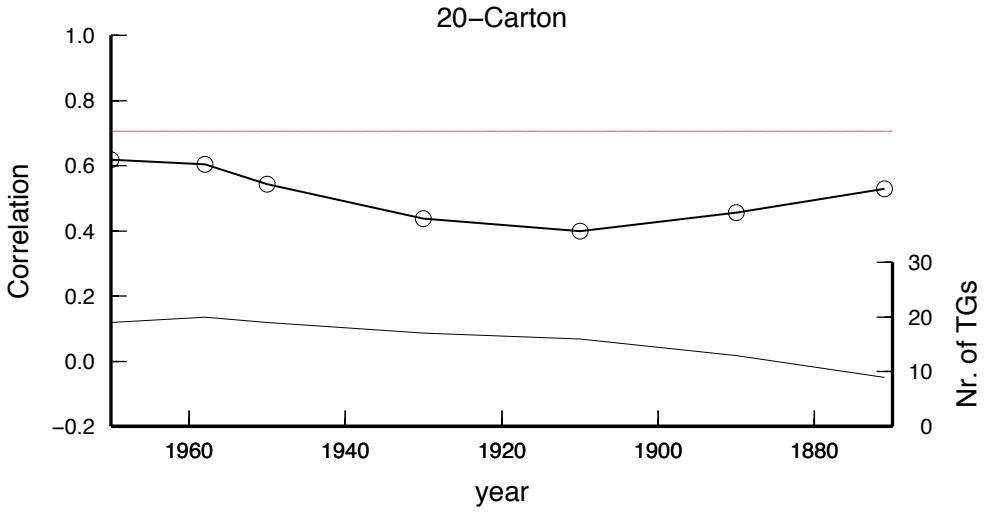

Figure 3.2: *Correlation of the 20 TG sites selected by Carton and Giese (2008) as a function of the starting epoch of the time span. The thin line shows the number of available TGs.*

(2008). When considering the entire time span of SODAv2, we observe

a decrease of the correlation (Equation 3.2) from $R = 0.61$ for the same time spans used by Carton et al. (2005) to $R = 0.54$. It should be noted that, given the unavailability of some of the TGs in the early stages of SODAv2, their number falls down to nine (Figure 3.2).

To increase the robustness of this test and to provide different perspective of the same problem, we repeated it with three additional subsets of TG time series. Namely: *a)* the 23 TGs chosen by Douglas (1991), by means of a rigorous selection that included: length of the time series, vicinity to active plate boundaries, completeness, coherence with neighboring TGs and absence of contamination by GIA; *b)* all the TG time series with time span longer than 120 years and *c)* those with data completeness $> 90\%$ over the SODAv2 time span.

For the subset *a)* that follows the selection by Douglas (1991), the correlation diagram is displayed in Figure 3.3. For this subset we observe

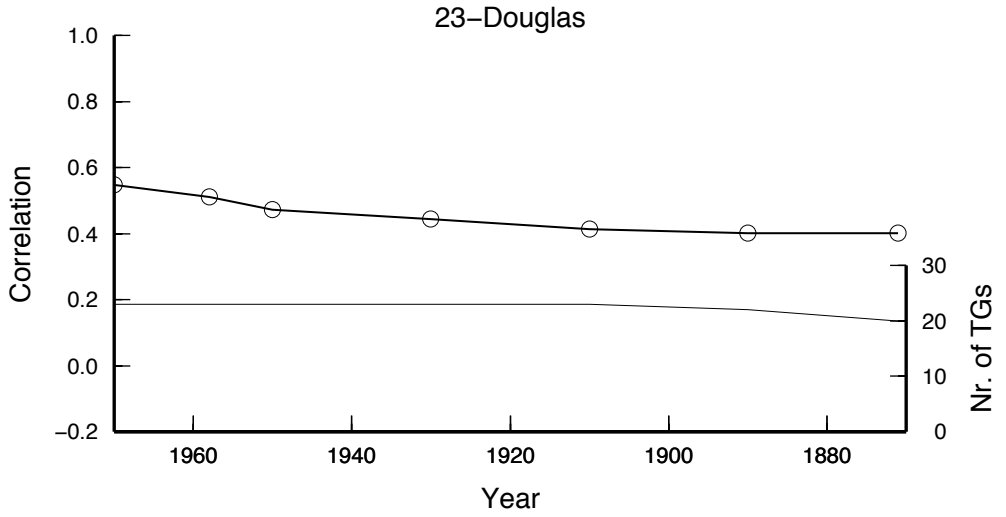

Figure 3.3: *Correlation of the 23 TG sites selected by Douglas (1991) as a function of the ending epoch of the time span.*

that the correlation decreases from $R = 0.55$ (1970–2008) to $R = 0.40$ (1871–2008). Subset *b)* consists of the 27 TGs with record length exceeding 120 years and with completeness $\geq 70\%$. Their correlation, displayed in Figure 3.4, varies from $R = 0.68$ for the period 1970–2008 to $R = 0.57$ for 1871–2008.

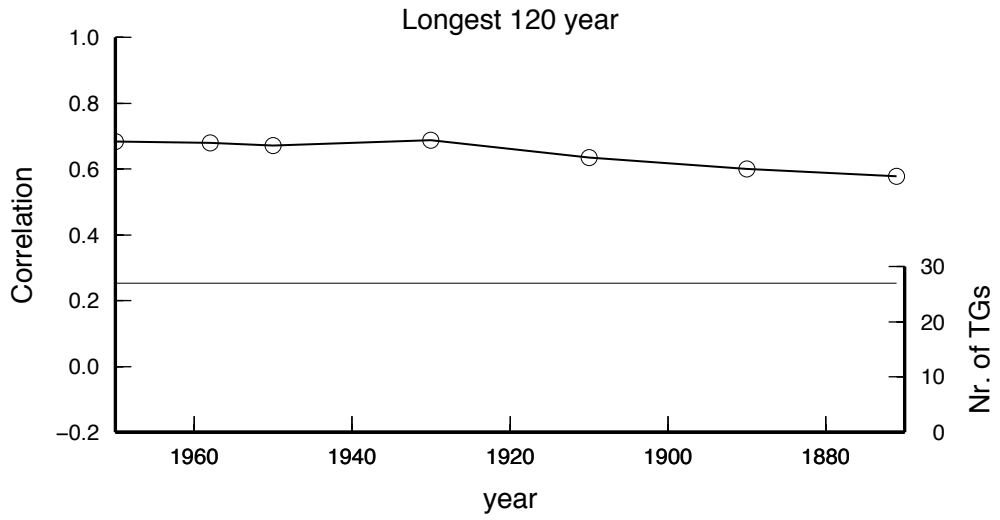

Figure 3.4: *Correlation of the TG sites whose time series exceeds 120 years as a function of the ending epoch of the time span.*

Finally, subsets *c)* leads to a large set of time series especially for the shorter and more recent time spans. The results are displayed in Figure 3.5. in which we can note that larger time spans correspond to smaller

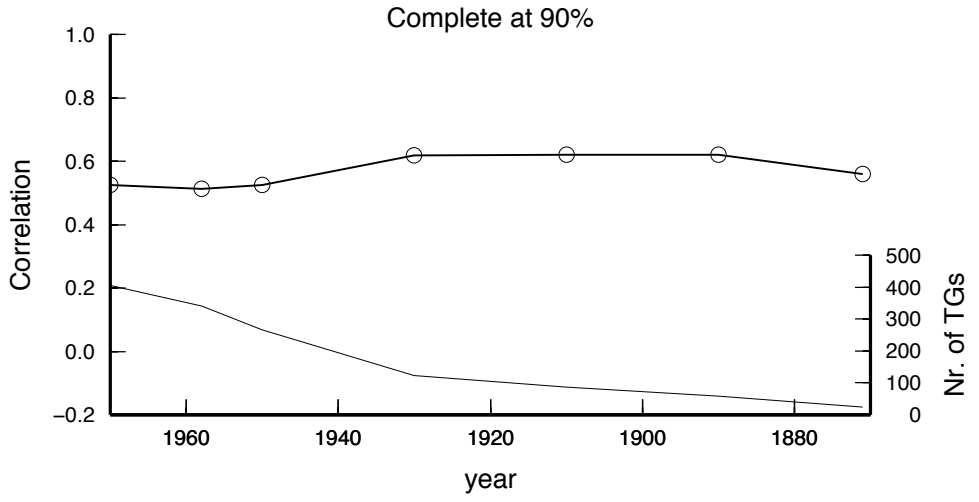

Figure 3.5: *Correlation of the TG sites whose time series completeness exceeds 90% as a function of the ending epoch of the time span.*

number of available TGs. This reflects in a rise for the correlation from $R = 0.52$ (period 1970–2008, 405 TGs) to $R = 0.62$ (period 1890–2008, 58 TGs). Finally, it levels out at $R = 0.56$ when the entire time span of

SODAv2 is considered.

The above analysis shows a persistent moderate positive correlation between TG time series and their corresponding synthetic ones in SODAv2. The correlation does not drop when the time span is extended from 1958–2008 to 1870–2008. The correlation for the four subsets and for the entire time span ($\overline{R}$= 0.52) indicates a decrease of about 10% with respect to that for the period 1958–2008 ($\overline{R}$=0.58). Overall, these results confirm that such a moderate correlation is maintained (values are in the range 0.5-0.6), in agreement with the findings of Chepurin et al. (2014).

The validation of SODAv2 in the open oceans before the altimetry era requires a different perspective, since no direct observations are available. Calafat et al. (2014) have observed that coastal and deep ocean sea–level signals are more correlated in SODAv2 than in the real world. However, they have acknowledged the reliability of SODAv2 for studying global scale sea–level variations, which is the main purpose of this work. In their conclusions the authors also suggests that the SODAv2 outcomes can be considered a realistic representation of the low-frequency sea-level variability at regional scale. In support to this hypothesis, Carton et al. (2012) have observed that extreme climate variability is reproduced by the reanalysis even back to the early years of the 20th century, while historical data were only able to resolve limited aspects of tropical and subtropical variability prior to the 40s.

3.4 Methodology

Given a sea–level time series, and consistently to the definitions given by Equation (1.5) and (1.7), we define the rate of sea–level rise as the slope ρ of the best fitting first-order polynomial in a ordinary linear regression and the acceleration α as twice the second order coefficient resulting from a quadratic fit.

The uncertainties associated with ρ and α will be the standard error and twice the standard error of the corresponding regression coefficients,

respectively. The application of least squares fitting could indeed be questioned, since it assumes stationarity and does not account for auto-correlation of time series (Bos et al., 2014). However, we stick to this definition to ease the comparison between our results and those from a number of previous works. We will first compute the values of ρ and α from global and coastal time series, and then check whether they provide values for these two regressors that are coherent, *i.e.* if the null hypothesis that one differs from each other can be rejected at a certain level of confidence. This analysis will be applied to the altimetry data (CSIRO, described in Sections 1.4 and 3.2) and to the ocean reanalysis SODAv2 described in Section 3.2.

To construct the global and coastal time series (either from CSIRO or from SODAv2), we will average at each time step all the grid points (for GMSL) or only those wet points surrounded by at least one dry point (for coastal sea level). A weighted average will be applied, since the area of the grid cells depends on latitude. The adoption of ordinary least squares is supported by the homoscedasticity of the time series (Figure 3.6). Furthermore, to emulate the reconstruction of GMSL from TG

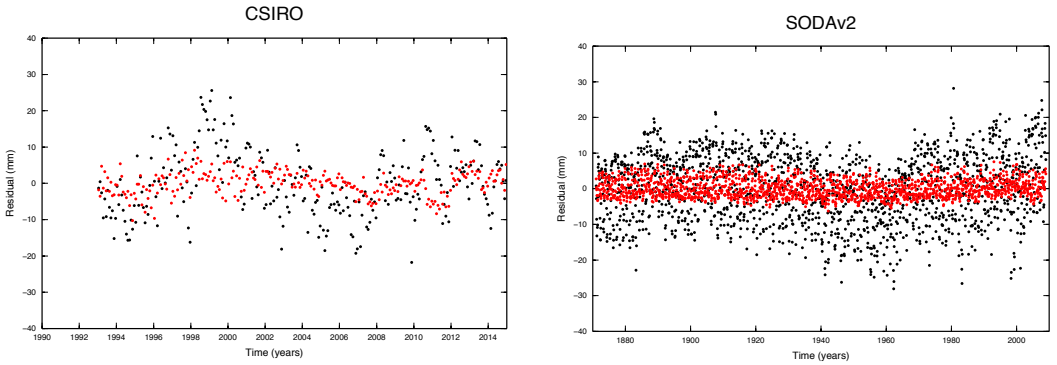

Figure 3.6: *a) distribution of the residuals for the coastal (red) and global CSIRO sea–level reconstructions. b): distribution of the residuals for the coastal (red) and global SODAv2 sea–level reconstructions.*

records, we will apply two of the methodologies commonly in use, stacking and RSOI, to the synthetic dataset PSMSL-SODA. In details, we will follow the stacking technique of Olivieri and Spada (2013) which

consists in averaging, at one year steps, all the time series with record length ≥ 60 years (this selection provides 226 sites, whose distribution is given in Figure 3.7), while for the the RSOI method, we will use the implementation proposed by Calafat et al. (2014). RSOI is based on the computation of the EOFs from altimetry data, assuming stationarity *i.e.* that the EOFs obtained for the altimetric period are also representative of previous decades. The sea–level pattern is then recovered globally by determining the combination of EOFs that best fits the available TG records. The advantage of using an optimal interpolation technique is that, contrary to stacking, it naturally accounts for the irregular distributions of TGs, down-weighting the redundant stations. Finally, the impact of the IB response will be assessed comparing ρ and α values obtained with and without application of the IB correction prior to the GMSL reconstruction.

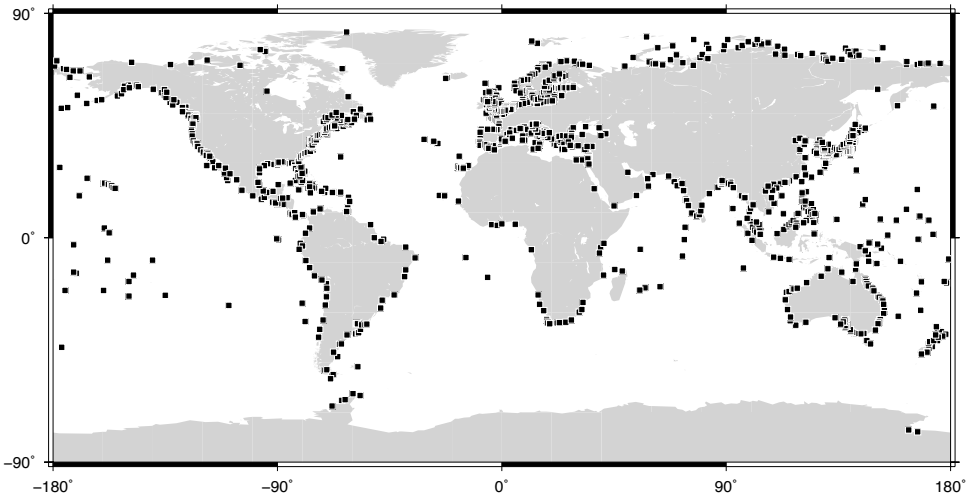

Figure 3.7: *Distribution of the* 226 *PSMSL RLR TG sites with records longer than* 60 *years used for the global mean sea–level reconstructions in this work.*

3.5 Results from satellite altimetry

Satellite altimetry provides an almost instantaneous image of sea level and by putting together a series of snapshots over time, global changes

of the sea level can be determined. One of the outcomes of these comprehensive measurements is the provision of the time history of the sea level (Figure 1.9a). This opens the possibility to determine the rate of sea–level rise that results to be $\rho = (3.4 \pm 0.4)$ mm yr^{-1} over the period 1993–2014 with slight fluctuations between different agencies or institutions (Nerem et al., 2010)[2]. As suggested by Figures 1.8 and 1.9a sea–level change has not a uniform behavior nor spatially neither over time.

Using CSIRO (1993–2014) with all corrections applied (IB, GIA, and seasonal cycle), we find $\rho = (3.17 \pm 0.30)$ mm yr^{-1} and $\rho = (3.53 \pm 0.90)$ mm yr^{-1} for the global and coastal time series (Figure 3.8a), if the global value is consistent with previous assessments for the rate of GMSLR, the coastal one significantly (95% confidence) overestimates the first by 0.36 mm yr^{-1}.

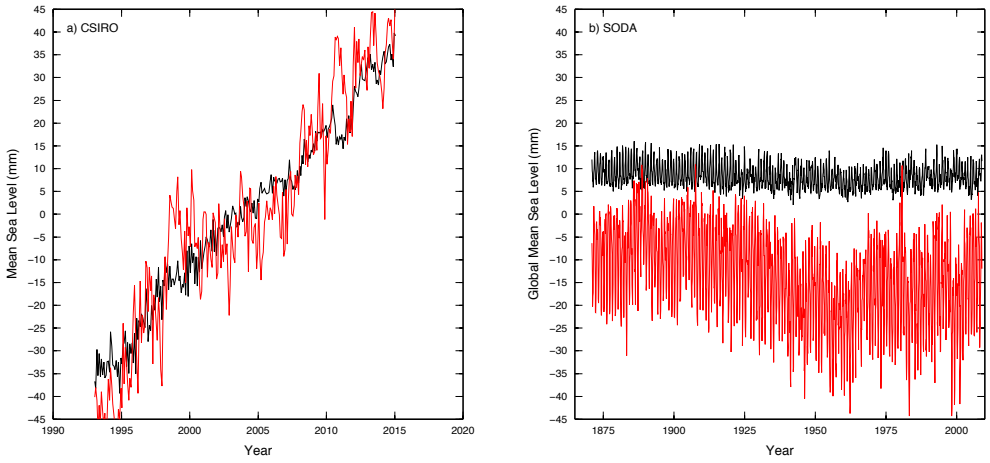

Figure 3.8: *a) global (black) and coastal (red) mean sea level as a function of time for CSIRO. b): same as in panel a) for the case of SODAv2.*

The above result suggests that global and coastal sea level might evolve differently at the time scale of few decades, in contrast with Prandi et al. (2009) but in agreement with what proposed by Cabanes et al. (2001) for the longer time period 1955-1996. To further validate the

[2]and further updates at http://sealevel.colorado.edu/content/global-mean-sea-level-time-series-seasonal-signals-removed.

discrepancy between coastal and global mean rate of sea–level rise we plotted the two distributions of rates computed for the total set of cells (global) and only for those representing the coastal points (Figure 3.9). A Student t-test with Welch (1947) correction suggests (95% confidence)

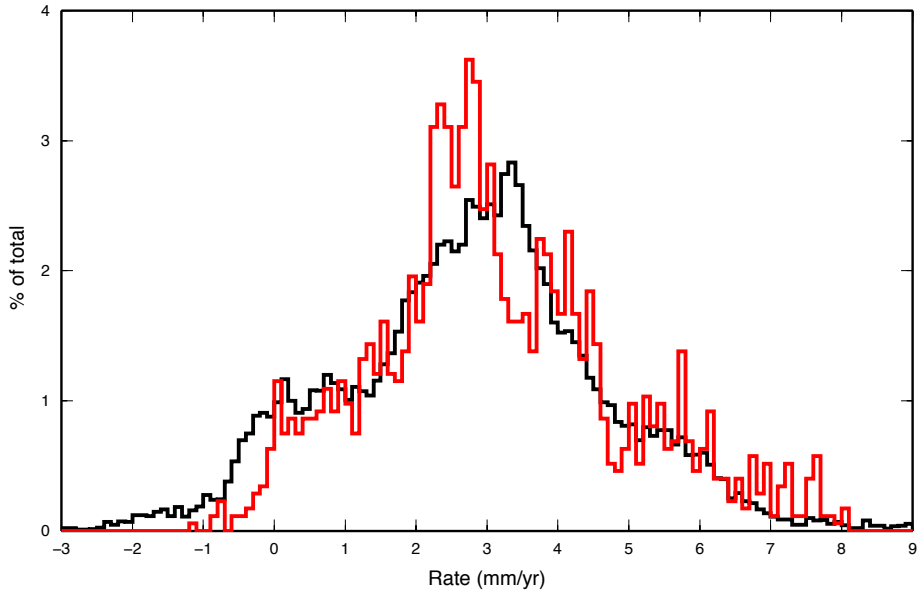

Figure 3.9: *Histogram of the percentage of observed CSIRO mean sea–level rates at global scale (black) and at coastal points (red). The rates have been computed from CSIRO altimetry data spanning the period 1993-2014. The bins are 0.1 mm yr^{-1} wide. Given the apparent multi-modal structure of the two histograms, the mean values do not coincide with the mode of the histograms.*

that the two distributions are statistically different. Concerning sea–level acceleration, we find that the global and coastal values for α computed for the two CSIRO time series are not statistically significant; that is, the quadratic regression does not improve the linear regression (95% confidence). As expected (Douglas, 1992; Scafetta, 2013), the existing secular acceleration cannot emerge above the variability during the 22 year period spanned by altimetry. The above results are summarized in Table 3.2.

Data set	ρ mm yr^{-1}	$\Delta\rho$ mm yr^{-1}	α myc	$\Delta\alpha$ myc
1. CSIRO Global	3.17 $\pm$ 0.30		Not Significant	
2. CSIRO Coastal	3.53 $\pm$ 0.90	0.36	Not Significant	No evidence
3. SODAv2 Global	-0.01 $\pm$ 0.02		0.05 $\pm$ 0.08	
4. SODAv2 Coastal	-0.09 $\pm$ 0.01	0.08	0.21 $\pm$ 0.03	0.17
5. SODAv2 TGs (stacking)	1.28 $\pm$ 0.05	1.28	-0.66 $\pm$ 0.28	0.66
6. SODAv2 TGs (RSOI)	0.05 $\pm$ 0.02	0.06	0.45 $\pm$ 0.15	0.40
7. IB TGs (stacking)	0.04 $\pm$ 0.01	0.04	-0.26 $\pm$ 0.01	-0.26
8. IB TGs (RSOI)	0.053 $\pm$ 0.005	0.053	-0.06 $\pm$ 0.01	-0.06

Table 3.2: *Comparison between coastal and global rates ρ and accelerations α as obtained for the different cases described in the paper. Column $\Delta\rho$ gives the difference relative to the global rate for the same type of data. Same for column $\Delta\alpha$ but for global acceleration.*

3.6 Results from SODAv2

The limitations imposed by the short period spanned by altimetry can be overcome by considering long time series extracted from the output of a numerical model like SODAv2. The motivation in support of the use of this model and its validation are described in Section 3.2. The same procedure described for CSIRO has been applied to SODAv2, which accounts for IB and is unaffected by GIA, see Figure 3.8b. Globally, the ρ and α values obtained are (-0.01 ± 0.02) mm yr^{-1} and (0.05 ± 0.08) myc, respectively (see Table 3.2), which do not differ significantly from zero (95% confidence). This merely reflects the fact that SODAv2 accounts for neither mass changes due to ice melting nor for globally uniform thermal expansion or contraction. When the computations are carried out at all coastal sites, they provide non-vanishing rate of sea–level rise $\rho = (-0.09 \pm 0.01)$ mm yr^{-1} and non-vanishing acceleration $\alpha = (0.21 \pm 0.03)$ myc, with the latter significantly improving (95% confidence) the fit of the linear model. In other words, the coastal ρ and α significantly differ from the global estimates by -0.08 mm yr^{-1} and 0.16 myc, respectively. The observed rate difference (-0.08 mm yr^{-1}), although statistically significant, is not relevant since it represents a neg-

ligible fraction ($< 5\%$) of the typical observed rate at this time scale. Conversely, the acceleration difference represents a significant fraction of the typical observed acceleration; moreover, unlike for CSIRO, it is now statistically significant, possibly as a consequence of the different time periods spanned by the two data sets.

To assess the stability of the acceleration over time, we have evaluated α from SODAv2 over different timespans, all of them beginning in 1871 and increasing at 5 years steps. The results indicate that the small positive acceleration stabilizes for timespans $\gtrsim 100$ years (Figure 3.10), confirming that the acceleration obtained for the whole SODAv2 (138 years long record) is robust, while this is not the case during the period spanned by CSIRO (22 years).

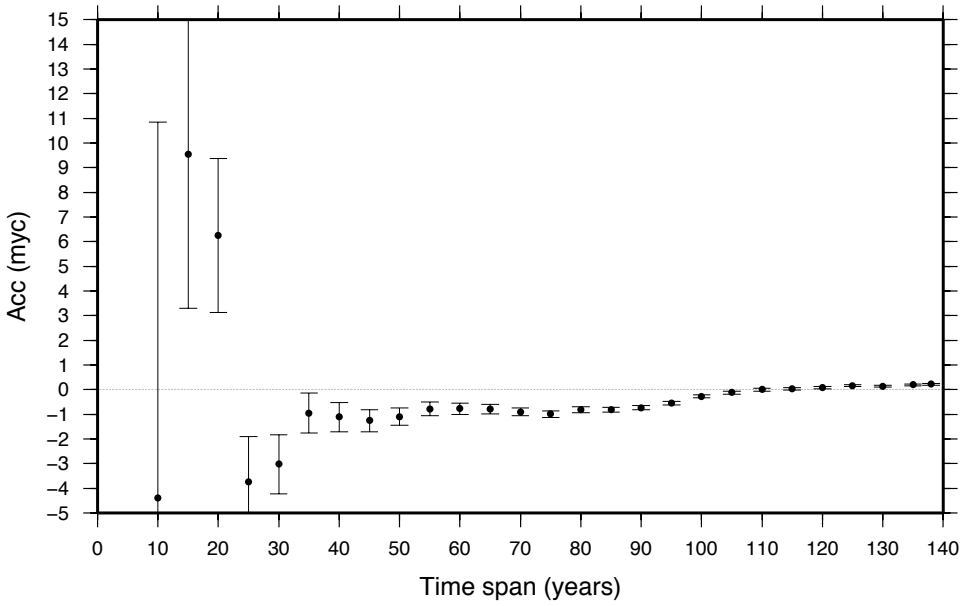

Figure 3.10: *Observed acceleration α versus time span since 1871 for the case of SODAv2 coastal time series.*

3.7 Effects on sea–level reconstructions at tide gauge sites

We have just shown that the secular sea level rate averaged along all the coasts essentially coincides with the actual GMSLR, while this is not the

case for the acceleration. However, contrary to the SODAv2 coastal subset, the actual TG distribution along the coastlines is sparse and not uniform, which could affect GMSL reconstructions. Two methods, stacking and RSOI (see details in Section 3.4), are applied to the synthetic dataset PSMSL-SODA for which the null global rate and acceleration are a priori known. The goal is to evaluate the effect of this sizable spatial subsampling on the reproducibility of the known GMSL in SODAv2.

To mimic the previous GMSL reconstruction of Olivieri and Spada (2013), we selected the 226 TG stations with record length ≥ 60 years (see Figure 3.7) but replacing actual TG time series with the synthetic ones from PSMSL-SODA. The stacking of these synthetic TG time series provides the curve depicted in Figure 3.11a (top), characterized by a rate ρ = (1.28 ± 0.05) mm yr^{-1}, which substantially corresponds to the deviation from the null GMSLR in SODAv2 (see Table 3.2). For the acceleration, we obtain $\alpha = (-0.66 \pm 0.28)$ myc that significantly differs from the SODAv2 GMSLA $\alpha = (0.05 \pm 0.08)$ myc (95% confidence). Since SODAv2 synthetic time series do not contain signals from GIA nor from local ground deformation, the large discrepancies found on ρ and α can be only attributed to the effect of the uneven distribution of the selected TGs along the coastlines. When comparing the stacked SODAv2 curve with that obtained by Olivieri and Spada (2013) using actual TGs, reproduced in Figure 3.11a (bottom), we note strong similarities. Indeed, the coherence of the two time series is confirmed by a Pearson (1931) correlation coefficient of 0.86 over the time span (1871-2008). This suggests that the reconstruction by Olivieri and Spada (2013) discussed in Section 2.4 is affected by a similar bias. Applying the RSOI method to the same set of synthetic TG time series yields different results. On one hand, we obtain a rate for the GMSLR $\rho = (0.05 \pm 0.02)$ mm yr^{-1}, that is, only slightly in excess of the actual vanishing GMSLR of SODAv2. On the other hand, for GMSLA we obtain $\alpha = (0.45 \pm 0.15)$ myc, significantly different from zero and almost opposite to the value

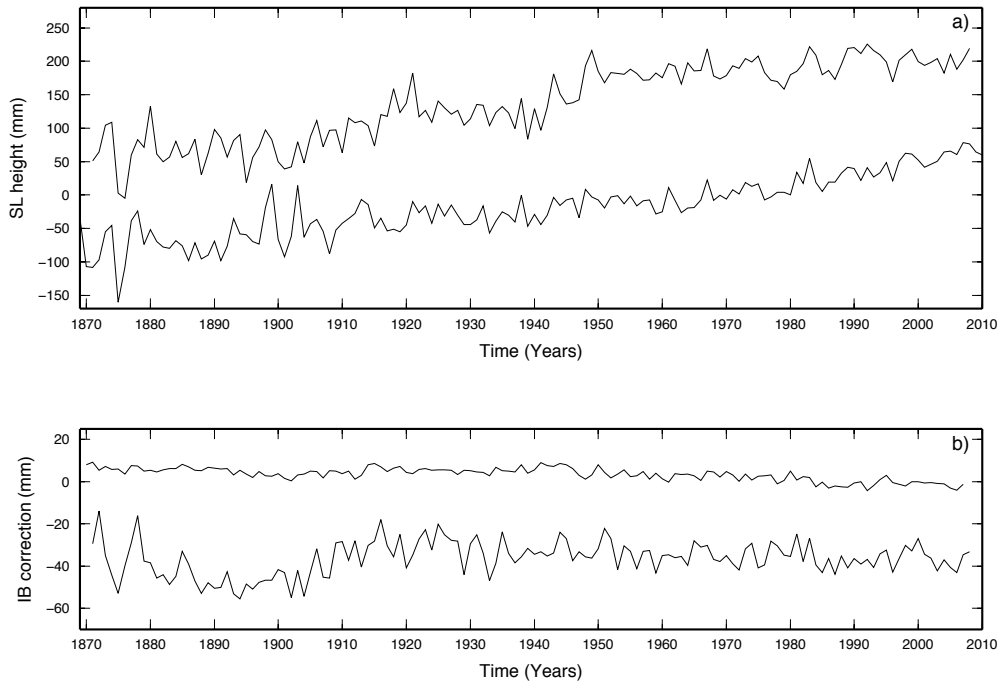

Figure 3.11: *Frame (a) shows the sea–level reconstruction of Olivieri and Spada (2013) (bottom) and the one obtained by stacking synthetic TG time series from SODAv2 model (top). The mean values of the time series are shifted to ease the comparison. The two IB reconstructions are shown in (b): the one obtained by stacking IB time series (bottom) and the one by RSOI (top).*

obtained from the stacking. These findings show that: *i)* the reconstruction by means of the RSOI technique yields an accurate GMSLR, while this is not the case when a stacking technique is used; ii) for GMSLA none of the techniques yields an accurate result.

3.8 Role of the inverted barometer correction at coastlines

As a last test, we have also evaluated the importance of applying the IB correction prior to recovering GMSL from TG data. Following the above approach, we have selected the IB correction values corresponding to the location and timespan of actual TG records with length ≥ 60 years and we created two "IB reconstructions" by applying the stacking and the RSOI methods respectively (Figure 3.11). From the "IB reconstruction" based on stacking we obtain a rate $\rho = (0.04 \pm 0.02)$ mm yr^{-1} and an

acceleration $\alpha = (-0.26 \pm 0.01)$ myc (Table 3.2). Since stacking is a linear process, these values coincide with the difference between the results obtained from stacking SODAv2 synthetic TGs and those obtained by adding first the atmospheric forcing to SODAv2. Most importantly, these results show that neglecting the IB correction prior to reconstructing GMSL would result in a negligible difference in the rates (< 0.1 mm yr^{-1}) but in a significant underestimation of the acceleration (0.26 myc). The IB reconstruction based on RSOI similarly results in a negligible rate (-0.05 ± 0.01) mm yr^{-1} (Table 3.2). More important, for the RSOI case, also the acceleration results to be negligible (-0.06 ± 0.01) myc.

3.9 Results

Concerning the problems posed in the Section 3.1, the results obtained can be summarized as follows:

i) About the extent to which coastal sea level is representative of GMSL, we can state that coastal data substantially follow the global ocean in terms of secular rate, showing a minor discrepancy (~ 0.08 mm yr^{-1}) that falls within the error-bar commonly associated with GMSLR assessments. Conversely, coastal data do not follow the same acceleration of the global ocean, since they overestimate GMSLA even at secular scale by ~ 0.2 myc during time period (1871-2008). This value constitutes a significant fraction of the GMSLA previously assessed in the literature (Spada et al., 2015). Accepting that for secular sea–level variability most of GMSL change is captured by the rate, with the acceleration being of second order, then coastal sea level could be considered representative of GMSL.

ii) About the extent to which the limited sampling provided by TG records allows a robust estimate of GMSL, we conclude that it does in term of GMSLR as long as the RSOI method is used. The discrepancy obtained is, in this case, essentially negligible (< 0.1 mm yr^{-1}). Con-

versely, stacking could not yield the right answer; when it is applied to SODAv2, it overestimates GMSLR by ~ 1 mm yr^{-1}. For GMSLA, none of techniques we have applied to synthetic TG records provides the right answer; the difference with respect to the actual GMSLA is -0.6 myc when using RSOI and 0.45 myc when using stacking.

iii) The IB correction produces a negligible bias in the computation of GMSLR from TGs (< 0.1 mm yr^{-1}). However it can produce a significant bias in the computation of GMSLA (~ 0.26 myc) when a simple stacking techniques is used.

We remark here some similarities with the recently published work by Thompson et al. (2016) in which the authors concluded that TG locations could be considered not in the right place for properly represent the global nature of sea level.

CHAPTER 4

Discussion

4.1 What we have learned

The data analyses and the consequent results in Chapters 2 and in Chapter 3 led to some important conclusions and some good lessons that are summarized in the following. Some of these are original in the sense that, to my knowledge, were not previously discussed by other authors.

First, I could quantify the relevance of long period oscillations in the determination of the rate of sea–level rise and of its acceleration at century and comparable time scales. This is strongly related with the common approach for the assessment of rate and acceleration, i.e. ordinary least squares linear and quadratic regression. From a set of synthetic time series on which I superimposed sinusoidal signals at different periods and amplitudes, it became apparent that the effects of periodic signals cancel only when a sufficient number of cycles is included ($N \gg 5$) and this would not be the case for multidecadal signals in century long time series. A reasonable workaround would be to move forward from

the standard definitions for rate and acceleration: slope of the best fitting first-order polynomial and twice the second order coefficient resulting from a quadratic fit, respectively. More realistic approaches are becoming necessary and these should also include an advanced determination of the contaminating long period signals. These signals, indeed, can strongly differ from a stationary sinusoid (constant amplitude and period). The reanalysis of the sea–level reconstruction by Jevrejeva et al. (2008), in the framework of a re-evaluation of the work by Chambers et al. (2012), confirmed (95% confidence) our hypothesis (Section 2.3).

Second, the distinct rate and acceleration observed for the cases of global and coastal sea–level change at different time scales suggest that ocean circulation is likely (95% confidence) to introduce a bias when global sea–level change is observed from coastal locations. This effect becomes more prominent when the number of coastal samples is reduced to those where long-lasting TGs have been sited. In details, we observed that sea–level reconstructions based on TG time series could not provide realistic estimates for the long term acceleration. For the case of the rate of GMSLR, sophisticated reconstructions based on RSOI method provide consistent representation of the long term global rate while stacking could not yield the right answer.

Finally, I could confirm that the undersampling of the ocean surface by TGs prevents the IB correction from vanishing as it occurs when global averages are considered. For this reason, the effect of the atmospheric pressure cannot be omitted when sea level is reconstructed from TG time series. In addition, most of the works cited in this dissertation, as well as this dissertation for consistency with previous works, neglected the apparent autocorrelation of sea–level time series. Autocorrelation stems from the fact that sea–level height at time t_k is certainly not independent from the sea–level height at time t_{k-1}. This fact breaks the hypotheses underlying the OLS method. The argument was exhaustively discerned by Foster and Brown (2015) who discussed the effect of cor-

related colored noise in regression models. The authors could conclude that, as expected from theory, autocorrelation mainly produces underestimated errors for the regressors but it does not bias the central values. It can be demonstrated, and visually observed from Figure 4.1 in which the regression residuals for the site of San Francisco (USA) are plotted as a function of time, that moving from heights $H(t_k)$ to its first differences $D(t_k) = H(t_k) - H(t_{k-1})$ removes most of the autocorrelation existing in sea–level time series.

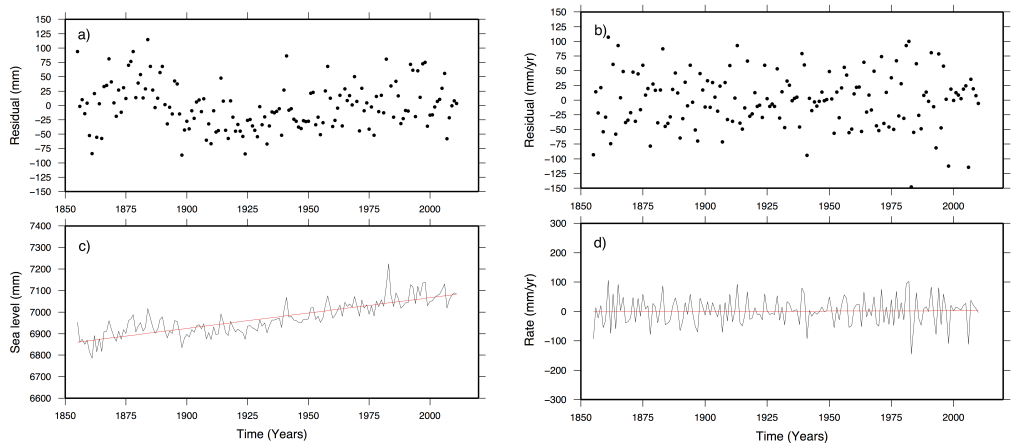

Figure 4.1: *Autocorrelation as observed for the annual mean sea level at San Francisco (USA). Frames a) and b) represent the residual (data minus regression model) as a function of time for the two case of sea–level height $H(t)$ and of its first differences $D(t)$, respectively. Frames c) and d) show the corresponding time series $H(t)$ and $D(t)$ and their best-fitting regression model (red line).*

From a physical point of view, this means to move from displacement to velocity, i.e. rate of sea–level rise. Although the discrete derivative enlarges the error-bar associated to each sample data (Olivieri and Spada, 2016), it also resolves the ambiguity in consequence of the use of different reference frames for different TG sites (Olivieri and Spada, 2016).

In the next sections of this Chapter, the above conclusions will be used to set the path for a new sea–level reconstruction that covers the last century. The aim will be to remove those biases induced by the sparse sampling of TG data, to remove the autocorrelation by moving from the time-domain to velocity and to account for multidecadal oscil-

lations. This pathway to sea–level reconstruction from TG records would rely on SODAv2 model as a correction for the effects of ocean circulation as discussed in Chapter 3 and explained in the following.

4.2 Tide gauge correction for ocean circulation

In Chapter 3, we could demonstrate that coastal points are biased in representing, at short- and the long-term, the nature of the sea–level change in terms of its rate and its acceleration. By using SODAv2 ocean reanalysis, that does not account neither for the mass change nor the thermosteric effect, we could argue that these biases originate from the ocean circulation, whose average effect do not vanish at coasts as it does globally (under the assumption of water incompressibility). This work relied on the PSMSL-SODA data set (details in Section 3.3) in which each of the TG time series was replaced by its corresponding synthetic one extracted from SODAv2. Under the assumption that SODAv2 is representative for the ocean circulation at TGs, PSMSL-SODA time series can be used as a correction for removing the long-term effects of ocean circulation on true data.

Using the formalism of Eq (1.1), I define S^n_{corr}, the corrected sea–level change at site n, as:

$$S^n_{corr}(t_i) = S^n_{obs}(t_i) - \rho^n_{GIA} \cdot t_i - S^n_{IB}(t_i) - S^n_{OC}(t_i), \qquad (4.1)$$

where n represents the PSMSL id of each TG time series, t_i is the epoch of each monthly observation, S_{obs} is the true RLR monthly time series, ρ_{GIA} is the rate of relative sea–level rise consequence of the glacial isostatic adjustment described in Section 1.2, S_{IB} is the time dependent IB correction for the atmospheric pressure at the site n, and S_{OC} is the sea–level correction for Ocean Circulation (OC), in this case obtained from SODAv2 model.

Before applying the OC, I first test if the good average agreement between data and SODAv2 models reflects in a variance reduction at each

of the long-lasting TGs. This would be an empirical proof for the quality of the correction. To perform this test I create two subsets: a) those TGs with completeness $> 50\%$ over the entire time span covered by SODAv2 (1871–2008) and b) those TGs with completeness $> 70\%$ over the time span 1958–2008 in which SODAv2 is considered more reliable. Results are gathered in Figure 4.2, in which I color-coded the variance change to discriminated those sites for which a reduction is observed. For a small

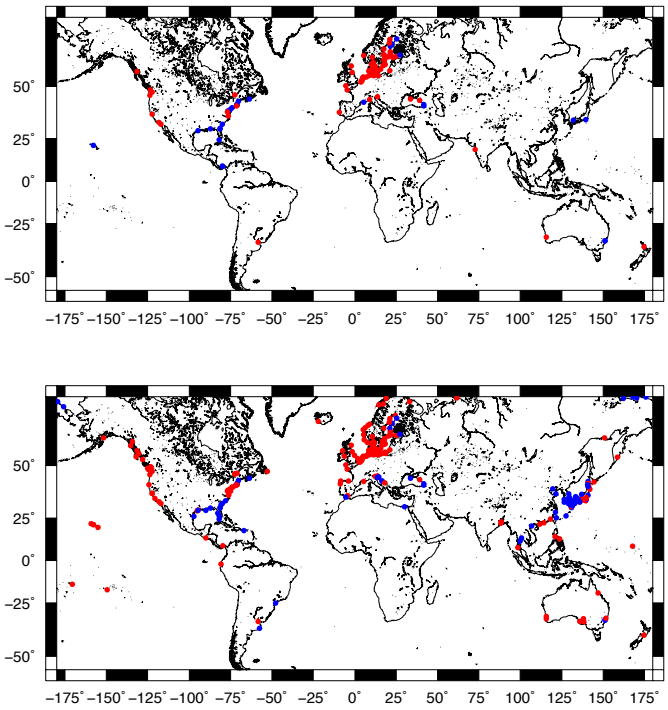

Figure 4.2: *Characterization of the variance change resulting from the OC correction at each tide gauge by means of SODAv2. Red squares mark those sites who observed a variance reduction, blue squares a variance increase. Two examples are displayed: a) time span 1871–2008 and time series completeness > 50% (68 years of data); b) time span 1958–2008 and completeness > 70% (35 years of data).*

portion of the selected sites (27% and 37% of the total respectively) the OC correction leads to an increase in the variance. Apart from those sparse samples, some patterns of coherent variance change can be recognized for both the selected time spans, suggesting the absence of any time dependence. In details, the Baltic Sea and the eastern coast of the Pacific Ocean show an homogeneous reduction. Conversely, along the

coasts of Florida (USA) and in Japan, the OC correction results in an increase of the variance for all the TGs. If the variance reduction is an indicator for the goodness of the model, the variance increase can point to a low resolution of the model in the vicinity of the coastline for the corresponding region. A detailed analysis of this hypothesis is out of the purpose of this work.

The discrepancy between the two maps, the lower accuracy for SODAv2 (Carton et al., 2012) in the epoch before 1900, and the sparse global sampling for the early decades of the PSMSL archive suggest to restrict the following analysis and the forthcoming sea–level reconstruction to the period 1900–2000. Further benefit from this choice would be an easier comparison of the results with the previous ones that are, as shown by other authors (e.g. Dean and Houston, 2013; Church et al., 2013; Spada et al., 2015), time dependent.

By choosing an arbitrary data completeness of 70 % over the time span 1900–2000, we restrict the dataset to 77 TG sites. The OC correction results ineffective (increased variance) for 20 sites that have been discarded. The remaining 55 sites[1] (S55 in the following) are plotted in Figure 4.3 in which we can notice that they sample the majority of the basins although with diverse densities. In detail: 30 TGs are sited in the Baltic Sea, 13 in the North Sea, 5 in the North Pacific Ocean, 3 in the North Atlantic Ocean, while just one TG results available along the coastlines of the Mediterranean Sea, the South Pacific Ocean, the South Atlantic Ocean, the Norwegian Sea and the North Indian Ocean. This again emphasizes the strong uneven capability of the existing TGs to equally sample all the basins.

To prevent the autocorrelation effects (Section 4.1), I then applied to each of the selected S^n_{corr} time series a discrete "two points centered"

[1] the two TGs located in the Black Sea were discarded since these are contaminated by huge subsidence effects (Spada and Galassi, 2012).

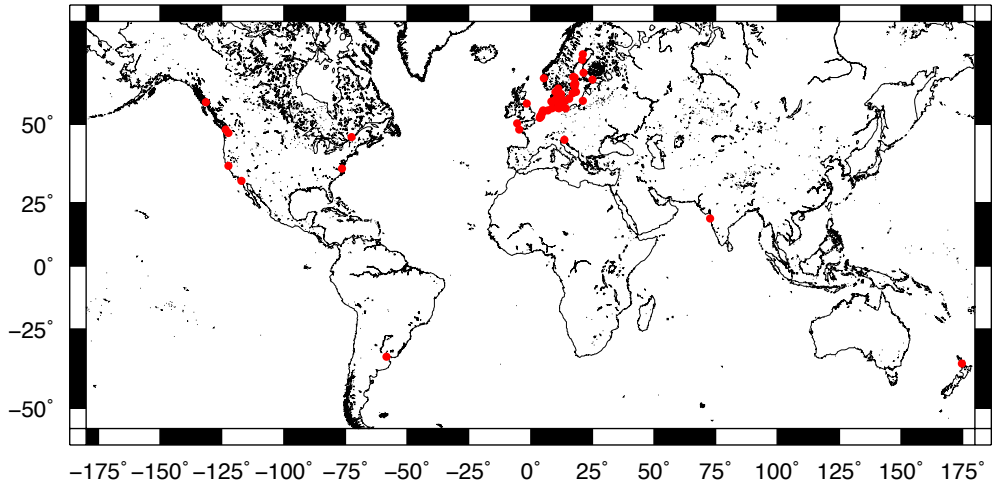

Figure 4.3: *Spatial distribution for the S55 TG selection with completeness > 70% over the time span 1900–2000, for which the application of the ocean circulation correction OC resulted in a variance reduction.*

derivative that, for a generic time series $F(t_n)$, reads:

$$F'(t_n) = \frac{F(t_{n+1}) - F(t_{n-1})}{t_{n+1} - t_{n-1}}, \tag{4.2}$$

where, in absence of gaps, the time interval $(t_{n+1} - t_{n-1})$ can be replaced by twice the sample rate of the time series. Time series are then down-sampled to annual mean values to remove the seasonal component of sea level.

I first focus on the Baltic Sea, a semi-enclosed basin for which S55 provides the largest and densest number of TGs. In Figure 4.4, annual mean corrected rates have been plotted for each of the 30 selected sites together with the "basin function" time series BF resulting from the stacking of all the TG time series associated to that basin:

$$BF(t_n) = \frac{1}{M_n} \sum_{k=1}^{M_n} S^k_{corr}(t_n), \tag{4.3}$$

where M is the number of sites that, as discussed in Section 2.4 can vary over time in consequence of the different level of completeness of the selected TGs. The coherence between the different sites, apparent

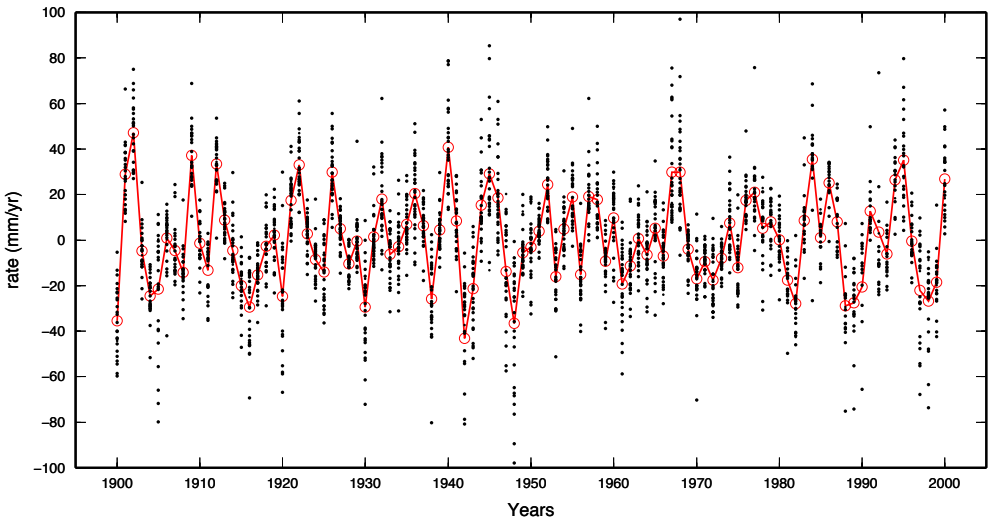

Figure 4.4: *Annual mean rate of sea–level for the Baltic Sea as observed by the different available TGs (Black dots) and its average resulting from the stacking (red circles and thick red line).*

in Figure 4.4, reduces the efficiency of the stacking because the oscillations dominate the common signal and do not cancel in BF, as one would expect in presence of incoherent noise. Consequently, this fluctuation dominates the basin function $BF(t)$ and it limits the constraint for the mean rate providing a standard deviation of the mean equal to 1.9 mm yr^{-1}.

To discriminate the apparent periodic signal from the expected long term behavior of sea level at basin scale, I apply the EMD analysis (Section 2.1) to the BF time series that results in the three IMFs plotted in Figure 4.5. We can observe that IMF1 is dominated by a signal with period of about 3.5 years and it contains almost 80% of the energy of the input signal, while IMF2 contains oscillations at about 10 years and $\sim 16\%$ of the energy. Finally, the IMF3 has periodicity in the range between 30–35 years and about 1% of the remaining energy. The residual is not monotonic with a minimum at year 1953 and negative values in the time span 1935–1967 (Figure 4.6). The average sea–level rate is ~ 1.2 mm yr^{-1} and a trend, corresponding to a positive ~ 0.5 myc acceleration, results from the best-fit of a first order polynomial. Error-bars are

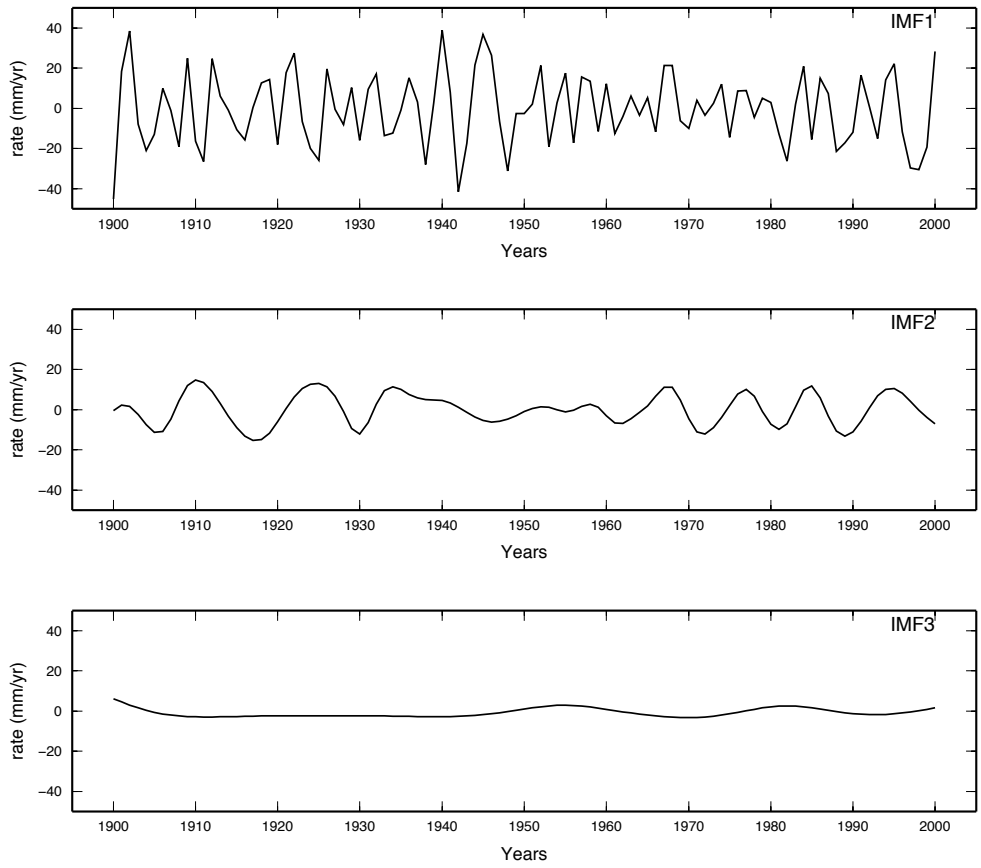

Figure 4.5: *From top bottom, IMF of increasing period as resulting from the EMD analysis applied to the stacking for the Baltic Sea.*

intentionally omitted and the reason will be discussed in the following. To visually remark how an incautious simplification of the model can lead to misleading conclusions, I also plotted (Figure 4.6) the sum of the residual RES plus the $IMFmax$, i.e. the the higher degree IMF that represents the low frequency part of the periodic content of the input time series. This represents what I will call "long term" basin function BF_{lt}:

$$BF_{lt}(t_n) = RES(t_n) + IMF_{max}(t_n). \tag{4.4}$$

We can notice that, when the low frequency oscillation is included, the long term sea level is not constant neither linear, even in the velocity domain. Moreover, detailed conclusions can be inappropriate, e.g. the 1953 minimum disappears when the IMFmax is considered.

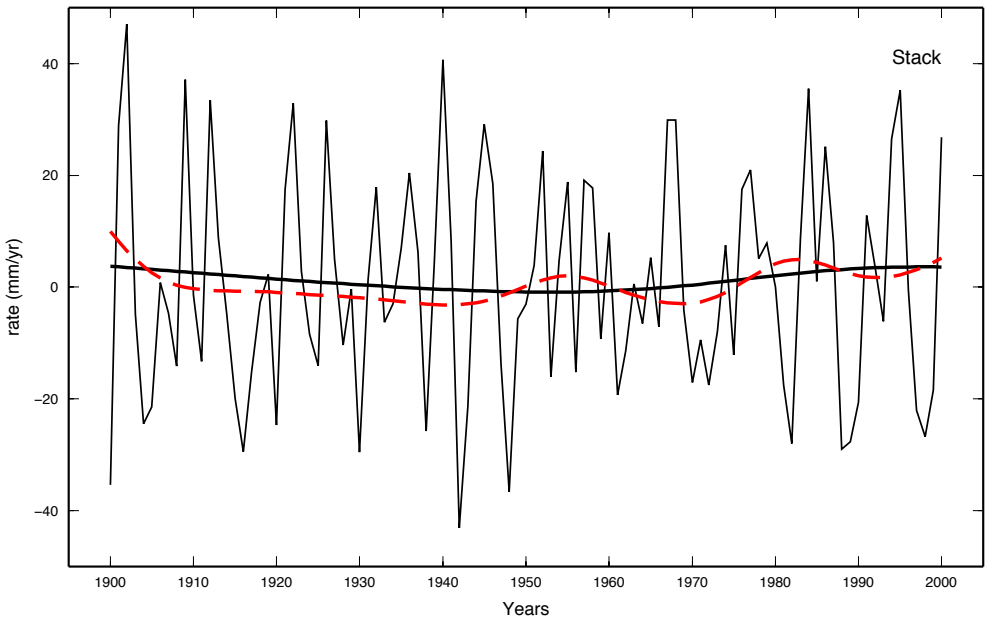

Figure 4.6: *The residual from the EMD analysis (thick line) superimposed to the original sea–level reconstruction resulting from the stacking (thin line). The red dashed line represents the combination of the residual plus the IMFmax.*

4.3 Towards a new sea–level reconstruction

With the aim of creating a global sea–level reconstruction, I extend the above approach to each of the basins for which data are available within S55. As mentioned above, some of the basins are sampled by only one site. This is the case, for example, of the Mediterranean Sea (Trieste, Northern Adriatic Sea), for the South Pacific Ocean (Auckland, Australia) and for the South Atlantic Ocean (Buenos Aires). Conscious of the limitations arising from the use of just one site to represent an entire ocean or the Mediterranean semi-enclosed basin, I extend the BF definition (Equation 4.3) to the case $M = 1$ in which BF corresponds to the unique available time series. To each of the "basin function" BF, I then applied the EMD analysis to discriminate cyclic from non-cyclic signals.

Following the conclusions of the previous Section, I represent the long term sea level for each of the basin by BF_{lt} according to Equation (4.4) This choice goes also along with the idea, discussed in Section

4.1, that multidecadal signals contained in sea–level data should not be removed since their removal could lead to a simplified model, not representative of the real long-term behavior of the ocean. Each BF_{lt} is represented, without its associated error-bar, in one of the frames of Figure 4.7. The figure also includes two tentative reconstructions of the

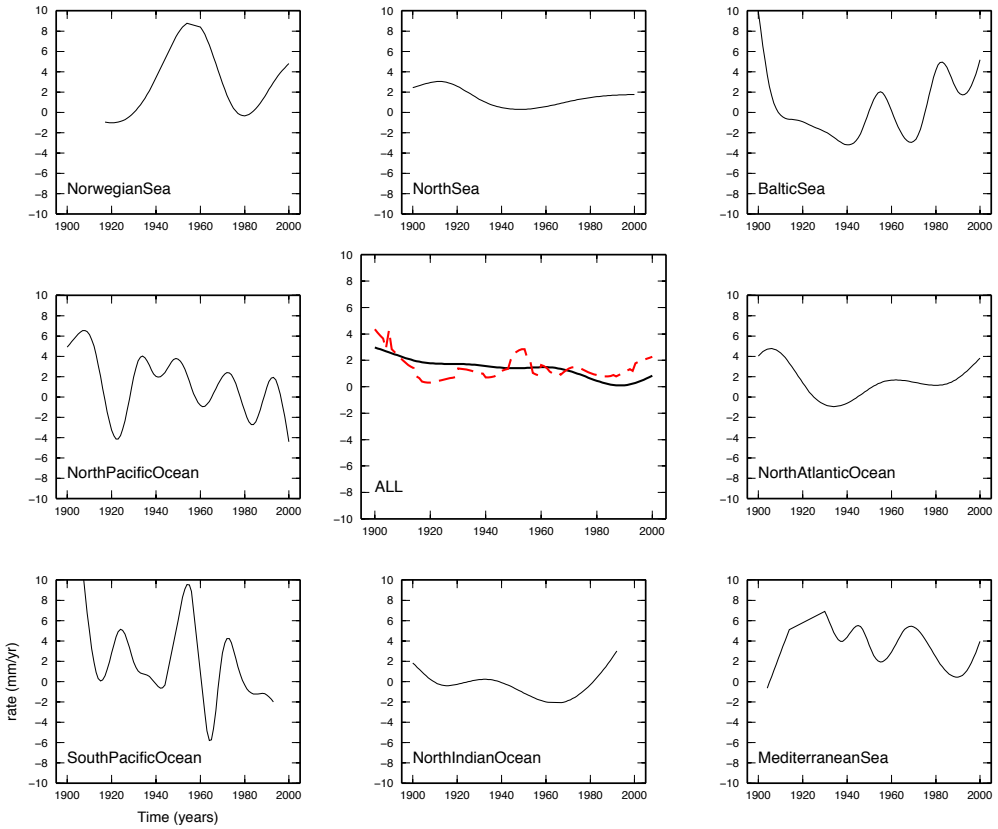

Figure 4.7: *Each frame represents the BF_{lt} for one of the basin listed in Section 4.2. This is the result of the stacking of all the available TG time series for the basin and of the sum of the residual plus the IMFmax obtained from the EMD analysis. The central frame are two tentative global sea–level reconstructions:* i) *the stacking of these sea–level reconstructions (red line),* ii) *the stacking of the original BFs to which the EMD analysis has been then applied.*

global sea level in which the combination of stacking and EMD have been applied in two different manners. In one case, I stacked all the original BFs time series and on the resulting one I applied the EMD. For this case, the sum of RES and IMFmax is displayed (thick black line); second, I stacked all the BF_{lt} representative of each basin (red dashed

line). The two global time series show large differences, however, the mean rate of sea–level rise results similar (1.38 and 1.56 mm yr^{-1} over the time span 1900–2000), and comparable with previous results (see Figure 1 and Table S1 in Spada et al., 2015).

I intentionally omitted any error-bar while plotting the time series in this Chapter as well as in any assessment provided in this Section. This choice, although wrong, remarks two points. First, results without error-bars are meaningless, regardless the reliability of the author or the plausibility of the applied methodology. Second, but even more important, the error propagation should cover the entire path, from data to results. In this work, we learned how to reconstruct the global sea level with an innovative approach that accounts for the undersampling of the oceans by tide gauges and that would prevent some of the biases also consequence of the processing methods. However, to complete the task, we still miss a robust propagation of the errors that entirely covers the processing flow from the uncertainty in input data to the assessment for rate or acceleration. This issue will remain open and it will require a dedicated research project.

4.4 Extemporary events: the case of the Pinatubo eruption

When searching for the GMSL long term rate and acceleration, major attention has been devoted to the presence of periodic signals that contaminate the sea level and that can introduce a bias in the rate and acceleration assessment. There are however also extraordinary episodic events that can impact the climate and consequently the sea level at global scale. When looking at the last decades, of the most important was the Pinatubo eruption in the Philippines. This eruption started beginning of June, 1991 and it culminated, June 15, in the second largest eruption of the 20^{th} century. The eruption lasted for about 9 hours and the massive column of ashes and debris was as high as about 34 km (Self et al., 1996). From a climatic point of view, this meant a significant injection of aerosols

and dust into the stratosphere, in particular sulfur dioxide (SO_2). The stratospheric cloud lasted for almost three years causing the temperature rise in the stratosphere itself in consequence of the increased absorption. But, more important, this caused a reduction in the normal amount of sunlight that resulted in a decrease by about $0.6\,^{\circ}\mathrm{C}$ in the Northern Hemisphere temperature and by $0.4\,^{\circ}\mathrm{C}$ globally. The decrease in temperature reflected in a thermosteric effect on global sea level dropping its height by about 6 mm from the start of the eruption to 1994 (Grinsted et al., 2007; Fasullo et al., 2016). Such a thermosteric effect on GMSL slowly recovered at a rate of ~ 0.5 mm yr^{-1} (Figure 2 in Fasullo et al., 2016).

This observation points the attention on a different aspect of sea–level change at decadal and longer time scale, but also at the time scale of satellite altimetry. The Pinatubo eruption occurred one year in advance of the satellite altimetry era. For this reason, if we distinguish the "natural" from the "Pinatubo induced" sea–level change, one could argue that the steady trend provided by the GMSL curve is an "eruption artifact" and, if corrected, this would result in a positive acceleration (Nerem, personal communication). Conversely, such a disruptive eruption can be one of the natural phenomena that drive the global sea–level change in which the GMSL alternates sudden decreases with slow recovers. Looking at catalogues for the largest eruptions associated to aerosol and ash injection in the stratosphere, the one that preceded the 1991 Pinatubo eruption, occurred in 1883 at Kratatoa (Dutch East Indies, now Indonesia), 108 year before, while several smaller eruptions with comparable stratospheric injection occurred in between (Church et al., 2005). Rampino and Self (1984) count 8 eruptions in the last ~ 250 years that induced some cooling (between 0.0 and $-1.0\,^{\circ}\mathrm{C}$) in the Northern Hemisphere. If we extend the validity of the model for the sea–level change that followed the Pinatubo eruption (Fasullo et al., 2016): i.e. fast decrease (~ 3 years) and slow recover (~ 10 years), we depict a decadal oscillation

with variable amplitude and phase. The first is somehow a function of the amount of aerosols injected in the stratosphere, and the second related to the time interval between one eruption and the following Rampino and Self (between 2 and 61 years for the events considered 1984).

Stratospheric eruptions are indeed episodic events occurring on different place of the Earth from time to time and whose effect is a short-lived change in sea–level height. This observation recalls one of the conclusion drawn by Olivieri and Spada (2013) and discussed in Section 2.4: the constant global acceleration observed in sea–level reconstruction from TG time series can originate from few bi-modal TG time series in which sudden rate changes occur.

CHAPTER 5

Conclusions

The underlying aim of this research work was the study of the sea–level change with specific attention to the sea–level acceleration for the last century or longer. The focus on this specific time span was driven by three main reasons. First, satellite altimetry is observing an almost steady sea–level rise at rate of $\sim$3.3 mm yr^{-1} since 1993. Models for the preceding decades are then mandatory to characterize any acceleration presently acting. Second, human induced global warming is supposed to start during the last century, then the identification of its effects on the sea–level would help to define any mitigation action. Finally, future scenarios of sea–level rise set their target date at year 2100. "One century" is then the appropriate time-scale at which cyclical sea–level variations should be explored to contribute realistic roots for future scenarios.

Tide gauge monthly observations form the only dataset that covers this time span. Their uneven spatio-temporal distribution, and their location confined at the coastlines, prevent the definition of realistic sea–

level reconstructions necessary to provide reliable assessments for the rate and acceleration of the global sea level.

The main lesson from this study is that the choice of using simple models for the global sea level at century scale is inappropriate. This can lead to biased results or to unrealistic reduced error-bars. We could also show that coastal observation provides a limited perspective for modeling the global sea level and that multidecadal oscillations should be accounted even though, again, simple models could be misleading.

This given, the path for a new sea–level reconstruction is depicted and this includes an innovative approach for correcting the bias consequence of the tide gauge distribution. This path is capable to account for the long period oscillations by using adaptive data analysis. What however is missing in this work as well as in the majority of the published ones, is a robust estimate for the errors to be associated to results. This estimate should be able to account for the error on data and to propagate them along the processing (stacking, interpolations, filtering, best-fitting, etc) in a realistic manner and without neglecting any source of error as for the case of autocorrelation.

In conclusion, despite the fact that the apparent acceleration can always be computed and that a realistic guess over the time span 1900–2000 is ~ 1 myc, what I learned is that it is misleading to a-priori assume and search the sea level for constant and global values over an arbitrary time-span. Although a positive sea level acceleration exists this has a significant spatial and temporal variability that cannot be considered "of the second order" and then neglected.

In view of the above considerations it would be more realistic and usable to create models representative for the variability at basin, as well as at decadal, scale in which perturbations, periodic or short-lived, are accounted and not filtered out. This would also help to wash out the wrong idea that improved global models for any past-to-present epoch would be more representative of the present-to-future time.

Acknowledgements

The majority of this research was done at the Università “Carlo Bo” di Urbino and part of it at the IMEDEA (Balearic Island). I am grateful to Giorgio (Prof. Giorgio Spada) for supervising my Ph.D. project, for the pleasure for discussing with him about sea level, geophysics, and other subjects, for sharing with me his curiosity about facts and for his patience. I am also grateful to Prof. Maurizio Bonafede, for his support to my idea of enrolling in a Ph.D. program more than 20 years after being the supervisor of my degree thesis. Prof. Damiá Gomis and Gabriel Jordá were my hosts at IMEDEA and it was a pleasure to work with them. Thanks also to the Istituto Nazionale di Geofisica e Vulcanologia that acknowledged to me the necessary three year leave with financial support and to Gaia Galassi for the fruitful discussions.

The Biblioteca di Cesenatico lecture room, with its fantastic view over the “Canale Leonardesco”, was the perfect site for writing this thesis while looking at the sea.

Tide Gauge observations have been retrieved from the PSMSL (Permanent Service for Sea Level, http://www.psmsl.org) in different epochs during the different stages of this work. The CSIRO altimeter products were extracted from (*http://www.cmar.csiro.au/ sealevel/sl_data_ cmar.html*), last access July 9, 2015; the SODAv2 reanalysis was ex-

tracted from (*http://www.atmos.umd.edu/∼ocean/data.html*), on June 18, 2015; Atmospheric pressure data were provided by the NOAA-ESRL Physical Sciences Division, Boulder Colorado at *http://www.esrl.noaa .gov/psd/*, last access June 20, 2015.

Figures have been generated by GMT (Wessel and Smith, 1998). Figure 2.3 and 2.12 are an exception since these result from the graphical output of SAC (SEISMIC ANALYSIS CODE) version 101.6_beta. Figure 1.1, 1.6, 1.7, 2.16 and 2.15 have been reproduced with permission as properly acknowledged in their corresponding caption.

Thanks to Eleonora for her support during this Ph.D., for suggesting the epigraph of this thesis and for all the rest. The writing pace for this thesis was superbly set by the smiles, the cries, the sleeps and the meals of Carlo.

Bibliography

Antonov, J., Levitus, S., Boyer, T., 2005. Thermosteric sea level rise, 1955–2003. Geophysical Research Letters 32 (12).

Barlow, N. L., Shennan, I., Long, A. J., Gehrels, W. R., Saher, M. H., Woodroffe, S. A., Hillier, C., 2013. Salt marshes as late Holocene tide gauges. Global and Planetary Change 106, 90–110.

Blanchon, P., 2011. Meltwater pulses. In: Encyclopedia of Modern Coral Reefs. Springer, pp. 683–690.

Bonaduce, A., Pinardi, N., Oddo, P., Spada, G., Larnicol, G., 2016. Sea-level variability in the Mediterranean Sea from altimetry and tide gauges. Climate Dynamics, 1–16.

Bos, M., Williams, S., Araújo, I., Bastos, L., 2014. The effect of temporal correlated noise on the sea level rate and acceleration uncertainty. Geophysical Journal International 196, 1423–1430.

Cabanes, C., Cazenave, A., Le Provost, C., 2001. Sea level rise during past 40 years determined from satellite and in situ observations. Science 294 (5543), 840–842.

Calafat, F., Chambers, D., Tsimplis, M., 2014. On the ability of global

sea level reconstructions to determine trends and variability. Journal of Geophysical Research: Oceans 119 (3), 1572–1592.

Camuffo, D., Pagan, E., Sturaro, G., 2005. The extraction of Venetian sea-level change from paintings by Canaletto and Bellotto. In: T, F. C. S. (Ed.), Flooding and Environmental Challenges for Venice and Its Lagoon: State of Knowledge. Cambridge University Press, Cambridge, pp. 129–142.

Carbognin, L., Teatini, P., Tomasin, A., Tosi, L., 2010. Global change and relative sea level rise at Venice: what impact in term of flooding. Clim. Dynam. 35, 6, 1039–1047.

Carson, M., Köhl, A., Stammer, D., 2015. The impact of regional multidecadal and century-scale internal climate variability on sea level trends in CMIP5 models. Journal of Climate 28 (2), 853–861.

Carton, J., Giese, B., 2008. A reanalysis of ocean climate using Simple Ocean Data Assimilation (SODA). Mon. Weather Rev. 136, 2999–3017.

Carton, J. A., Giese, B. S., Grodsky, S. A., 2005. Sea level rise and the warming of the oceans in the Simple Ocean Data Assimilation (SODA) ocean reanalysis. Journal of Geophysical Research: Oceans 110 (C9).

Carton, J. A., Seidel, H. F., Giese, B. S., 2012. Detecting historical ocean climate variability. Journal of Geophysical Research: Oceans 117 (C2).

Cazenave, A., Llovel, W., 2010. Contemporary sea level rise. Annual Review of Marine Science 2, 145–173.

Cazenave, A., Nerem, R. S., 2004. Present-day sea level change: Observations and causes. Rev. Geophys. 42 (3).

Chambers, D. P., 2015. Evaluation of empirical mode decomposition for quantifying multi-decadal variations and acceleration in sea level records. Nonlinear Processes in Geophysics 22 (2), 157–166.

Chambers, D. P., Cazenave, A., Champollion, N., Dieng, H., Llovel, W., Forsberg, R., von Schuckmann, K., Wada, Y., 2016. Evaluation of the global mean sea level budget between 1993 and 2014. Surveys in Geophysics, 1–19.

Chambers, D. P., Merrifield, M. A., Nerem, R. S., 2012. Is there a 60-year oscillation in global mean sea level? Geophysical Research Letters 39 (18).

Chao, B., Wu, Y., Li, Y., 2008. Impact of artificial reservoir water impoundment on global sea level. Science 320, 212–214.

Chepurin, G. A., Carton, J. A., Leuliette, E., 2014. Sea level in ocean reanalyses and tide gauges. Journal of Geophysical Research: Oceans 119 (1), 147–155.

Chow, G. C., 1960. Tests of equality between sets of coefficients in two linear regressions. Econometrica 28, 3, 591–605.

Church, J., Clark, P., Cazenave, A., Gregory, J., Jevrejeva, S., Levermann, A., Merrifield, M., Milne, G., Nerem, R., Nunn, P., Payne, A., Pfeffer, W., Stammer, D., Unnikrishnan, A., 2013. Sea Level Change. In: Stocker, T., Qin, D., Plattner, G.-K., Tignor, M., Allen, S., Boschung, J., Nauels, A., Xia, Y., Bex, V., Midgley, P. (Eds.), Climate Change 2013: The Physical Science Basis. Contribution of Working Group I to the Fifth Assessment Report of the Intergovernmental Panel on Climate Change. Cambridge University Press, Cambridge, pp. 1138–1191.

Church, J. A., White, N. J., 2006. A 20th century acceleration in global sea–level. Geophys. Res. Lett. 33, L01602.

Church, J. A., White, N. J., 2011. Sea–level rise from the late 19th to the early 21st century. Survey in Geoph. 32 4, 585–602.

Church, J. A., White, N. J., Arblaster, J. M., 2005. Significant decadal-scale impact of volcanic eruptions on sea level and ocean heat content. Nature 438 (7064), 74–77.

Church, J. A., White, N. J., Coleman, R., Lambeck, K., Mitrovica, J. X., 2004. Estimates of the regional distribution of sea level rise over the 1950-2000 period. J. Clim. 17 (13), 2609–2625.

Church, J. A., White, N. J., Konikow, L. F., Domingues, C. M., Cogley, J. G., Rignot, E., Gregory, J. M., van den Broeke, M. R., Monaghan, A. J., Velicogna, I., 2011. Revisiting the Earth's sea-level and energy budgets from 1961 to 2008. Geophysical Research Letters 38 (18).

Clark, J. A., Farrell, W. E., Peltier, W. R., 1978. Global changes in post-glacial sea level: a numerical calculation. Quaternary Research 9 (3), 265–287.

Clark, P. U., Mitrovica, J., Milne, G., Tamisiea, M., 2002. Sea-level fingerprinting as a direct test for the source of global meltwater pulse IA. Science 295 (5564), 2438–2441.

Conrad, C. P., 2013. The solid Earth's influence on sea level. Geological Society of America Bulletin 125 (7-8), 1027–1052.

Dean, R., Houston, J., 2013. Recent sea level trends and accelerations: comparison of tide gauge and satellite results. Coastal Engineering 75, 4–9.

Delvecchio, M., 2016. Il livello del mare a Cesenatico (FC): nuove osservazioni dal 1939. Tesi di laurea, Anno Accademico 2014/2015, Università degli Studi di Urbino Carlo Bo.

Douglas, B., 1991. Global sea level rise. Journal of Geophysical Research 96 (C4), 6981–6992.

Douglas, B., 1992. Global sea level acceleration. Journal of Geophysical Research 97 (C8), 12,699–12,706.

Dyurgerov, M. B., Meier, M. F., 2005. Glaciers and the changing Earth system: a 2004 snapshot. Vol. 58. Institute of Arctic and Alpine Research, University of Colorado Boulder.

Ezer, T., 2013. Sea level rise, spatially uneven and temporally unsteady: Why the US East Coast, the global tide gauge record, and the global altimeter data show different trends. Geophysical Research Letters 40 (20), 5439–5444.

Fairbanks, R. G., 1989. A 17, 000-year glacio-eustatic sea level record: influence of glacial melting rates on the younger dryas event and deep-ocean circulation. Nature 342 (6250), 637–642.

Farrell, W., 1972. Deformation of the Earth by surface loads. Reviews of Geophysics 10 (3), 761–797.

Farrell, W., Clark, J., 1976. On postglacial sea-level. Geophys. J. Roy. Astr. S. 46, 647–667.

Fasullo, J., Nerem, R., Hamlington, B., 2016. Is the detection of accelerated sea level rise imminent? Scientific Reports 6, 31245.

Fleming, K., Lambeck, K., May 2004. Constraints on the Greenland Ice Sheet since the Last Glacial Maximum from sea-level observations and glacial-rebound models. Quaternary Science Reviews 23, 1053–1077.

Florido, E., Auriemma, R., Faivre, S., Rossi, I. R., Antonioli, F., Furlani, S., Spada, G., 2011. Istrian and dalmatian fishtanks as sea-level markers. Quaternary international 232 (1), 105–113.

Foster, G., Brown, P. T., 2015. Time and tide: analysis of sea level time series. Climate Dynamics 45 (1-2), 291–308.

Fu, L.-L., Christensen, E. J., Yamarone, C. A., Lefebvre, M., Menard, Y., Dorrer, M., Escudier, P., 1994. TOPEX/POSEIDON mission overview. Journal of Geophysical Research: Oceans 99 (C12), 24369–24381.

Galassi, G., Aprile 2015. Global and regional sea level variations in the recent past and future: insight from observations and modeling. Ph.D. thesis, Università degli Studi di Bologna.

Galassi, G., Spada, G., 2015. Linear and non-linear sea-level variations in the Adriatic Sea from tide gauge records (1872-2012). Annals of Geophysics 57 (6).

Gehrels, W. R., Woodworth, P. L., 2013. When did modern rates of sea–level rise start? Global and Planetary Change 100, 263–277.

Giese, B. S., Ray, S., 2011. El Niño variability in simple ocean data assimilation (SODA), 1871–2008. Journal of Geophysical Research: Oceans 116 (C2).

Gilbert, F., Dziewonski, A., 1975. An application of normal mode theory to the retrieval of structural parameters and source mechanisms from seismic spectra. Phil. Trans. R. Soc. A 278, 187–269.

Goldstein, P., Dodge, D., Firpo, M., Minner, L., 2003. 85.5 sac2000: Signal processing and analysis tools for seismologists and engineers. International Geophysics 81, 1613–1614.

Grinsted, A., Moore, J., Jevrejeva, S., 2007. Observational evidence for volcanic impact on sea level and the global water cycle. Proceedings of the National Academy of Sciences 104 (50), 19730–19734.

Gutenberg, B., 1941. Changes in sea level, postglacial uplift, and mobility of the Earth's interior. Geol. Soc. Am. Bull. 52 (5), 721–772.

Hamlington, B., Thompson, P., 2015. Considerations for estimating the 20th century trend in global mean sea level. Geophysical Research Letters 42 (10), 4102–4109.

Hansen, B. E., 2001. The new econometrics of structural shange: dating breaks in U.S. labor productivity. Journal of Economic Perspectives 15, 4, 117–128.

Harrison, C., 1990. Long-term eustasy and epeirogeny in continents. In: Revelle, R. (Ed.), Sea-level change. National Academy Press Washington, DC, pp. 141–158.

Holgate, S. J., Matthews, A., Woodworth, P. L., Rickards, L. J., Tamisiea, M. E., Bradshaw, E., Foden, P. R., Gordon, K. M., Jevrejeva, S., Pugh, J., 2013. New data systems and products at the permanent service for mean sea level. Journal of Coastal Research 29 (3), 493–504.

Houghton, K. J., Vafeidis, A. T., Neumann, B., Proelss, A., 2010. Maritime boundaries in a rising sea. Nature Geoscience 3 (12), 813–816.

Huang, N., Shen, Z., Long, S., Wu, M., Shih, H., Zheng, Q., Yen, N.-C., Tung, C., Liu, H., 1998a. The empirical mode decomposition and the Hilbert spectrum for nonlinear and non-stationary time series analysis. Proceedings of the Royal Society of London. Series A: Mathematical, Physical and Engineering Sciences 454 (1971), 903–995.

Huang, N. E., Shen, S. S., 2005. Hilbert–Huang transform and its applications. Vol. 5. World Scientific.

Huang, N. E., Shen, Z., Long, S. R., Wu, M. C., Shih, H. H., Zheng, Q., Yen, N.-C., Tung, C. C., Liu, H. H., 1998b. The empirical mode decomposition and the Hilbert spectrum for nonlinear and non–stationary time series analysis. Proceedings of the Royal Society of London. Series A: Mathematical, Physical and Engineering Sciences 454 (1971), 903–995.

Huang, N. E., Wu, Z., 2008. A review on Hilbert-Huang transform: Method and its applications to geophysical studies. Reviews of Geophysics 46 (2).

Jevrejeva, S., Grinsted, A., Moore, J., Holgate, S., 2006. Nonlinear trends and multiyear cycles in sea level records. J. Geophys. Res: Oceans (1978–2012) 111 (C9).

Jevrejeva, S., Moore, J., Grinsted, A., Matthews, A., Spada, G., 2014. Trends and acceleration in global and regional sea levels since 1807. Global Planet. Change 113, 11–22.

Jevrejeva, S., Moore, J., Grinsted, A., Woodworth, P., 2008. Recent global sea level acceleration started over 200 years ago? Geophysical Research Letters 35 (8).

Jordà, G., Gomis, D., 2013. On the interpretation of the steric and mass components of sea level variability: the case of the Mediterranean basin. Journal of Geophysical Research: Oceans 118 (2), 953–963.

Kalinin, G., Klige, R., 1978. Variation in the world sea level. World Water Balance and Water Resources of the Earth, 581–585.

Kaplan, A., Kushnir, Y., Cane, M. A., Blumenthal, M. B., 1997. Reduced space optimal analysis for historical data sets: 136 years of Atlantic sea surface temperatures. Journal of Geophysical Research: Oceans 102 (C13), 27835–27860.

Kopp, R. E., Kemp, A. C., Bittermann, K., Horton, B. P., Donnelly, J. P., Gehrels, W. R., Hay, C. C., Mitrovica, J. X., Morrow, E. D., Rahmstorf, S., 2016. Temperature-driven global sea-level variability in the common era. Proceedings of the National Academy of Sciences, 201517056.

Lambeck, K., Nakiboglu, S., 1983. Long-period Love numbers and their frequency dependence due to dispersion effects. Geophysical Research Letters 10 (9), 857–860.

Larsen, C. F., Echelmeyer, K. A., Freymueller, J. T., Motyka, R., 2003.

Tide gauge records of uplift along the northern Pacific–North American plate boundary, 1937 to 2001. J. Geoph. Res. 108 (B4), 2216.

Le Traon, P., Morrow, R., 2001. Ocean currents and eddies. In: Lee-Lueng Fu, L., Cazenave, A. (Eds.), Satellite Altimetry and Earth Sciences – A Handbook of Techniques and Applications. Academic Press, pp. 171–216.

Leuliette, E. W., Miller, L., 2009. Closing the sea level rise budget with altimetry, Argo, and GRACE. Geophysical Research Letters 36 (L04608).

McMichael, A. J., Woodruff, R. E., Hales, S., 2006. Climate change and human health: present and future risks. The Lancet 367 (9513), 859–869.

Meehl, G., Stocker, T., Collins, W., Friedlingstein, P., Gaye, A., Gregory, J., Kitoh, A., Knutti, R., Murphy, J., Noda, A., Raper, S., Watterson, I., Weaver, A., Zhao, Z.-C., 2007. Climate change 2007: The physical science basis, intergovernmental panel on climate change. In: Solomon, S., Qin, D., Manning, M., Chen, Z., Marquis, M., Averyt, K., Tignor, M., Miller, H. (Eds.), Global Climate Projections. Cambridge University Press, Cambridge, pp. 747–845.

Meier, M. F., 1984. Contribution of small glaciers to global sea level. Science 226 (4681), 1418–1421.

Melini, D., Piersanti, A., Spada, G., Soldati, G., Casarotti, E., Boschi, E., 2004. Earthquakes and relative sealevel changes. Geophysical research letters 31 (9).

Miller, L., Douglas, B. C., 2004. Mass and volume contributions to twentieth-century global sea level rise. Nature 428 (6981), 406–409.

Mitrovica, J. X., Peltier, W., 1991. On postglacial geoid subsidence over

the equatorial oceans. Journal of Geophysical Research: Solid Earth 96 (B12), 20053–20071.

Müller, R. D., Sdrolias, M., Gaina, C., Steinberger, B., Heine, C., 2008. Long-term sea-level fluctuations driven by ocean basin dynamics. Science 319 (5868), 1357–1362.

Navarra, A., Simoncini, V., 2010. A Guide to Empirical Orthogonal Functions for Climate Data Analysis. Springer Science & Business Media.

Nerem, R., Chambers, D., Choe, C., Mitchum, G., 2010. Estimating mean sea level change from the TOPEX and Jason altimeter missions. Marine Geodesy 33 (S1), 435–446.

Nerem, R., Mitchum, G., 2002. Estimates of vertical crustal motion derived from differences of TOPEX/POSEIDON and tide gauge sea level measurements. Geophysical Research Letters 29 (19).

Olivieri, M., Spada, G., 2013. Intermittent sea–level acceleration. Global and Planetary Change 109, 64–72.

Olivieri, M., Spada, G., 2016. Spatial sea-level reconstruction in the Baltic Sea and in the Pacific Ocean from tide gauges observations. Annals of Geophysics 59 (3), P0323.

Olivieri, M., Spada, G., Antonioli, A., Galassi, G., 2013. Mazara del Vallo Tide Gauge Observations (1906-16): Land Subsidence or Sea-Level Rise? Journal of Coastal Research 31 (1), 69–75.

Passaro, M., Cipollini, P., Vignudelli, S., Quartly, G. D., Snaith, H. M., 2014. ALES: A multi-mission adaptive subwaveform retracker for coastal and open ocean altimetry. Remote Sensing of Environment 145, 173–189.

Pearson, E. S., 1931. The test of significance for the correlation coefficient. Journal of the American Statistical Association 26 (174), 128–134.

Peltier, W., 1998. Postglacial variations in the level of the sea: Implications for climate dynamics and solid-earth geophysics. Reviews of Geophysics 36 (4), 603–689.

Peltier, W., 2004. Global glacial isostasy and the surface of the ice-age Earth: the ICE-5G (VM2) model and GRACE. Annu. Rev. Earth Planet. Sci. 32, 111–149.

Peltier, W., Andrews, J., 1976. Glacial-isostatic adjustment I. The forward problem. Geophysical Journal International 46 (3), 605–646.

Peltier, W., Argus, D., Drummond, R., 2015. Space geodesy constrains ice age terminal deglaciation: The global ICE-6G_C (VM5a) model. Journal of Geophysical Research: Solid Earth 120 (1), 450–487.

Peltier, W. R., 1994. Ice age paleotopography. Science 265 (5169), 195–195.

Pilkey, O. H., Cooper, J. A. G., 2004. Society and sea level rise. Science 303 (5665), 1781–1782.

Pinardi, N., Bonaduce, A., Navarra, A., Dobricic, S., Oddo, P., 2014. The mean sea level equation and its application to the Mediterranean Sea. Journal of Climate 27 (1), 442–447.

Pirazzoli, P., 1986. Secular trends of relative sea-level (RSL) changes indicated by tide-gauge records. Tech. rep., CNRS-INTERGEO, 191 Rue Saint Jacques, 75005 Paris, France.

Prandi, P., Cazenave, A., Becker, M., 2009. Is coastal mean sea level rising faster than the global mean? A comparison between tide gauges and satellite altimetry over 1993–2007. Geophysical Research Letters 36 (5).

PSMSL, 2015. Permanent Service for Mean Sea Level, Tide Gauge data. http://www.psmsl.org/obtaing, [Online; retrieved 01-February-2015].

Quandt, R., 1960. Tests of the hypothesis that a linear regression obeys two separate regimes. J. Am. Stat. Ass. 55, 324–330.

Rahmstorf, S., 2007. A semi-empirical approach to projecting future sea-level rise. Science 315 (5810), 368–370.

Rampino, M. R., Self, S., 1984. Sulphur-rich volcanic eruptions and stratospheric aerosols. Nature 310, 677–679.

Rato, R., Ortigueira, M., Batista, A., 2008. On the HHT, its problems, and some solutions. Mechanical Systems and Signal Processing 22 (6), 1374–1394.

Ray, R., Douglas, B., 2011. Experiments in reconstructing twentieth-century sea levels. Prog. Oceanogr. 91, 495–515.

Regehr, E. V., Laidre, K. L., Akçakaya, H. R., Amstrup, S. C., Atwood, T. C., Lunn, N. J., Obbard, M., Stern, H., Thiemann, G. W., Wiig, Ø., 2016. Conservation status of polar bears (Ursus maritimus) in relation to projected sea-ice declines. Biology Letters 12 (12), 20160556.

Santamaría-Gómez, A., Gravelle, M., Collilieux, X., Guichard, M., Míguez, B. M., Tiphaneau, P., Wöppelmann, G., 2012. Mitigating the effects of vertical land motion in tide gauge records using a state-of-the-art GPS velocity field. Global and Planetary Change 98, 6–17.

Scafetta, N., 2013. Discussion on common errors in analyzing sea level accelerations, solar trends and global warming. Pattern Recognition in Physics 1, 37–57.

Self, S., Zhao, J.-X., Holasek, R. E., Torres, R. C., King, A. J., 1996. The atmospheric impact of the 1991 Mount Pinatubo eruption. In: Newhall,

C., Punongbayan, R. (Eds.), Fire and Mud: The eruptions and Lahars of Mount Pinatubo, Philippines. Washington University Press, pp. 1089–1116.

Silver, N., 2012. The signal and the noise: Why so many predictions fail-but some don't. Penguin, New York, NY.

Sivareddy, S., November 2015. A Study on Global Ocean Analysis from an Ocean Data Assimilation System and its Sensitivity to Observations and Forcing fields. Ph.D. thesis, Andhra University.

Slangen, A., Katsman, C., Van de Wal, R., Vermeersen, L., Riva, R., 2012. Towards regional projections of twenty-first century sea-level change based on IPCC SRES scenarios. Climate dynamics 38 (5-6), 1191–1209.

Smith, M. L., Dahlen, F., 1981. The period and Q of the Chandler wobble. Geophysical Journal International 64 (1), 223–281.

Spada, G., 2017. Glacial isostatic adjustment and contemporary sea level rise: An overview. Surveys in Geophysics 38 (1), 153–185.

Spada, G., Bamber, J., Hurkmans, R., 2013. The gravitationally consistent sea-level fingerprint of future terrestrial ice loss. Geophysical Research Letters 40 (3), 482–486.

Spada, G., Galassi, G., 2012. New estimates of secular sea level rise from tide gauge data and GIA modelling. Geophysical Journal International 191 (3), 1067–1094.

Spada, G., Melini, D., Galassi, G., Colleoni, F., 2012. Modeling sea level changes and geodetic variations by glacial isostasy: the improved SELEN code. arXiv preprint 1212.5061.

Spada, G., Olivieri, M., Galassi, G., 2014. Anomalous secular sea-level acceleration in the Baltic Sea caused by isostatic adjustment. Annals of Geophysics 57 (4), S0432.

Spada, G., Olivieri, M., Galassi, G., 2015. A heuristic evaluation of long-term global sea level acceleration. Geophysical Research Letters 42, 4166–4172.

Spada, G., Stocchi, P., 2006. The Sea Level Equation, Theory and Numerical Examples. Aracne, Roma.

Spada, G., Stocchi, P., 2007. SELEN: a Fortran 90 program for solving the "Sea Level Equation". Comput. and Geosci. 33 (4), 538–562.

Stocchi, P., Spada, G., 2009. Influence of glacial isostatic adjustment upon current sea level variations in the Mediterranean. Tectonophysics 474 (1), 56–68.

Stocker, T. F., Qin, D., Plattner, G.-K., Tignor, M., Allen, S. K., Boschung, J., Nauels, A., Xia, Y., Bex, V., Midgley, P. M., 2013. Climate Change 2013: The Physical Science Basis. IPCC, Working Group I Contribution to the IPCC Fifth Assessment Report (AR5).

Storto, A., Masina, S., 2017. Objectively estimating the temporal evolution of accuracy and skill in a global ocean reanalysis. Meteorological Applications.

Sturges, W., Hong, B., 2001. Decadal variability of sea level. In: Douglas, B. C., Kearney, M. S., Leatherman, S. P. (Eds.), Sea level rise: History and consequences. International Geophysics Series (75), pp. 165–180.

Thompson, P., Hamlington, B., Landerer, F., Adhikari, S., 2016. Are long tide gauge records in the wrong place to measure global mean sea level rise? Geophysical Research Letters 43 (19).

Trupin, A., Wahr, J., 1990. Spectroscopic analysis of global tide gauge sea level data. Geophys. J. Int. 100 (3), 441–453.

Tsimplis, M., Woodworth, P., 1994. The global distribution of the seasonal sea level cycle calculated from coastal tide gauge data. Journal of Geophysical Research: Oceans 99 (C8), 16031–16039.

Tsimplis, M. N., Raicich, F., Fenoglio-Marc, L., Shaw, A. G., Marcos, M., Somot, S., Bergamasco, A., 2012. Recent developments in understanding sea level rise at the Adriatic coasts. Physics and Chemistry of the Earth, Parts A/B/C 40, 59–71.

Turcotte, D. L., Schubert, G., 2014. Geodynamics. Cambridge University Press.

Tushingham, A., Peltier, W., 1991. ICE-3G - A new global model of late Pleistocene deglaciation based upon geophysical predictions of post-glacial relative sea level change. Journal of Geophysical Research 96 (B3), 4497–4523.

Vermeer, M., Rahmstorf, S., 2009. Global sea level linked to global temperature. Proceedings of the National Academy of Sciences 106 (51), 21527–21532.

Visser, H., Dangendorf, S., Petersen, A. C., 2015. A review of trend models applied to sea level data with reference to the "acceleration-deceleration debate". Journal of Geophysical Research: Oceans 120 (6), 3873–3895.

Wada, Y., van Beek, L., Chao, B., Wu, Y., Bierkens, M., 2012. Past and future contribution of global groundwater depletion to sea-level rise. Geophysical Research Letters 39, L09402.

Welch, B. L., 1947. The generalization of Student's problem when several different population variances are involved. Biometrika 34 (1/2), 28–35.

Wessel, P., Smith, W. H. F., 1998. New, improved version of Generic Mapping Tools released. Eos T. Am. Geophys. Un. 79 (47), 579.

Winer, B. J., 1962. Statistical principles in experimental design. McGraw–Hill.

Woodward, R., 1888. On the form and position of mean sea level. USGS Bulletin 48, 87–170.

Woodworth, P., White, N., Jevrejeva, S., Holgate, S., Church, J., Gehrels, W., 2009. Evidence for the accelerations of sea level on multi–decade and century timescales. Int. J. Climatol. 29, 777–789.

Woodworth, P. L., 1990. A search for accelerations in records of European mean sea level. Int. J. Climatol. 10, 129–143.

Wöppelmann, G., Marcos, M., 2016. Vertical land motion as a key to understanding sea level change and variability. Reviews of Geophysics 54, 64–92, 2015RG000502.

Wöppelmann, G., Marcos, M., Coulomb, A., Míguez, B. M., Bonnetain, P., Boucher, C., Gravelle, M., Simon, B., Tiphaneau, P., 2014a. Rescue of the historical sea level record of Marseille (France) from 1885 to 1988 and its extension back to 1849–1851. Journal of Geodesy 88 (9), 869–885.

Wöppelmann, G., Marcos, M., Santamaría-Gómez, A., Martín-Míguez, B., Bouin, M.-N., Gravelle, M., 2014b. Evidence for a differential sea level rise between hemispheres over the twentieth century. Geophysical Research Letters 41 (5), 1639–1643.

Wöppelmann, G., Miguez, B. M., Bouin, M.-N., Altamimi, Z., 2007. Geocentric sea-level trend estimates from GPS analyses at relevant tide gauges world-wide. Global and Planetary Change 57 (3), 396–406.

Wunsch, C., Stammer, D., 1997. Atmospheric loading and the oceanic "inverted barometer" effect. Reviews of Geophysics 35 (1), 79–107.

Glossary

C

CP — Change Point. 15, 26, 48

D

DFT — Discrete Fourier Transform. 31–33, 42

E

EMD — Empirical Mode Decomposition. 33, 34, 41, 42, 45, 52, 80–83

EOF — Empirical Orthogonal Function. 21, 25, 56, 64

G

GIA — Glacial Isostatic Adjustment. 3, 6, 7, 9, 10, 17, 20, 24, 41–43, 46, 47, 52, 57, 65, 67, 70, 76

GMSL — Global Mean Sea Level. 18, 22, 24, 25, 27, 28, 56, 64, 65, 69, 71, 84, 85

GMSLA — Global Mean Sea Level Acceleration. 25, 55–57, 70, 71

GMSLR Global Mean Sea Level Rise. 55, 56, 66, 69–71, 74

GPS Global Positioning System. 22

I

IB Inverted Barometer. 57, 65, 67, 68, 70, 71, 74, 76

IMF Intrinsic Mode Function. 33–35, 41, 42, 45, 80–83

IPCC AR5 Intergovernmental Panel on Climate Change, Fifth Assessment Report. 25, 27, 40

L

LGM Last Glacial Maximum. 3–5, 8, 9, 12, 13

M

MWP Melt Water Pulses. 4

O

OC Ocean Circulation. 76–78

OLS Ordinary Least Square. 12, 13, 34, 55, 74

P

PGR Post Glacial Rebound. 3

PSMSL Permanent Service for Mean Sea Level. 29–32, 39, 41, 59, 65, 78

R

RLR Revised Local Reference. 30–32, 38, 47, 59, 65, 76

RSOI Reduced Space Optimal Interpolation. 20, 47, 56, 57, 64, 68–72, 74

S

SLE Sea-Level Equation. 10, 11

SODA Simple Ocean Data Assimilation. 57–64, 66–71, 76–78

SSH Sea Surface Heights. 57, 58

T

TG Tide Gauge. 11, 18, 20–22, 24–33, 35, 38–42, 45–47, 49, 51, 55–65, 68–72, 74–80, 83, 86